Liver Steatosis and Insulin-Resistance: Reversal by *Sutherlandia frutescens*

Stephen Clarke (207048868)

Submitted in partial fulfilment of the requirements for the degree of *Magister Scientiae* (MSc) in the Department of Biochemistry and Microbiology in the Faculty of Science at the Nelson Mandela Metropolitan University.

JANUARY 2014

Supervisor: Dr G Dealtry
Co-supervisor: Dr H Davids

Contents

Declaration

Name: Stephen Clarke

Student Number: 207048868

Qualification: MSc. (Biochemistry)

Title: Liver Steatosis and Insulin-Resistance: Reversal by *Sutherlandia frutescens*

Declaration:

In accordance with rule G4.6.3, I hereby declare that the above-mentioned dissertation is my own work and that it has not previously been submitted for assessment to another University or for another qualification.

Signature: _____

Date: ___13/01/2014____

Acknowledgements

Without the Lord my God, Who had bestowed upon me the ability and graceful opportunity to learn about His Creation, I would not have been in power to perform the tasks I have in the past year. I thank thee, my Lord.

To my friends and family: thank you for your support in times that all felt lost. You gave me hope and inspiration when I needed it most - this will forever be remembered.

Dr Gill Dealtry and Dr Hajierah Davids, you have blessed me with your vast knowledge of Biochemistry and this I thank you for. Your guidance has helped me better my abilities as an aspiring scientist.

To the NMMU maintenance staff, Lawyer especially, thank you for your help and maintenance of the laboratory.

Thank you to Dr Trevor Koekemoer for his assistance in the cell laboratory and advice.

Melissa Fortuin, thank you for your assistance using the qBasePLUS software.

Finally, I would like to thank NMMU, South Africa and the NRF for funding this project.

I dedicate this document to my parents who have supported me throughout the entire course of my studies.

List of Figures

List of Tables

List of Abbreviations

α	Alpha
β	Beta
γ	Gamma
δ	Delta
ε	Epsilon
ζ	Zeta
η	Eta
θ	Theta
κ	Kappa
λ	Lambda
μ	Mu
μL	Microlitre
˚C	Degrees Celsius
ACC	Acetyl-CoA Carboxylase
AMP	Adenosine 5'-Monophosphate
AMPK	AMP-activated Protein Kinase
aPKC	Atypical Protein Kinase C
AS160	Akt Substrate of 160kDa
ATP	Adenosine 5'-Triphosphate
ATP5B	Mitochondrial Adenosine 5'-Triphosphate synthase subunit β
BH_4	Tetrahydrobiopterin
BSA	Bovine Serum Albumin
Ca^{2+}	Calcium
CaMKKβ	Calcium/Calmodulin-dependent Protein Kinase Kinase β
cAMP	Cyclic Adenosine 5'-Monophosphate
CAT	Carnitine Acetyltransferase
CBP	CREB-binding Protein
ChREBP	Carbohydrate Response Element Binding Protein
COP1	Coat Protein 1
cPKC	Classical Protein Kinase C
CPT-1	Carnitine Palmitoyltransferase 1
CREB	cAMP Response Element-binding Protein
CRTC2	CREB-regulated Transcription Co-activator 2, also TORC2
C_q	Quantification Cycle
DAG	Diacylglycerol
DCF	2',7'-Dichlorodihydrofluorescein
DCFH	2',7'-Dichlorodihydrofluorescin
DCFH-DA	2',7'-Dichlorodihydrofluorescin Diacetate
ddH_2O	Deionised Distilled Water
DGAT2	Diacylglycerol acetyltransferase 2
DM	Diabetes Mellitus
DMSO	Dimethyl Sulfoxide
DPBSA	Dulbecco's Phosphate Buffered Saline A
dsDNA	Double Stranded DNA
EGP	Endogenous Glucose Production

eIF2B	Eukaryotic Initiation Factor 2B
EMEM	Eagle's Minimum Essential Medium
ER	Endoplasmic Reticulum
ERK1/2	Extracellular Regulated Kinase 1/2
F1P	Fructose 1-Phosphate
F16BP	Fructose 1,6-Bisphosphate
F6P	Fructose 6-Phosphate
FADH2	Flavin Adenine Dinucleotide
FAF-BSA	Fatty Acid-free Bovine Serum Albumin
FBS	Foetal Bovine Serum
FFA	Free Fatty Acid
FITC	Fluorescein Isothiocyanate
FK	Fructokinase
FoxO1	Forkhead Box Protein O 1
g	Gram
G6P	Glucose 6-Phosphate
G6Pase	Glucose 6-Phosphatase
GAP	GTP-activating Protein
GC	Gas Chromatography
GC-MS	Gas Chromatography-Mass Spectrometry
GLUT	Glucose Transporter
Grb-2	Growth Factor Receptor-binding Protein 2
GS	Glycogen Synthase
GSK-3	Glycogen Synthase Kinase 3
GTP	Guanosine 5'-triphosphate
GTPase	Guanosine 5'-triphosphatase
H_2O_2	Hydrogen Peroxide
HBSS	Hank's Balanced Salts Solution
HDL	High Density Lipoprotein
HEPES	N'-2-Hydroxyethylpiperazine-N'-2-ethanesulfonic Acid
HGP	Hepatic Glucose Production
HIV/AIDS	Human Immunodeficiency Virus/Acquired Immunodeficiency Syndrome
HK	Hexokinase
HMGA1	High-mobility Group Protein A1
HPLC	High Performance Liquid Chromatography
HSD	High Sucrose Diet
IF	MCDB-201 medium supplemented with Insulin and Fructose
IFM	IF medium supplemented with metformin
IFSF	IF medium supplemented with *S. frutescens*
IGF-I	Insulin-like Growth Factor I
IGF-IR	Insulin-like Growth Factor I Receptor
IKK	IκB Kinase
iNOS	Inducible Nitric Oxide Synthase
IR	Insulin Receptor
IRR	Insulin Receptor-related Receptor
IRS	Insulin Receptor Substrate
JIP1	JNK-interacting Protein 1
JNK	c-Jun N-terminal Kinase

kDa	Kilo Dalton
L	Litre
LC-MS/MS	Liquid Chromatography-tandem Mass Spectrometry
LKB1	Liver Kinase B1
m	Milli
M	Molar
MAG	Monoacylglycerol
MAPK	Mitogen Activated Protein Kinase
IF	MCDB Supplemented with Insulin and Fructose
MKK7	MAPK Kinase 7
MPB	MCDB Supplemented with Palmitate-BSA
mRNA	Messenger Ribonucleic Acid
mTOR	Mammalian Target of Rapamycin
MTT	4,5-dimethylthiazol-2,5-diphenyltetrazolium bromide
NAD^+	Nicotinamide Adenine Dinucleotide (Oxidised)
NADH	Nicotinamide Adenine Dinucleotide (Reduced)
NaOH	Sodium Hydroxide
NEAA	Non-essential Amino Acids
NED	Naphthylethylenediamine Dihydrochloride
NFκB	Nuclear Factor κB
NO	Nitric Oxide
NOS	Nitric Oxide Synthase
nPKC	Novel Protein Kinase C
NTC	No Template Control
O_2^-	Superoxide
OB	MCDB-201 medium supplemented with Oleate-BSA conjugate
OCT-1	Organic Cation Transporter 1
OM	OB medium supplemented with metformin
OSF	OB medium supplemented with *S. frutescens*
PB	MCDB-201 medium supplemented with Palmitate-BSA conjugate
PBS	Phosphate Buffered Saline
PDH	Pyruvate Dehydrogenase
PDK	Phosphoinositide-dependent Protein Kinase
PEP	Phosphoenolpyruvate
PEPCK	Phosphoenolpyruvate Carboxykinase
PGC-1α	Proliferator-activated Receptor-γ Coactivator-1α
PI3K	Phosphoinositide 3-kinase
PIP_2	Phosphatidylinositol 4,5-bisphosphate
PIP_3	Phosphatidylinositol 3,4,5-trisphosphate
PKB	Protein Kinase B
PKC	Protein Kinase C
PM	PB medium supplemented with metformin
PP1	Protein Phosphatase 1
PP2A	Protein Phosphatase 2A
PPARα	Peroxisome Proliferator-activated Receptor α
PPARγ	Peroxisome Proliferator-activated Receptor γ
PSF	PB medium supplemented with *S. frutescens*
PTP1B	Protein Tyrosine Phosphatase 1B

qRT-PCR	Quantitative Reverse Transcriptase Polymerase Chain Reaction
ROS	Reactive Oxygen Species
RT	Reverse Transcriptase
SCD-1	Stearoyl-CoA Destaturase-1
SH2	*Src* Homology 2
SHP	Small Heterodimer Partner
SIRT1	Sirtuin 1
SOCS	Suppressor of Cytokine Signalling
SOS	Son of Sevenless
SREBP-1c	Sterol Regulatory Element Binding Protein 1c
STK11	Serine/Threonine Kinase 11
T2DM	Type 2 Diabetes Mellitus
T_a	Annealing Temperature
TAG	Triacylglycerol
TATA-BP	TATA Binding Protein
TCA	Tricarboxylic Acid
TG	Triglyceride
TLC	Thin-layer Chromatography
TNF-α	Tumour Necrosis Factor alpha
TORC2	Transducer of Regulated CREB 2
VLDL	Very Low Density Lipoprotein
X5P	Xylulose-5-Phosphate

Abstract

Type 2 diabetes mellitus (T2DM) is rapidly emerging as one of the greatest global health issues of the 21st century. Insulin-resistance is a condition associated with T2DM and in the cell it is defined as the inadequate strength of insulin signalling from the insulin receptor downstream to the final substrates of insulin action involved in multiple metabolic, gene expression, and mitogenic aspects of cellular function. To investigate the potential mechanisms involved in the development of insulin-resistance, two *in vitro* liver cell models were established using palmitate or a combination of insulin and fructose as inducers. The development of insulin-resistance was determined via the capacity of the hepatocytes to maintain normal glucose metabolism functionality by measuring hepatic gluconeogenesis and glycogenolysis. It was established that the treatments induced the development of insulin-resistance after 24 hours chronic exposure. Previous studies have investigated the potential of *Sutherlandia frutescens* extracts as therapeutic agents for insulin-resistance. The aim of this study was thus to investigate the ability of a hot aqueous extract of *S. frutescens* to reverse the insulin-resistant state, via measuring gluconeogenesis and glycogenolysis, the associated changes in cellular physiology (lipid accumulation, oxidative stress, and acetyl-CoA levels), and changes in mRNA expression. The results showed that *S. frutescens* had a significant effect on reversing the insulin-resistant state in both models of insulin-resistance. Furthermore, *S. frutescens* was capable of reducing lipid accumulation in the form of triacylglycerol in the high insulin/fructose model, while this was unaffected in the palmitate model. However, *S. frutescens* did reduce the accumulation of diacylglycerol in the palmitate model. Oxidative stress, seen to be associated with the insulin-resistant state, was successfully treated using the extract, as indicated by a reduction in reactive oxygen species. However no change was seen in the nitric oxide levels, in either model. Interestingly, although *S. frutescens* had no effect on the level of acetyl-CoA in the insulin/fructose model, it was found to increase this in the palmitate model. It is suggested that this may be due to increased β-oxidation and metabolic activity induced by the extract. The analysis of mRNA expression gave some insight into possible mechanisms by which insulin-resistance develops, although the results were inconclusive due to high variability in samples and the possibility of the RNA being compromised. Future studies will address this issue. The results of this study reflect different proposed clinical causes of insulin-resistance through the responses seen in the two cell models. These indicate that liver steatosis and insulin-resistance are induced by high palmitate as well as high insulin and fructose levels, and reversed by *S. frutescens*. Therefore the potential of *S. frutescens* to be used as a therapeutic agent in the treatment of insulin-resistance is indicated by this study.

Chapter 1
Introduction and Literature Review

Introduction

Diabetes mellitus (DM) is the most common endocrine disorder in man, currently (Diabetes Atlas statistics for the year 2013) affecting over 382 million people worldwide and, potentially, over 592 million by the year 2035 (Sicree *et al*., 2011). Type 2 DM (T2DM) is rapidly emerging as one of the greatest global health issues of the 21st century. Furthermore, it is also expected to trigger a rise in the complications associated with diabetes, such as ischemic heart disease, stroke, neuropathy, retinopathy, and nephropathy (Cornier *et al*., 2008). As well as pancreatic β-cell failure, the major pathophysiological event contributing to the development of T2DM is the resistance of target tissues to insulin (called insulin-resistance), which is usually associated with abnormal insulin secretion. Clinically, the term "insulin-resistance" implies that elevated concentrations of insulin are required to maintain normoglycaemia. At the cellular level, it defines the inadequate strength of insulin signalling from the insulin receptor downstream to the final substrates of insulin action involved in multiple metabolic, gene expression, and mitogenic aspects of cellular function (Saini, 2010).

The pathogenesis of T2DM involves abnormalities in both insulin action and secretion. The precise pathophysiological mechanism which leads to insulin-resistance is still largely unknown, but recent studies have contributed to a greater understanding of the underlying molecular mechanisms. These mechanisms involve alterations in the insulin signalling process through mutations in the genes encoding signalling molecules, hyperinsulinaemia and hyperglycaemia. In addition, free fatty acids (FFAs) have been shown to activate a serine kinase cascade, which leads to insulin signalling defects downstream of the insulin receptor (IR). The latter two mechanisms (hyperinsulinaemia/hyperglycaemia and FFA action) affect insulin signalling by inducing insulin-resistance in target cells (Saini, 2010). In recent studies, cell models have been used to study the molecular mechanisms underlying T2DM (Ruddock *et al*., 2008; Williams, 2010). These studies have shown that either combined high concentrations of insulin and fructose (Williams, 2010) or palmitate (Ruddock *et al*., 2008) result in the development of insulin-resistance in hepatic cell cultures. Furthermore, Williams (2010) investigated the potential of South African medicinal plant extracts as

therapeutic agents and showed that aqueous extracts of *Sutherlandia frutescens* were capable of reversing the insulin-resistant state through increasing the expression of genes associated with vesicle transport and insulin signalling.

The current study aims at investigating the changes in gene expression at the mRNA level which are involved in insulin signalling and the associated protein synthesis, as well as changes in cellular physiology. The two insulin-resistant cell models, cells in which insulin-resistance is induced using palmitate or insulin/fructose and then treated with a hot aqueous extract of *S. frutescens*, will be compared. This comparison will aid in providing more insight into the mechanism of insulin-resistance, its reversal, and potential treatment.

Literature Review

1 Insulin and Its Function in Blood Glucose Homeostasis

1.1 Insulin and the Insulin Receptor

Insulin is produced by the pancreatic β-cells and is a major anabolic hormone that is involved in growth, development and homeostasis of glucose, fat, and protein metabolism. Insulin is a pleiotropic molecule which affects amino acid uptake, protein synthesis, and proteolysis (Cornier *et al*., 2008). Glucose levels are regulated by insulin at many sites; reducing hepatic glucose output and increasing the rate of glucose uptake, primarily into striated muscle and adipose tissue. Lipid metabolism is affected by insulin that increases lipogenesis in hepatocytes and adipocytes, and attenuating fatty acid release from triglycerides (TGs) in fat and muscle. Insulin mediates its effects on metabolism and gene expression through interaction with its receptor present on target cell surfaces (Pessin and Saltiel, 2000).

The IR is a member of the receptor tyrosine kinase family that also includes the type 1 insulin-like growth factor I (IGF-I) receptor (IGF-IR) and the orphan receptor: insulin receptor-related receptor (IRR). The complete insulin receptor is a heterotetrameric glycoprotein composed of two α-subunits and two β-subunits linked by disulphide bonds. The α-subunits are extracellular and contain the insulin binding site. The β-subunit is composed of an extracellular domain, a transmembrane domain, and an intracellular domain, which possesses the intrinsic tyrosine kinase activity (Figure 1). The insulin receptor mRNA

is subject to alternative splicing events of exon 11 due to hormonal and/or metabolic factors in a tissue-specific manner, giving rise to two functionally unique isoforms (Mosthaf *et al*., 1990). Isoform B, also named $Ex11^{+}$, contains a 12-amino-acid peptide at the carboxyl-terminus of the α-subunit. Isoform A, also named $Ex11^{-}$, lacks this amino acid insertion (Sesti, 2006).

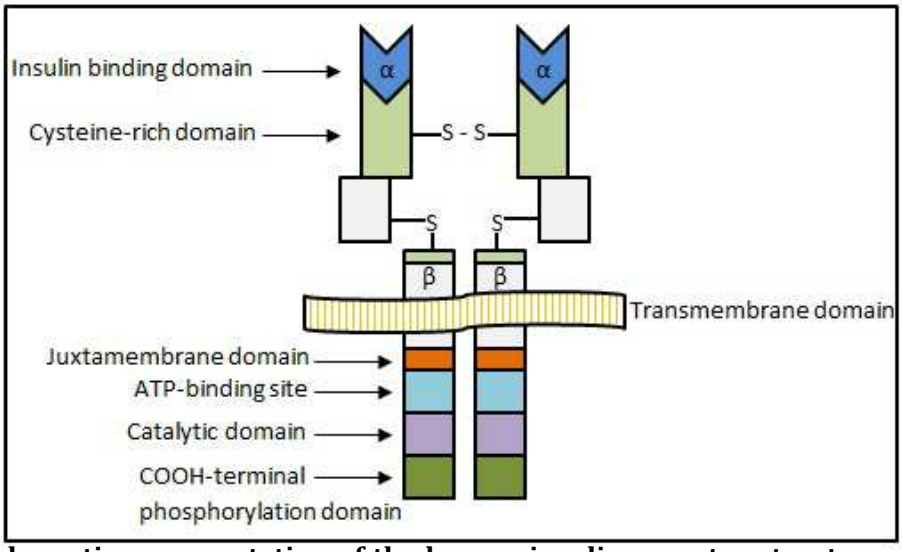

Figure 1: Schematic representation of the human insulin receptor structure. The insulin receptor is a heterotetrameric glycoprotein composed of two extracellular α-subunits and two β-subunits comprising of an extracellular and transmembrane domain (adapted from Sesti, 2006).

The $Ex11^{-}$ isoform shows a two-fold higher affinity for insulin as compared to the $Ex11^{+}$ isoform. This difference in ligand binding affinity is concomitant with a higher sensitivity for both anabolic and metabolic actions of insulin. Furthermore, the $Ex11^{-}$ isoform appears to have higher rates of internalization, recycling, and is a better activator of phosphoinositide 3-kinase (PI3K) class Ia. Thus, increased expression of the $Ex11^{+}$ isoform in skeletal muscle has been positively correlated with both hyperglycaemia and hyperinsulinaemia (Norgren *et al*., 1994; Sesti, 2006).

1.2 Insulin Signalling

There are two general models of *in vitro* insulin signalling: insulin signalling in adipocytes and myocytes (Figure 2), and insulin signalling in hepatocytes. The adipocyte/myocyte model is the best studied and understood, and it is accepted that the general mechanism of insulin signalling that occurs in adipocytes/myocytes also occurs in hepatocytes. These two

signalling models differ slightly in that hepatocytes do not maintain the glucose transporter 4 (GLUT4), and thus do not contain any signalling pathways leading to the translocation of GLUT4 to the plasma membrane from its intracellular pool (Sesti, 2006). Hepatocytes do, however, maintain isoforms of the GLUT4 protein, namely GLUT2 and GLUT8. In hepatocytes, GLUT2 is predominantly expressed that allows facilitated diffusion of glucose across the plasma membrane. GLUT8 is a high-affinity glucose transporter which cycles between intracellular vesicles and the plasma membrane (Gorovits *et al*., 2003). It is, therefore, proposed that GLUT8 functions similarly to the GLUT4 of adipocytes and myocytes.

The insulin signalling cascade is divided into three major pathways namely, (i) the PI3K-Akt pathway which is mainly involved in the regulation of metabolic actions by insulin (glucose, lipid, and protein metabolism), (ii) the mitogen-activated protein kinase (MAPK) pathway, mediating the mitogenic, growth and cell differentiation effects, and (iii) signal transduction through the CAP/Cbl/Tc10 pathway, which controls the GLUT4 (and GLUT2/8) translocation event (Leclercq *et al*., 2007). The latter pathway involves the interactions between Cbl associated protein (CAP), the E3 ubiquitin-protein ligase Cbl, which was first identified as a product of the *Cbl* proto-oncogene, and Tc10, belonging to the G protein members of the Rho family of guanosine triphosphatases (GTPases). This is a well-established insulin signalling pathway that influences the actin cytoskeleton and assembly of the exocytosis complex required for GLUT4 translocation to the plasma membrane.

The physiological control of the glucose fluxes across the plasma membrane is solely dependent on the intracellular glucose phosphorylation/dephosphorylation ratio. Insulin does, however, indirectly stimulate glucose influx in hepatocytes through the activation of glucokinase (or hexokinase) and thus the use of glucose for energy consumption, glycogen, and lipid synthesis (Leclercq *et al*., 2007).

1.3 Adipocytes and Myocytes

Due to the extensive studies performed on insulin signalling in adipocytes and myocytes, the insulin signalling mechanisms described here use the adipocyte/myocyte model; however the focus of this project is on insulin signalling in hepatocytes. GLUT4 translocation is a complex process involving release of GLUT4 from its intracellular reservoir compartment,

translocation, and docking and fusion to the plasma membrane. This signalling cascade is initiated by the binding of insulin to the extracellular α-subunit of the IR. This binding event results in the autophosphorylation of tyrosine residues located in the cytoplasmic region of the transmembrane β-subunit of the IR (Sesti, 2006). The activated receptor recruits and phosphorylates a variety of substrates (Figure 2).

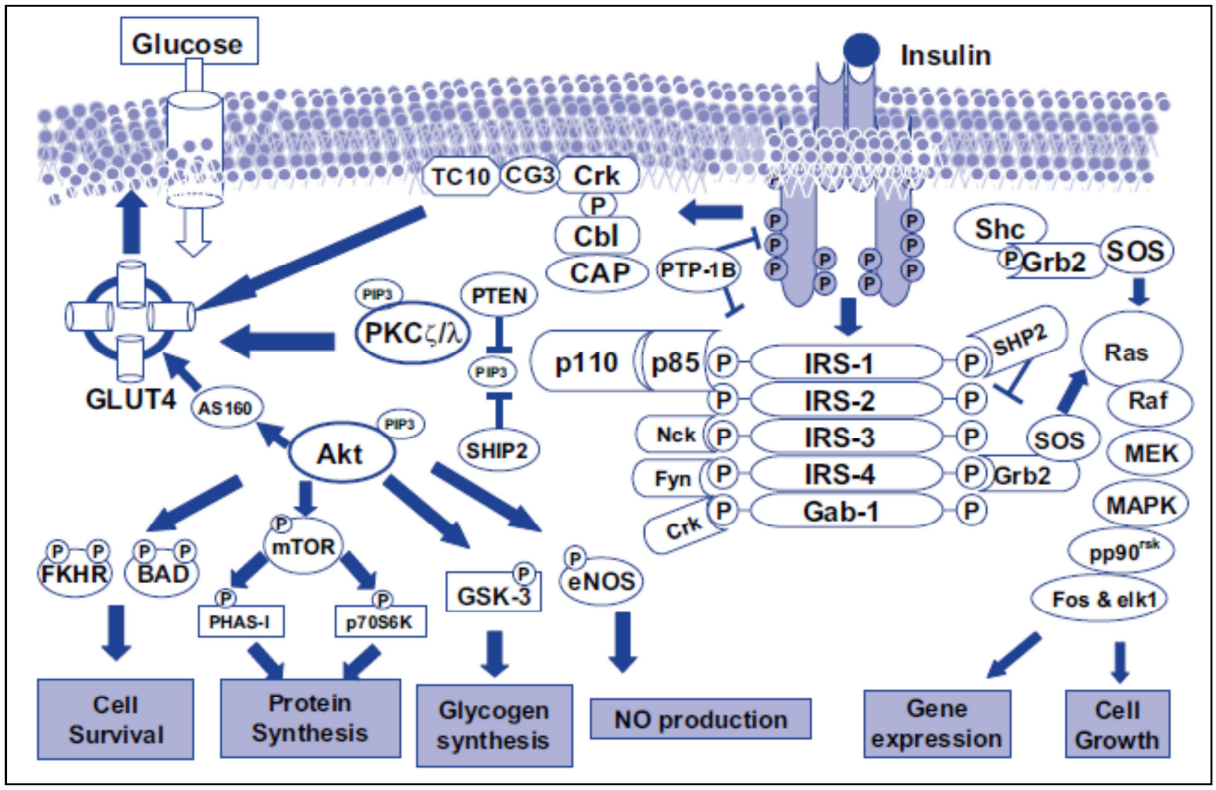

Figure 2: Schematic representation of the insulin signalling cascade (Sesti, 2006).

These substrate molecules consists, amongst others, of the insulin receptor substrate (IRS) molecules (IRS1 to IRS6), which appear to be the adapter molecules playing a major role in linking the PI3K, protein kinase B (PKB also known as Akt), and MAPK downstream kinases (Fröjdö *et al*., 2009; Sesti, 2006). Other molecules include the Shc adaptor protein, Gab-1 and Cbl. Once these molecules are phosphorylated, IRS proteins bind to several *Src* homology 2 (SH2) domain proteins, including p85 (the regulatory subunit of PI3K), recruiting PI3K (Fröjdö *et al*., 2009), tyrosine kinases Fyn and Csk, the tyrosine protein phosphatase small heterodimer partner 2 (SHP-2), several smaller adapter molecules such as the growth factor receptor-binding protein 2 (Grb-2), Crk, and Nck (Sesti, 2006) to the plasma membrane. Once recruited and activated, PI3K proceeds to produce the second messenger phosphatidylinositol 3,4,5,-trisphosphate (PIP_3), which activates a serine/threonine

phosphorylation cascade of PH domain-containing proteins (as summarised in figure 2) (Fröjdö *et al*., 2009).

This serine/threonine phosphorylation cascade consists of the initial phosphorylation of the phosphoinositide-dependent protein kinase (PDK) by PIP_3, which in turn phosphorylates and activates two classes of serine/threonine kinases, Akt/PKB and the atypical protein kinase C (aPKC) isoforms ζ and λ (PKCζ/λ) on threonine residues located in the activation loop of the catalytic domain (Sesti, 2006; Fröjdö *et al*., 2009). Both Akt/PKB and PKCζ/λ are thought to be important in the mediation of glucose transport effects of insulin in muscle and adipose tissue. However, Akt, rather than aPKCs, is important in stimulating glycogen synthesis and promoting glucose storage in muscle, adipose, and liver tissue, as well as diminishing gluconeogenesis and glucose secretion by the liver (Sesti, 2006). Protein kinase B targets glycogen synthase kinase 3 (GSK-3) and Akt substrate of 160 kDa (AS160) [containing a GTPase-activating protein (GAP) domain], of which the phosphorylation of AS160 has been found to be essential for the insulin-induced translocation of GLUT4 to the plasma membrane in 3T3-L1 adipocytes (Fröjdö *et al*., 2009; Sano *et al*., 2003). Glycogen synthase kinase 3 is inactivated by PKB-mediated phosphorylation at the serine-9 residue in parallel to protein-phosphatase-1 (PP1) activation, counteracting the inhibitory phosphorylation of glycogen synthase (GS), resulting in the synthesis of glycogen (Fröjdö *et al*., 2009). Furthermore, PKB regulates the insulin-stimulated translocation of GLUT4 to the plasma membrane through the inhibitory phosphorylation of AS160. The inhibition of AS160 favours the GTP-loaded state of Rab, counteracting the inhibitory effect towards GLUT4 translocation from intracellular compartments to the plasma membrane. Complementing the function of PKB in regulating GLUT4 translocation is the aPKCs, acting in parallel to, or even being substitutive for, PKB (Fröjdö *et al*., 2009).

Parallel to the PI3K-mediated pathway, IRS recruits Grb2, which associates with the Son of Sevenless (SOS) protein, and activates the extracellular regulated kinase 1/2 (ERK1/2) MAPK pathway. Additionally, the p38 and c-jun N-terminal kinase (JNK) stress-activated kinases, which are mainly dependent on activation through stress signals and inflammatory cytokines, have been shown to be activated (via phosphorylation) in response to insulin (Fröjdö *et al*., 2009).

1.4 Hepatocytes

Hepatic insulin signalling occurs in the same manner as described for the adipocytes and myocytes. The only difference is that the GLUT4 translocation event is omitted due to the absence of GLUT4 in hepatocytes, which is replaced by GLUT2, which is independent of insulin-stimulated regulation.

1.4.1 Control of Hepatic Glucose Production

Insulin mediates the activation of several signalling proteins upon binding to the IR. The cascade mediated by this follows through IRS activation by the IR, subsequently activating two main pathways: (1) the PI3K pathway is mainly involved in the control of metabolic actions by insulin (glucose, lipid and protein metabolism), protein synthesis [(via the Mammalian Target of Rapamycin (mTOR)] and control of cell survival, and (2) the MAPK pathway which mediates the mitogenic, growth and cell differentiation effects. Activation of PI3K induces the conversion of phosphatidylinositol bisphosphate (PIP_2) to PIP_3, followed by recruitment and activation of PDK and PKB/Akt by PIP_3. Thereafter, PKB/Akt proceeds to phosphorylate GSK-3, preventing its inhibition of GS, thereby facilitating the synthesis of glycogen. This inhibition of GSK-3 by PKB/Akt is achieved through activation of forkhead box protein o 1 (FoxO1) by PKB/Akt, which leads to the transcription of key enzymes involved in gluconeogenesis, namely phosphoenolpyruvate carboxykinase (PEPCK), and glucose-6-phosphatase (G6Pase). Hence, through the activation of PI3K and PKB/Akt, insulin promotes the storage of glucose as glycogen and inhibits glucose synthesis and output via inactivation of GSK-3 and activation of FoxO1 (Leclercq *et al.*, 2007).

1.4.2 Transcriptional Control of Hepatic Lipogenesis

The effects of insulin on lipogenesis are controlled by the transcription factor sterol regulatory element-binding protein 1c (SREBP-1c) through its regulatory function on mono-unsaturated fatty acid synthesis (Figure 3). Its precursor is maintained within the endoplasmic reticulum (ER), being freed in times of sterol depletion. The SREBP-1c in itself is subject to complex regulation through the activities of sterol depletion and tumour necrosis factor (TNF) (in an insulin-independent manner). It is suggested that insulin is responsible for the regulation of SREBP-1c's transcription, maturation, and activity (Foufelle & Ferre,

2002), as well as the transcription of Insig2a (participating in the retention of SREBP-1c in the ER) (Leclercq *et al*., 2007). Hence, these regulatory pathways of SREBP-1c remain insulin sensitive. Furthermore, inhibitory phosphorylation of SREBP-1c by GSK-3 or ERK modulates its activity. In insulin-resistant states, expression of TNF-α is increased, which stimulates the maturation and activity of SREBP-1c. Thus, TNF participates in increased intrahepatic lipogenesis (Leclercq *et al*., 2007).

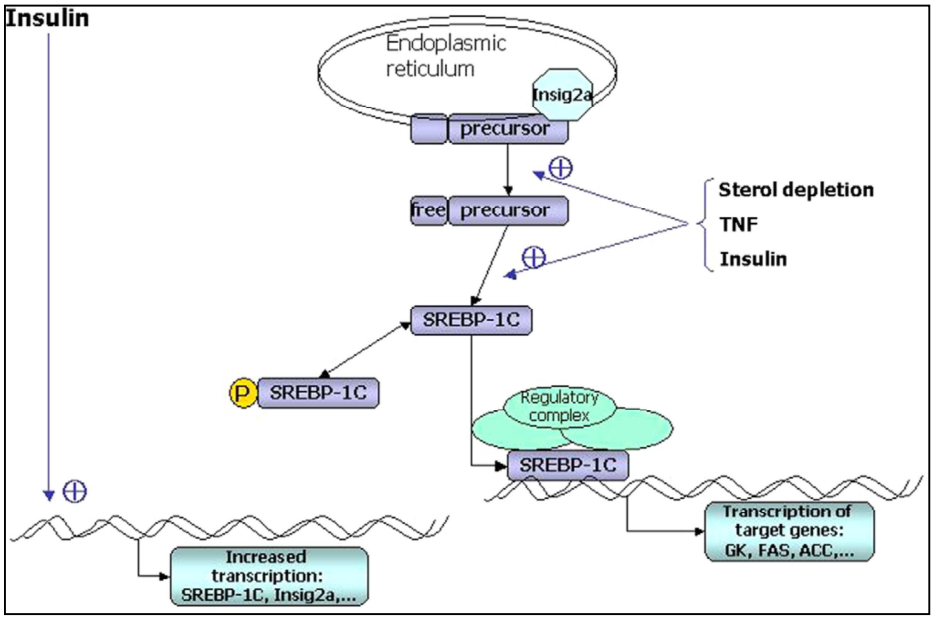

Figure 3: Regulation of SREBP-1c (Leclercq *et al.*, 2007).

1.4.3 Cell Growth, Proliferation, and Survival

The MAPK cascade is activated downstream of IR phosphorylation via IRS, Gab1, and Shc (Figure 2). The MAPK pathway is associated with the mitogenic and proliferative effects of insulin via the control of the cell cycle; however it does not appear to have any role in mediating hepatic glucose production or the anabolic effects of insulin. The PKB/Akt pathway also functions in mediating the effect of insulin on cell growth and survival. When phosphorylated, PKB promotes anti-apoptotic effects and protein synthesis. Eukaryotic initiation factor 2B (eIF2B), a guanine nucleotide exchange factor which is inhibited upon phosphorylation by GSK-3, controls the initiation phase of protein translation. This protein biosynthesis stimulated by PKB/Akt is dependent on phosphorylation of mTOR (Leclercq *et al*., 2007).

1.5 Insulin Signalling Alterations in Type 2 Diabetes Mellitus

Insulin signalling is altered in the insulin-resistant and diabetic states. Four major defects have been identified as the causes of impaired insulin signalling, namely (1) mutations or post-translational modifications of the IR or any of its downstream effector molecules, (2) increased degradation of the IR, (3) defective binding of insulin to the IR, and (4) defect(s) in the post-binding insulin signalling cascade (Fröjdö *et al*., 2009).

The IR is subject to inhibition by serine/threonine phosphorylation – inhibiting the intrinsic tyrosine kinase activity of the receptor. Thus, the downstream signalling cascade is decreased in proportion to this inhibition (Sesti, 2006). It has been found that PKCs and MAPKs are capable of phosphorylating the IR at these serine/threonine residues (Saini, 2010). The same inhibitory effect is seen when IRS proteins are phosphorylated at serine residues (discussed in more detail in section 3), resulting in decreased downstream insulin signalling. Serine phosphorylation is also induced by the pro-inflammatory cytokine, TNF-α (Saini, 2010). During the pro-inflammatory state, the suppressor of cytokine signalling (SOCS) is activated, which in turn alters the insulin signalling cascade. The SOCS is able to compete with IRS1/2 for IR binding, thus attenuating tyrosine phosphorylation and downstream signalling of IRS1/2, and is capable of inducing IRS degradation (Qatanani and Lazar, 2007). Free fatty acids and FFA derivatives [such as diacylglycerol (DAG) and acyl-Coenzyme A (CoA)] are also capable of increasing serine phosphorylation of IRS through activation of several serine/threonine protein kinases, such as PKCs, JNK, and the inhibitor of nuclear factor-κB kinase-β (IkkB); decreasing the insulin signalling cascade (Lee *et al*., 2010).

2 Mechanism of Insulin-Resistance

The state in which the body has a decreased capacity of circulating insulin for the regulation of nutrient metabolism is referred to as insulin-resistance. Several mechanisms may act individually or in synergy to inhibit insulin signalling. These mechanisms include: elevated insulin secretion (hyperinsulinaemia) due to elevated blood glucose levels (hyperglycaemia), elevated levels of serum FFAs (Zick, 2001; Van Epps-Fung *et al*., 1997), oxidative stress, ER stress, glycated proteins and their products, and adipokines (such as leptin). This can occur via three major processes: first, signal propagation can be altered through decreased expression or increased degradation of any one of the components of the insulin signalling

cascade. Increases in protein expression and/or activation may also act as negative feedback signals. Post-translational modifications such as phosphorylation are the second mechanism by which insulin signalling can be altered. The third mechanism is through interactions with inhibitory proteins (Leclercq *et al*., 2007).

2.1 Insulin/Fructose-induced Insulin-Resistance

Characteristics of the insulin-resistant state are increased glycaemia and the subsequent compensatory hyperinsulinaemia, both of which are factors that exacerbate the insulin-resistant state (Meshkani and Adeli, 2009). Hyperinsulinaemia induces down-regulation of IR expression at the protein level via ligand internalization and degradation, followed by resistance downstream of the receptor by increased degradation of IRS and other insulin signalling molecules. Furthermore, hyperinsulinaemia can damage the pancreatic β-cells, participating in reduced insulin secretion and T2DM. Also, hyperglycaemia may reduce the activation step from PI3K to PKB/Akt, but does not affect the proximal part of the IR-mediated pathway (Saini, 2010).

The motivation for using high levels of both insulin and fructose for inducing insulin-resistance in experimental procedures is, firstly, that high circulating insulin levels are associated with insulin-resistance and thus high levels of insulin are used to mimic the hyperinsulinaemic state of T2DM. Secondly, following ingestion of a meal containing complex carbohydrates or glucose, the liver becomes a glucose-consuming organ, accounting for 20–30% of the total dietary carbohydrate disposal. Most of this glucose is used to replenish glycogen stores, with the remainder primarily directed to glycolysis. Upon ingestion of fructose or fructose-containing carbohydrates (sucrose), the liver becomes more active in absorption of carbohydrates. This is due to the highest fructokinase concentrations being expressed in the liver. Thus, fructose extraction from blood by the liver is elevated. Furthermore, fructose-1-phosphate (the product of fructokinase) stimulates glucose uptake in the liver. Therefore, the replacement of glucose or complex carbohydrates by sucrose or fructose results in an increase in the contribution of the liver to carbohydrate disposal (Wei *et al*., 2007).

Wei *et al*. (2007) performed studies on the effect of high fructose diets on the liver by feeding rats a high sucrose diet (HSD). It was found that the liver concentrations of xylulose 5-

phosphate (X5P), lactate and DAG were significantly increased, while levels of inorganic phosphate were significantly decreased in the HSD compared to the standard diet. The liver was found to express elevated levels of phosphorylated cyclic adenosine 5'-monophosphate (cAMP) responsive element binding protein (CREB) and increased JNK activity and subsequent serine phosphorylation of IRS1. Here, CREB regulates transcription of genes controlled by the cAMP-mediated pathways of signal transduction. Such genes include the *G6Pase* and *PEPCK* genes. Furthermore, hepatic gluconeogenesis was increased in HSD-fed rats while insulin-stimulated suppression of hepatic glucose production (HGP) was decreased. The same effect was seen in rats fed the high-fructose diets. Additionally, tyrosine phosphorylation of IRS1/2, association of IRS1/2 with PI3K, PI3K activity, and phosphorylation of PKB/Akt were significantly reduced in HSD livers. Therefore, fructose is able to impair post-receptor insulin signalling in the liver (Wei *et al*., 2007). This has also been observed in models using high fructose levels under hyperinsulinaemic conditions (Wei *et al*., 2004).

The mechanism by which fructose mediates the development of insulin-resistance is attributed to the activities of protein tyrosine phosphatase 1B (PTP1B) and JNK (Wei *et al*., 2007). It is known that PTP1B negatively regulates IRS tyrosine phosphorylation (Gum *et al*., 2003). Furthermore, JNK interferes with the insulin signalling cascade through serine phosphorylation of IRS1. It has also been suggested that JNK is a critical component of the biochemical pathway responsible for development of insulin-resistance in the liver (Hirosumi *et al*., 2002). Fructose-mediated increases in PTP1B and activator protein-1 activity in the liver had been observed in rat models fed HSD, resulting in hepatic insulin-resistance. This demonstrates that fructose can activate hepatic JNK activity and that this activity contributes to the fructose-induced hepatic insulin-resistance through serine-phosphorylation of IRS1 (Wei *et al*., 2007). It has also been hypothesised that high rates of fructose delivery leads to accumulation of intermediates which serve as acute, short-term signals of sugar excess. This sugar excess inflicts a metabolic burden upon the hepatocytes; selectively increasing MAPK kinase 7 (MKK7), activation of JNK, and association of JNK with IRS and JNK-interacting protein-1 (JIP1). The association of JNK with IRS1/2 results in decreased tyrosine phosphorylation of IRS1/2 and consequently decreases insulin signalling (Figure 4) (Wei *et al*., 2007).

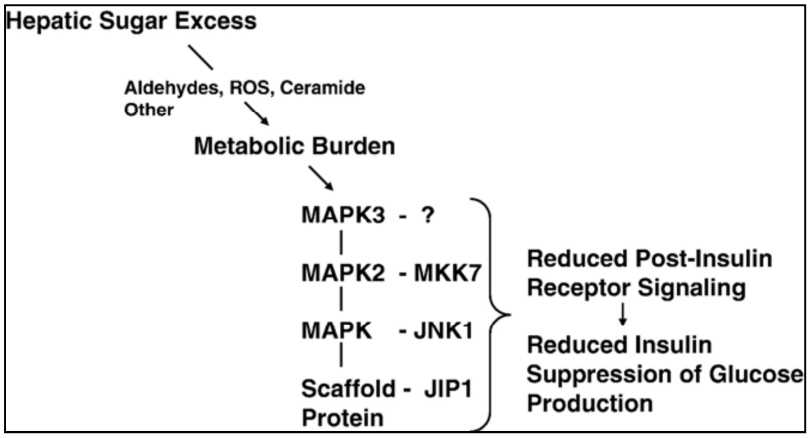

Figure 4: Working model for fructose-induced insulin-resistance in the liver (Wei *et al.*, 2007).

Williams (2010) found that exposing Chang liver cells to high concentrations of a combination of insulin and fructose was able to induce the insulin-resistant state *in vitro*. This state was determined through investigating changes in expression of a set of 84 diabetes-related genes. The study found that exposure to high doses of insulin and fructose resulted in decreased glucose uptake and increased lipid accumulation – characteristic of the insulin-resistant state. Furthermore, IRS1/2 and MAPK signalling molecules were up-regulated in the insulin-resistant state, while signalling from IRS1/2 to PI3K was decreased, resulting in an increase in hepatic gluconeogenesis. The increase in IRS1/2 and MAPK signalling molecules is likely in compensation for this reduced activity of insulin-induced stimulation of the insulin signalling cascade. Thus, the increase in hepatic gluconeogenesis leads to hyperglycaemia (Williams, 2010).

2.2 Lipid-induced Insulin-Resistance

It is well known that in addition to glucose uptake, adipose tissue lipolysis and suppression of hepatic glucose production are regulated by insulin. Lipolysis is highly sensitive to the action of insulin in adipose tissue, in which stored lipids are released into the circulation as FFAs and glycerol. During the insulin-resistant state, the anti-lipogenic activity of insulin is inhibited, resulting in increased release of FFAs by adipose tissue. This subsequently disrupts blood glucose homeostasis via the effects elevated circulating FFAs have on other tissues such as the liver (Stumvoll, 2005). Serum FFA, frequently elevated in obesity, has been implicated as an important causative link between obesity, insulin-resistance, hyperglycaemia, and T2DM (Chen *et al.*, 2006). This leads to the development of non-

alcoholic fatty liver due to an increase in hepatic FFA uptake, as the rate of hepatic FFA uptake is an unregulated process, solely dependent on the plasma concentration of FFAs (Lee *et al*., 2010).

Endogenous glucose production (EGP) is the only post-absorptive source of glucose, of which the liver is responsible for 80% of EGP and the remaining 20% by the kidneys. Excessive EGP is responsible for the hyperglycaemic state characteristic of T2DM. Furthermore, excessive EGP during T2DM usually occurs despite the presence of hyperinsulinaemia, suggesting that hepatic insulin-resistance is a key component of the pathogenesis of fasting hyperglycaemia (Stumvoll, 2005). In previous studies, plasma FFAs stimulated gluconeogenesis in healthy subjects. In patients with T2DM, an increase in FFA concentration also stimulated gluconeogenesis, which was consistent with findings in healthy subjects (Chen *et al*., 1999). Since EGP is derived from gluconeogenesis and glycogenolysis, it is suggested that FFAs interfere with the inhibitory action of insulin on these. The mechanism responsible for lipid-induced insulin-resistance in liver may be due to known mechanisms involved in insulin-induced T2DM. In T2DM, this may be explained by several observations: (1) increased plasma FFA levels increase FFA uptake by hepatocytes, leading to accelerated lipid oxidation and accumulation of acetyl-CoA. This stimulates pyruvate carboxylase and PEPCK, the rate-limiting enzymes for gluconeogenesis, as well as glucose 6-phosphatase (G6Pase), the rate-limiting enzyme for glucose release from hepatocytes, (2) increased FFA oxidation provides a source of energy for gluconeogenesis, and (3) an increase in plasma FFA leads to hepatic insulin-resistance by inhibiting the insulin signal transduction system similarly to skeletal muscle (Stumvoll, 2005).

Oxidation of FFAs (also referred to as β-oxidation) is only partly responsible for the FFA-induced decrease in hepatic insulin signalling, suggesting that hepatic PKC activation could be implicated in the FFA-induced decrease in insulin binding. It is known that FFAs are capable of activating PKC directly and/or through *de novo* synthesis of DAG (Diaz-Guerra *et al*., 1991). Also, insulin binding is reduced by the PKC stimulators, phorbol esters or DAG, and PKC activation may stimulate internalization of the IR (Chen *et al*., 2006).

Previous studies have shown that increased release of FFAs from adipocytes leads to insulin-resistance and TG accumulation in the liver, progressing to hepatic steatosis (Montell *et al*., 2001). More recent studies have shown that saturated long chain FAs are associated with the

defects of insulin signalling, of which palmitate was found to decrease IR mRNA and protein in hepatocyte cell lines, attenuating insulin signalling (Ruddock *et al*., 2008; Dey *et al*., 2007). HepG2 cells treated with either saturated fatty acid (palmitate) or unsaturated fatty acid (oleate) showed that palmitate significantly activated JNK and inactivated PKB. This confirmed the involvement of ER stress in palmitate-mediated insulin-resistance. Oleate, but not palmitate, significantly induced intracellular TG deposition and activated SREBP-1. The DAG levels and PKCε activity were significantly increased by palmitate, suggesting the possible role of DAG in palmitate-mediated lipotoxicity (Lee *et al*., 2010). Dasgupta *et al*. (2011) have shown that lipid-induced PKCε phosphorylation occurs via palmitoylation. Phosphorylated PKCε is transported by F-actin to the nuclear region where it impairs the high-mobility group protein A1 (HMGA1). Subsequently, this results in reduced IR expression, significantly decreasing insulin sensitivity in target cells.

3 Genes Associated with Insulin-Resistance

Williams (2010) has shown, using an RT^2 profiler, changes in the mRNA expression of signal transduction genes. This group includes several signal transduction molecules which are key intermediates in the insulin signalling cascade, namely IRS1/2, Akt, MAPK, JNK, and PKCε. The signalling cascade proteins involved in normal insulin signalling can be investigated in order to elucidate the mechanism by which insulin-resistance develops.

In normal insulin signalling, insulin binds to the α subunit of the IR and activates the tyrosine kinase in the β subunit (Figure 5). Once the tyrosine kinase of IR is activated, it promotes autophosphorylation of the β subunit, where phosphorylation of three tyrosine residues (Tyr-1158, Tyr-1162, and Tyr-1163) is required for amplification of the kinase activity. Most of the metabolic and anti-apoptotic effects of insulin are mediated by the signalling pathway involving the phosphorylation of the IRS proteins, and the activation of the PI3K, PKB/Akt, mTOR, and p70 S6 kinase. The IR tyrosine kinase phosphorylates the IRS proteins, and phosphotyrosine residues on IRS proteins become targets for the p85 regulatory subunit of PI3K. The activated PI3K generates PIP_3 via phosphorylation of PIP_2, which binds to and activates PDK1. Known substrates of the PDKs are PKB and also aPKCs (Saini, 2010).

Studies have shown that mutations in the IRS protein are associated with insulin-resistance as these disrupt the IRS-PI3K signalling (Figure 5). Furthermore, IRS is inactivated by serine

phosphorylation, reducing its ability to recruit and activate PI3K. This phosphorylation of IRS proteins also increases degradation of IRS and decreases tyrosine phosphorylation, decreasing the downstream effector functions of IRS. Physiological homeostasis depends on this inherent inactivation of IRS proteins in order to prevent insulin signalling when needed (Saini, 2010). Studies have shown a link between IRS dysfunction in skeletal muscle and adipocyte biology and lipotoxicity, meaning that circulating FFAs and the adipokine TNF-α may increase serine phosphorylation of IRS proteins, thereby causing impaired insulin signal transduction (White, 2002).

The fasting hyperglyceamia in patients with T2DM is the clinical link with increased glucose production by the liver due to insulin-resistance. This is the result of the lack of inhibition of the two key gluconeogenic enzymes, PEPCK and the G6Pase catalytic subunit. There is increasing evidence that FoxO-proteins are critically involved in the insulin-dependent regulation of gluconeogenic gene expression and insulin-resistance *in vivo* (Saini, 2010). Studies in hepatoma cells suggest that transcription of reporter genes containing insulin response elements from the PEPCK and G6Pase promoters are regulated by FoxO-1 and 3 (Hall *et al*., 2000; Guo *et al*., 2012). Furthermore, FoxO-1 is phosphorylated in an insulin-responsive manner by Akt. Reduced activity of Akt2 results in decreased phosphorylation of FoxO protein, allowing it to enter the nucleus and activate the transcription of these rate-limiting enzymes of gluconeogenesis (Figure 5) (Saini, 2010; Zhang *et al*., 2006).

The balance between the PI3K subunits provides another possible mechanism by which insulin-resistance occurs. PI3K exists as a heterodimer (class 1a of PI3K), consisting of a regulatory subunit, p85, tightly associated to the catalytic subunit, p110. Normally, the regulatory subunit exists in stoichiometric excess to the catalytic one, resulting in a pool of free p85 monomers not associated with the p110 catalytic subunit. However, there exists a balance between the free p85 monomer and the p85-p110 heterodimer, with the latter being responsible for the PI3K activity. The p85 monomers and p85-p110 heterodimers constantly compete for the tyrosine phosphorylated IRS protein-binding sites. Thus, an imbalance in monomer to heterodimer levels will lead to either an increase or decrease in PI3K activity. Studies have shown that elevated expression of the p85 monomer result in a decrease in PI3K signalling and subsequent interruption of insulin signalling, leading to insulin-resistance (Saini, 2010). The recent work of Williams (2010) shows decreased expression of PI3K

isotype genes when inducing insulin-resistance in Chang liver cells with high concentrations of insulin and fructose.

In recent years, research on the insulin-resistant state has shifted from a glucocentric to a lipocentric view. Here, the involvement of high fat diets is investigated in order to uncover the process by which insulin-resistance develops. The mechanism of FFA-induced insulin-resistance is still unclear; however it has been studied recently by Dasgupta *et al*. (2011) and Lee *et al*. (2010), suggesting the possible involvement of PKC isoforms in the insulin-resistant state. The molecular mechanism underlying defective insulin-stimulated glucose transport activity can be attributed to increases in intra-myocellular lipid metabolites such as fatty acyl CoAs and DAG, which in turn activate a serine/threonine kinase cascade, thus leading to defects in insulin signalling through the serine/threonine phosphorylation of IRS-1. Diacylglycerol has been shown to increase in muscle during both lipid infusions and fat feeding and it is also a known activator of novel PKC isoforms. PKC isoforms are classified as classical (cPKCα, βI, βII, γ), novel (nPKCδ, ε, θ, η) or atypical (aPKCζ, λ). cPKCs are activated by calcium (Ca^{2+}) and DAG, nPKCs are activated only by DAG, and aPKCs respond to neither Ca^{2+} nor DAG. Among these PKC isoforms, nPKCs are said to have a modulatory role in insulin signalling. Boden & Shulman (2002) have demonstrated a link between nPKCs and FFA-induced insulin-resistance. Lipid infusion in rats and humans impaired insulin-stimulated glucose disposal into the muscle and concomitantly activated PKCθ and PKCδ (Itani *et al*., 2002). The latter has been shown to be a possible candidate for phosphorylation of the IR on serine residues, resulting in defects in the insulin signalling pathway and inducing insulin-resistance (Figure 5) (Saini, 2010).

The IR is one of the major targets of FFA-induced impairment of insulin activity. *In vivo* studies have shown that glucose uptake rather than glucose metabolism is the rate-limiting step for FFA-induced insulin-resistance in humans (Shulman, 2000). Therefore, the accumulation of intracellular fatty acids, or their metabolites, results in the impairment of IRS/PI3K signalling and a decrease in GLUT4 recruitment to the cell membrane (Saini, 2010).

Phosphorylation of PKCs may be catalysed by PDK1 (Toker & Newton, 2000). PKCε phosphorylation, as well as PDK-1 independent phosphorylation due to FFA, is involved in development of insulin-resistance (Lee *et al*., 2010; Dey *et al*., 2007). This is possibly due to

a constitutive phosphorylation of PKCε by FFA in a PDK-1-independent manner as shown through incubation of HepG2 cells with myristic acid, resulting in myristoylation of PKCε and consequent phosphorylation of PKCε in the kinase domain. The same PDK-1-independent phosphorylation of PKCε was found through palmitoylation of PKCε. Therefore, FFA causes PDK-1-independent phosphorylation of PKCε, which in turn translocates to the nucleus; where upon entry into the nucleus coincides with inhibition of IR gene transcription through the possible phosphorylation of the transcription factor HMGA1 (Figure 5) (Dey *et al*., 2007; Reeves, 2001).

These studies all show the effect establishment of insulin-resistance has on the insulin signalling cascade through the effects hyperinsulinaemia/hyperglycaemia and FFAs have on the signalling molecules.

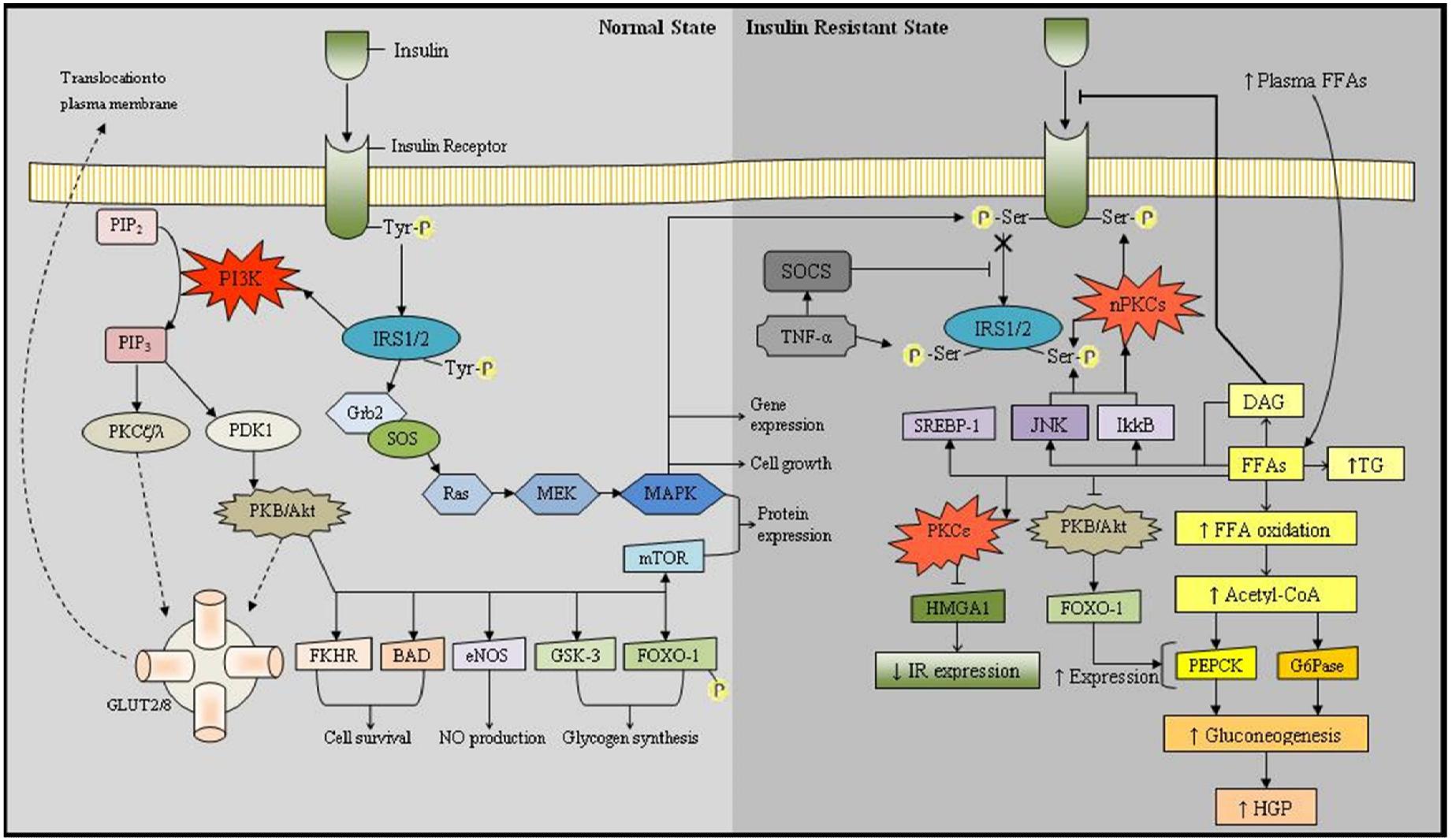

<u>Figure 5:</u> Insulin Signalling cascade in hepatocytes under normal or insulin-resistant conditions. (Sesti, 2006; Saini 2010; Lee *et al.*, 2010; Dasgupta *et al.*, 2011; Dey *et al.*, 2007; Guo *et al.*, 2012; White, 2002; Wei *et al.*, 2007)

4 Metformin

4.1 Background

The biguanide derivative, metformin (1,1-dimethylbiguanide), is the most widely prescribed drug to treat hyperglycaemia in individuals suffering from T2DM and is recommended, in addition to lifestyle changes, as the first line oral therapy in the guidelines of the American Diabetes Association, the European Association of the Study of Diabetes (Viollet *et al*., 2012), and the 2012 SEMDSA Guideline for the Management of Type 2 Diabetes (Amod *et al*., 2012). The drug was first clinically introduced in the 1950s although its mechanism of action is still not fully understood. However, it has been shown to have several therapeutic uses including anti-hyperglycaemic activity, treatment of diabetes-related disease (such as nephropathy), and more recently, anti-cancer activity (Viollet and Foretz, 2013).

4.2 Mechanism of Action

Early investigations into the mechanism of metformin activity indicated it to be most likely via the inhibition of gluconeogenesis. It has now been discovered to act through the activation of adenosine monophosphate (AMP)-activated protein kinase (AMPK) which plays a crucial role in the protection of cellular functions under energy-restricted conditions in the liver (Amod *et al*., 2012).

A rise in AMP levels paired with a fall in adenosine triphosphate (ATP) levels, during metabolic stress leads to the activation of AMPK. This increase in the ratio of AMP:ATP levels is indicative of a decreased cellular energy state as seen in glucose deprivation. The heterotrimeric protein requires the activation, through phosphorylation of Thr172, within its α-subunit. This phosphorylation is catalysed by upstream kinases, namely the tumour suppressor serine/threonine kinase 11 (STK11) or also known as liver kinase B1 (LKB1) and Calcium/calmodulin-dependent protein kinase kinase β (CaMKKβ). Once activated, AMPK switches cells from an anabolic to a catabolic state by switching ATP-consuming synthetic pathways off and restoring energy balance. This AMPK-governed regulation is achieved through phosphorylation of key metabolic enzymes, transcription factors, and co-activators modulating gene expression by AMPK. Ultimately, this results in attenuation of lipogenesis, protein synthesis, and cell growth, while promoting fatty acid oxidation and glucose uptake

(Viollet and Foretz, 2013). Metformin does not activate AMPK or affect its phosphorylation by LKB1, but rather activates AMPK as a secondary effect causative of its effect on the mitochondria (primary target of the drug). In the mitochondria, metformin inhibits the respiratory chain complex 1 in a time- and concentration-dependent fashion. This suggests that metformin activates AMPK through the inhibition of ATP production which, in turn, leads to an increase in ADP and AMP levels (Viollet and Foretz, 2013).

The anti-hyperglycaemic activity of metformin may be attributed to two possible mechanisms of which the first is the most well-known of explanations (Figure 6). Here metformin suppresses hepatic gluconeogenesis through the LKB1/AMPK signalling pathway. This pathway regulates the phosphorylation and nuclear exclusion of the transcriptional co-activator CREB-regulated transcription co-activator 2 (CRTC2) better known as the transducer of regulated CREB 2 (TORC2). TORC2 is a key regulator of HGP in response to fasting by directing transcriptional activation of the gluconeogenic pathway. This is achieved by the translocation of non-phosphorylated TORC2 to the nucleus, where it associates with phosphorylated CREB to drive the expression of peroxisome proliferator-activated receptor-γ coactivator-1α (PGC-1α) and subsequent gluconeogenic genes, PEPCK and G6Pase. Alternatively, metformin's inhibitory effect on TORC2-mediated gluconeogenesis involves the deacetylation of TORC2 by nicotinamide adenine dinucleotide (NAD^+ or NADH)-dependent sirtuin 1 (SIRT1). This results in the loss of protection by coat protein 1(COP1) mediated ubiquitinisation and subsequent degradation (Viollet and Foretz, 2013). It is likely that, in addition to this, other mechanisms involving the disassembly of the CREB-CBP (CREB binding protein)-TORC2 complex from gluconeogenic gene promoters, occur in parallel. The metformin-induced regulation of gluconeogenic gene expression is dependent on CBP phosphorylation through AMPK-induced aPKC activation and dissociation of the CREB co-activator complex. This suppression of gluconeogenic gene expression is further mediated through AMPK-induced up-regulation of the nuclear receptor, SHP. This nuclear receptor functions as a transcriptional repressor of CREB-dependent hepatic gluconeogenic gene expression through direct interaction with CREB and competing with TORC2 binding in the CREB-CBP complex (Viollet *et al*., 2012; Viollet and Foretz, 2013).

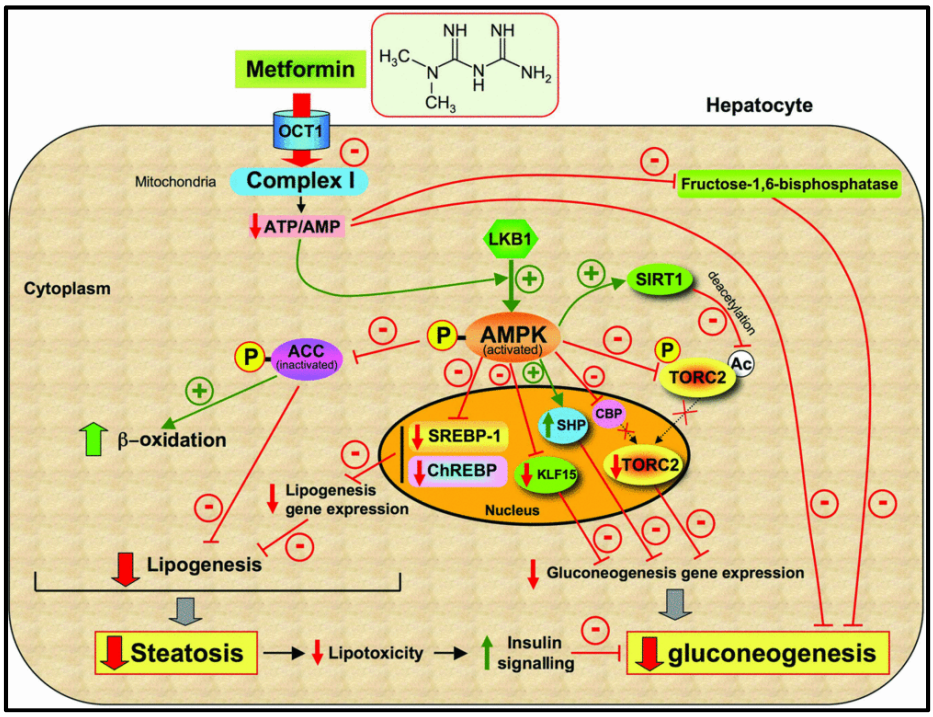

Figure 6: Potential molecular mechanisms of metformin action on hepatic steatosis and gluconeogenesis. After hepatic uptake through OCT1 (organic cation transporter 1), metformin exerts specific and AMPK-independent inhibition of respiratory-chain complex 1. The resultant mild decrease in energy status leads to acute and transient inhibition the energy-consuming gluconeogenic pathways. In addition, through AMPK-dependent and -independent regulatory points, metformin can lead to the inhibition of glucose production by disrupting gluconeogenic gene expression. In parallel, the LKB1-dependent activation of AMPK triggered by ATP depletion could reduce hepatic lipogenesis and exert an indirect effect on hepatic insulin sensitivity to control hepatic glucose output (Viollet *et al.*, 2012).

5 *Sutherlandia frutescens*

5.1 Botanical Information

The *Sutherlandia* genus belongs to the family of *Fabaceae* (Leguminosa) and is closely related to *Astragalus* L. and *Lessertia* DC. The genus can be divided into two species, namely *Sutherlandia tomentosa* and *Sutherlandia frutescens* (Figure 7). The latter occurs endemically in the western, central, and eastern parts of southern Africa, the majority of the Lesotho region, southern parts of Namibia, and the south-eastern corner of Botswana. *S. frutescens* is a perennial shrub, of 0.2-2.5m in height, with red flowers and large bladdery pods containing numerous seeds. Locally, *S. frutescens* is known as cancer bush, balloon pea, and turkey flower in English, and as kankerbos, gansies, wildekeur, and belbos in Afrikaans (Van Wyk and Albrecht, 2008).

5.2 Use as Medicinal Plant

Sutherlandia frutescens is widely used as a medicinal plant in southern Africa. Traditionally, medication is prepared by infusion of "two or three leafy twigs" in boiling water. The resultant tea, containing approximately 2.5-5g of dry material, is given as a daily dosage. It is used for a wide variety of conditions, including: cancer, diabetes, inflammation, back pain, stomach pain, eye disease, skin disease, influenza, human immunodeficiency virus/acquired immunodeficiency syndrome (HIV/AIDS), and many more. The traditional use of *S. frutescens* far exceeds that of *S. tomentosa* due to its limited localized distribution on coastal dunes of the Western Cape area of South Africa (Van Wyk and Albrecht, 2008).

Several biologically active compounds have been isolated and identified from *S. frutescens*, although many questions still remain about its mode of action. Recent studies conducted have focussed on its anti-cancer, -diabetic, -HIV, -inflammatory, and anti-oxidant properties. The known active compounds identified are: pinitol (patented for anti-diabetic properties) (Van Wyk and Albrecht, 2008), L-canavanine (L-arginine competitor, yielding anti-inflammatory and anti-cancer properties) (Akaogi *et al*., 2006), and triterpenoid glycosides (show anti-inflammatory and improved lipid metabolism) (Kawada *et al*., 2005).

Figure 7: ***Sutherlandia frutescens.*** *S. frutescens* is a perennial shrub, of 0.2-2.5m in height, with red flowers and large bladdery pods containing numerous seeds (Van Wyk *et al*., 2012).

Aims and Objectives

In recent studies, cell models have been used to study the molecular mechanisms underlying T2DM (Ruddock *et al*., 2008; Williams, 2010). These cell models have shown that high concentrations of insulin and fructose (*in vitro* hepatic cell culture) and high fat diets (*in vivo* rat model) are capable of inducing the insulin-resistant state. Furthermore, Williams (2010) investigated the potential of South African medicinal plant extracts as therapeutic agents and showed that extracts of *S. frutescens* were capable of reversing the insulin-resistant state. The current investigation aimed to measure changes in hepatocyte physiology and gene expression in insulin-resistant states and during their reversal. The action of a hot aqueous extract of *S. frutescens* on the insulin-resistant cell cultures was also analysed. This was done by investigating the changes in glucose metabolism and homeostasis, lipid accumulation, oxidative stress, cellular energy state in the form of acetyl-CoA, and gene expression of signalling proteins involved in normal and impaired insulin signalling, as well as their respective protein expression levels. Cells of the human HepG2 line was made insulin-resistant using palmitate or a combination of high levels of insulin and fructose, and the two models were compared biochemically. Investigating the effect of the hot aqueous *S. frutescens* extract on the two models of insulin-resistance may help in elucidating the mechanism of its anti-diabetic activity.

The objectives of this study were thus:

1 Establishing two insulin-resistant models using the insulin/fructose and palmitate methods in HepG2 human liver cell line.
2 Investigating changes in cellular physiology in the two models.
3 Comparison of the two insulin-resistant models in terms of cellular physiology, gene expression, and protein synthesis.
4 qRT-PCR analysis of selected gene expression.
5 Measurement of changes in signal transduction proteins.
6 Investigation of action *S. frutescens* has on the insulin-resistant cell models.

Chapter 2
Insulin-Resistant Cell Models

This chapter discusses the establishment of two cellular models of insulin-resistance using two different mechanisms. These models aim to reflect the physiological states during (1) hyperglycaemia and the compensatory hyperinsulinaemia, and (2) elevated serum FFAs. This was achieved by treating cells in culture with medium supplemented with either high levels of fructose and insulin, or high levels of the saturated FFA palmitate (Williams, 2010; Chavez and Summers, 2010).

In order to determine successful induction of insulin-resistance, hepatic glucose production via gluconeogenesis and cellular glycogen content was measured in the presence of insulin. As insulin acts to inhibit gluconeogenesis and promote glycogenesis, insulin-resistant cells would not respond to these effector functions.

Methods

1. Cell Culture

HepG2 cells were cultured in Eagle's Minimum Essential Medium (EMEM) (Lonza) supplemented with 10% (v/v) foetal bovine serum (FBS) (HyClone) and 1% (v/v) non-essential amino acids (HyClone) as growth medium. Cells were maintained at 37 °C in humidified air and CO_2 (5%).

2. Preparation of Stock Solutions

2.1. Preparation of *Sutherlandia frutescens* Aqueous Extract

Fresh leaves of *S. frutescens* were collected in September 2011 from a site in the Karoo, between Graaff Reinet and Murraysburg. The leaves were air dried for three days.

Dried leaves (15 g) were added to 700 mL boiling water, boiled for 10 minutes, and allowed to cool overnight following the procedure of Chadwick *et al*. (2007) which replicated the traditional procedure. The mixture was filtered on a Buchner funnel using filter paper (Whatman number 1), the extract frozen at -80 °C and then freeze-dried under vacuum over 2 days using the Savant Freeze Drying System. Dried material was collected, placed in Eppendorf microcapped tubes as 30 mg samples, sealed and kept in a desiccator until use. The *S. frutescens* extract was dissolved in 1 mL 50% (v/v) dimethyl sulfoxide (DMSO) in water, diluted in MCDB-201 medium (Sigma), filter sterilised using 0.2 µm acrodiscs (Pall), and used at a final concentration of 12 µg/mL (Williams, 2010).

2.2. Preparation of Metformin

Metformin, an established medication for the treatment of insulin-resistance and T2DM, was prepared as a 1 mM stock solution in DMSO. The stock solution was diluted to 20 µM with MCDB-201 medium for use at a final concentration of 1 µM as a positive control for treatment (Williams, 2010).

2.3. Conjugation of FFAs to FAF-BSA

To conjugate palmitate or oleate to fatty acid-free BSA (FAF-BSA) (Sigma), a 100 mM solution of palmitate in 0.1 M sodium hydroxide (NaOH) was heated to 65 °C with stirring until dissolved. A 0.1 mL aliquot of the resulting fatty acid solution was added, while stirring, into 1.3 mL 10% (w/v) FAF-BSA solution (Sigma) at 50 °C. After 15 min of slow stirring to allow clarification of the solution, 0.6 mL sterile deionised distilled water (ddH_2O) was added to bring the final concentration to 5 mM fatty acid. The solution was filter sterilised using an acrodisc (0.2 µm pore size) and stored in aliquots at -20 °C for up to 6 months (Pappas *et al*., 2002; Ruddock *et al*., 2008).

3. Induction of Insulin-Resistance

3.1. Insulin/Fructose Method

HepG2 cells were seeded at a density of 2.5×10^4 cells/mL and grown for 48 hours in EMEM containing 10% FBS and 1% non-essential amino acids in a humidified incubator at 37 °C and 5% CO_2. After 48 hours, the culture medium was aspirated and replaced with either serum-free MCDB-201 (Sigma) medium (control); or serum free MCDB-201 supplemented with 0.1 µM insulin (Roche) and 1 mM fructose (Sigma) (IF) to induce insulin-resistance. Additionally, cells were exposed to IF induction medium supplemented with either a 12 µg/mL (final concentration) aqueous extract of *S. frutescens* (IFSF) or 1 µM metformin (IFM) (positive control for treatment) for 24 hours (Williams, 2010).

3.2. Palmitate-BSA Method

HepG2 cells were grown in culture medium for 48 hours after which the culture medium was aspirated and replaced with either serum-free MCDB-201 medium (control); or serum-free MCDB-201 supplemented with palmitate-BSA (0.25 mM) (PB) to induce insulin-resistance. Parallel cultures were exposed to PB-induction medium supplemented with either 12 µg/mL (final concentration) aqueous extract of *S. frutescens* (PSF) or 1 µM metformin (PM) (positive control for treatment) for 24 hours (Ruddock *et al*., 2008).

4. Cell Viability Testing

The viable cell number was determined in parallel experimental plates using the 4,5-dimethylthiazol-2,5-diphenyltetrazolium bromide (MTT, Sigma) assay (Mosmann, 1983).

The assay measures the activity of mitochondrial reductase in viable cells to reduce the yellow MTT to formazan crystals (purple colour). The crystals were extracted from the cells by the addition of DMSO and absorbance measured spectrophotometrically against a DMSO blank at 540 nm.

5. Verification of Insulin-Resistance

5.1. Hepatic Glucose Production Assay

After 48 hours of growth in growth medium, the medium was aspirated and replaced with the various treatments as described in section 3 and incubated for a further 24 hours. Glucose production was monitored by the method of Gao *et al*. (2010). Briefly, the medium was aspirated and cells washed twice with phosphate buffered saline (1× PBS) (8 g/L NaCl, 0.2 g/L KH_2PO_4, 2.9 g/L Na_2HPO_4, and 0.2 g/L KCl, pH 7.4) to remove any residual glucose contained in the culture media. The cells were then incubated for 16 hours in glucose-production medium (glucose- and phenol red-free EMEM containing gluconeogenic substrates, 20 mM sodium lactate and 2 mM sodium pyruvate) (Sigma) with the addition of 0.1 µM insulin during the last three hours. Medium from each sample was analysed using glucose oxidase colourimetric determination of glucose content at 510nm.

5.2. Analysis of Glycogen Content

The cellular glycogen content was analysed after three hours incubation in the presence of 0.1 µM insulin using the anthrone test for carbohydrates. Briefly, culture medium was aspirated and cells boiled in the culture plate for 20 min in 30% (v/v) KOH followed by the addition of 95% (v/v) ethanol. The resultant mixture was thoroughly mixed, transferred to Eppendorf microcapped tubes, and centrifuged at 4000 $\times g$ for 15 min. The supernatant was removed and 0.01% (v/v) anthrone in 98% (v/v) sulphuric acid added to each sample. Samples were

placed at 4 °C for 10 min, boiled for 20 min, and left at room temperature for 20 min before spectrophotometric analysis at 620 nm (Chun and Yin, 1988).

6. Data analysis

Absorbance data were normalised to cell number as determined by the MTT assay and expressed as a percentage of the control (MCDB-201). Statistical analysis was performed by ANOVA (one- or two-way depending on the data set) with post-test analyses performed (Newman-Keuls or Bonferroni post-tests). Confidence levels were set to 95%.

Results and Discussion

1. Cell Viability

HepG2 cells cultured in the insulin-resistance induction media for 24, 48, and 72 hours were subjected to cell viability analysis using the MTT assay (Figure 8). The absorbance readings obtained from the extracted formazan crystals were compared to those obtained from a standard curve of serial dilution of cells seeded at densities from 75000 to 625 cells per well.

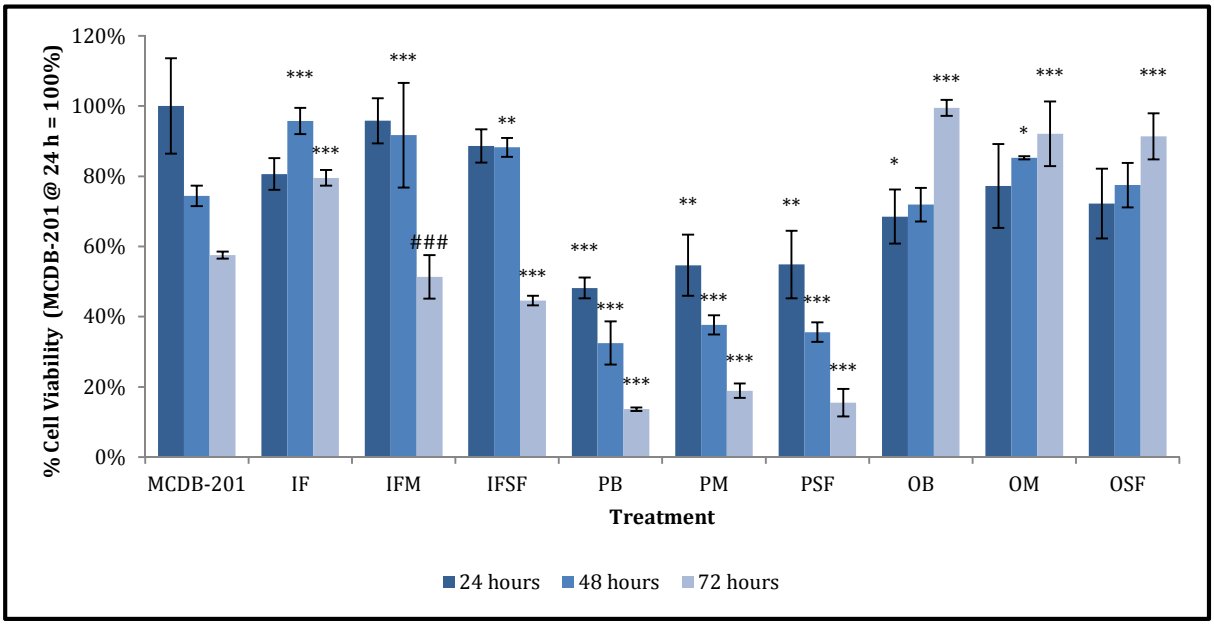

Figure 8: Cell viability of HepG2 cells. HepG2 cells were cultured in various conditions for 24, 48, and 72 hours followed by MTT cell viability analysis. The data is represented as mean percentages versus control (MCDB-201 at 24 hours) ± S.D. (n = 3). Statistical analysis performed using two-way ANOVA (n = 3). * = $p < 0.05$, ** = $p < 0.005$, *** or ### = $p < 0.0005$ (compared to control or IF, respectively). IF = Insulin and Fructose in MCDB-201 medium, IFM = IF supplemented with 1 µM metformin, IFSF = IF supplemented with 12 µg/mL *S. frutescens* aqueous extract, PB = Palmitate-BSA conjugate in MCDB-201 medium, PM = PB supplemented with metformin, PSF = PB supplemented with *S. frutescens* aqueous extract, OB = Oleate-BSA conjugate in MCDB-201 medium, OM = OB supplemented with metformin, and OSF = OB supplemented with *S. frutescens* aqueous extract.

The cell viability studies show, in comparison to the control, a relative decrease in cell viability over the 72 hour study in the control, IFM-, and IFSF treatments. This decline is mainly due to the depletion of nutrients from the culture wells, resulting in a decline in cell viability by 72 hours. In the 48 hour treated cells, significantly higher ($p < 0.0005$ for IF and IFM, $p < 0.005$ for IFSF) cell viability is seen in the IF-, IFM-, and IFSF treatments compared to the control group's 48 hour time point. This may be due to the presence of

fructose in the induction medium which adds to the nutritional capacity of the media, allowing it to sustain the cells for longer. Interestingly, the metformin and *S. frutescens* treatments yielded a more significant ($p < 0.0005$) decline in cell viability at 72 hours than the IF treated cells. This effect is comparable to the trend seen in the control cells, suggesting that the cause for the decline in cell viability may be similar. It is thought that this difference in viability between the metformin- or *S. frutescens*-treated cells and the IF-induced cells is due to the recovery of cellular glycolytic functions and the associated depletion of glucose from the media, resulting in the decline in cell growth and viability due to nutrient depletion. In the IF-induced cultures, however, cellular glycolysis is attenuated (as seen in the glucose oxidase study) resulting in a decline in the rate at which glucose is depleted from the culture medium. This combined effect of decreased glucose uptake and glycolysis results in the higher viability seen in the IF-induced cells as compared to metformin- and *S. frutescens*-treated cells. Furthermore, metformin acts on mitochondria to mildly inhibit ATP production, resulting in increased AMP levels (Viollet and Foretz, 2013). AMPK, therefore, becomes more active, which results in switching of the cells from an anabolic to a catabolic state. This causes ATP consuming processes to shut down in order to restore energy balance. As a result, lipid and protein synthetic pathways as well as cellular growth become inhibited while enhancing glucose uptake. This effect of metformin to mildly attenuate cellular growth is supported by the newly proposed use of the drug in cancer therapy (Viollet *et al*., 2012). In this respect, metformin would cause a decline in cell viability of the HepG2 cell line as it is a hepatoma culture. Hence, the metformin-induced reduction in cell viability may be attributed to the combinatory effect of the metformin-induced reduction in cell growth and depletion of media nutrients.

In the palmitate model, a reduction of approximately 50% in cell viability within 24 hours was seen. Further reduction in cell viability was observed at the 48 and 72 hour intervals ($p < 0.0005$). Palmitate mediates the production of reactive oxygen species (ROS) and induces ER stress (Gao *et al.*, 2010). Elevated ROS production and ER stress are implicated in cellular damage and apoptosis (Karaskov *et al*., 2006; Liu *et al*., 2007). In contrast, oleate treatment resulted in an initial reduction in cell viability, followed by an increase in cell survival over the time-course. Oleate stimulates the accumulation of lipid in hepatocytes which contributes to lipotoxicity, hence the initial reduction in cell viability (Lee *et al*., 2010). However, oleate also allows for the passage of long chain fatty acids into the mitochondrial matrix by increasing *Cpt-I* expression (Coll *et al*., 2008), allowing these to be utilized for

ATP production while also suppressing ROS production, ER stress, and inflammation. Cpt-I is involved in facilitating the transport of long chain fatty acids into the mitochondrial matrix, allowing these to be fed into β-oxidation. Furthermore, oleate has been shown to promote Akt phosphorylation, which induces downstream activation of cell survival signalling and cellular growth (Coll *et al*., 2008). This effect of oleate possibly attributes to the increase in cell viability seen after 24 hours. Increased β-oxidation increases the available energy the cells have access to, allowing for cellular growth.

The MTT assay allows for the exclusion of any effects which may be associated with the various treatments, such as apoptosis, as seen in the palmitate model (Yuzefovych *et al*., 2010). This exclusion allows for the analysis of all subsequent data in an unbiased fashion.

2. Verification of Insulin-Resistance

For the verification of successful induction of insulin-resistance by the two models, cellular responses to the induction or treatments in the presence of insulin were investigated. Here HGP and glycogen content were analysed (Figures 9 and 10, respectively). Lipid accumulation is also indicative of insulin-resistance in some, but not all cases, will be discussed in a later chapter. During the insulin-resistant state, the hepatocytes suffer from impaired regulation of glucose production, resulting in increased gluconeogenesis and glucose release. Glucose production is fuelled by the conversion of lactate to pyruvate with subsequent pyruvate conversion to phosphoenolpyruvate (PEP). This allows for the PEP to enter the gluconeogenic pathway. In order to monitor gluconeogenesis, the cells were supplemented with these two gluconeogenic substrates in the form of sodium lactate and sodium pyruvate. This supplementation avoids depletion of the substrates which would limit glucose production, as the study is focussed on monitoring gluconeogenesis alone. Gluconeogenesis and glycogenolysis feeds G6P into the ER lumen via the G6P transporter (T1). Here, G6P is converted to glucose by hepatic G6Pase, allowing export of glucose via the GLUT2 transporter (Kresge *et al*., 2005).

HepG2 cells treated with IF (0.1 µM insulin and 1 mM fructose) and PB (0.25 mM palmitate) showed a significant increase in HGP in both models, with the increase being greatest in the presence of palmitate ($p < 0.0005$). Furthermore, treatment with either metformin or *S. frutescens* yielded a significantly ($p < 0.05$ in IF and $p < 0.005$ in PB) suppressive effect on

the HGP (Figure 9). Concomitant decreases in glycogen content in the insulin-resistant cultures were observed with recovery of glycogen stores following metformin or *S. frutescens* treatment (Figure 10).

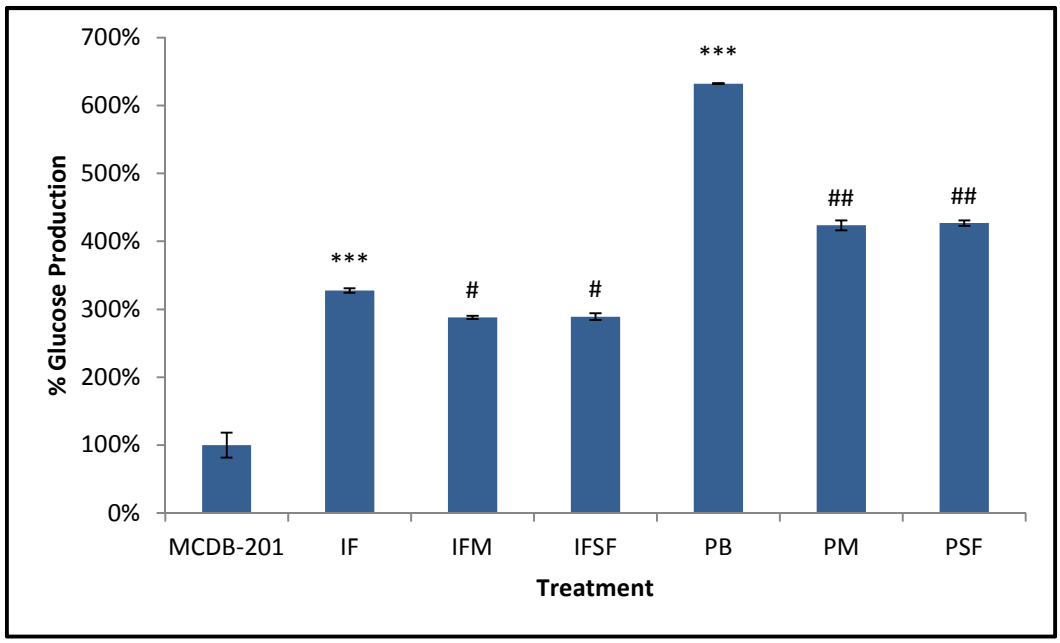

Figure 9: Hepatic glucose production. HepG2 cells were incubated in the presence of 0.1 µM insulin for three hours after 13 hours incubation in glucose-free medium. Glucose production was measured by glucose oxidase activity. Data is represented as mean percentage of the control (MCDB-201) ± S.D. Statistical analysis was performed using one-way ANOVA (n = 3). *** = $p < 0.0005$ (compared to control), # = $p < 0.05$, ## = $p < 0.005$ (compared to either IF or PB). IF = Insulin and Fructose in MCDB-201 medium, IFM = IF supplemented with 1 µM metformin, IFSF = IF supplemented with 12 µg/mL *S. frutescens* aqueous extract, PB = Palmitate-BSA conjugate in MCDB-201 medium, PM = PB supplemented with metformin, PSF = PB supplemented with *S. frutescens* aqueous extract.

Hepatic gluconeogenesis is regulated by SIRT1, an NAD^+-dependant protein deacetylase, which is involved in the deacetylation of PGC1-α, leading to increased glucose production (Rodgers *et al*., 2005). Hepatic SIRT1 is also implicated in the regulation of genes involved in cholesterol and lipid metabolism and is able to induce lipogenesis (Chen *et al*., 2008). Caton *et al*. (2011) demonstrated the role of fructose in SIRT1 activation and subsequent gluconeogenesis. Therefore, one mode by which the IF model may induce gluconeogenesis is through this SIRT1-dependant mechanism. The SIRT1-induced gluconeogenesis has been shown to act initially through an acute activation of JNK after which SIRT1 activation occurs in a JNK-independent manner within 30 minutes of fructose exposure (Caton *et al*., 2011).

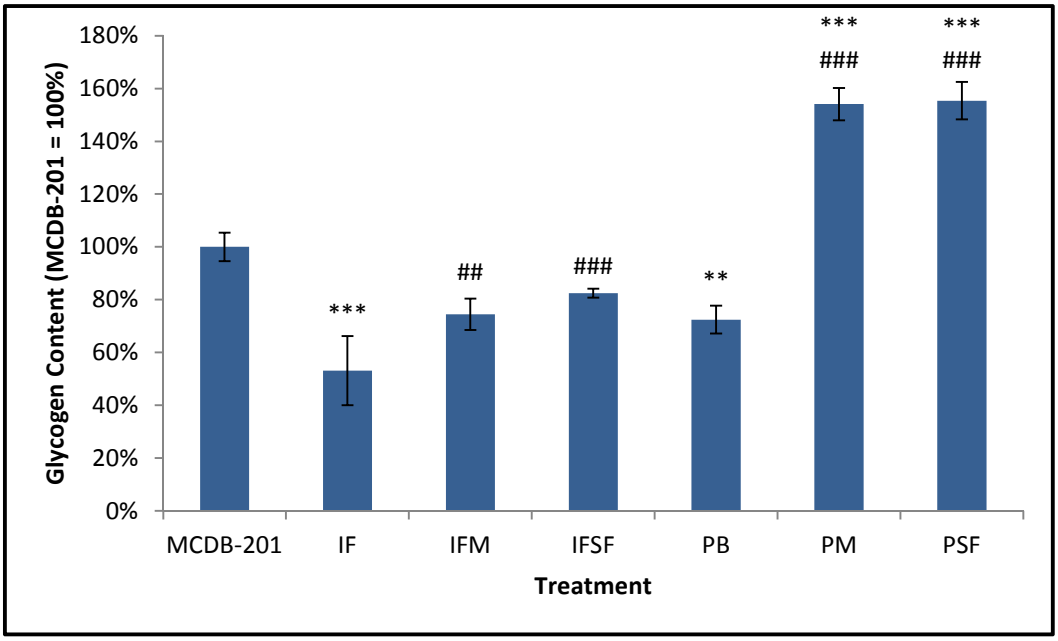

<u>Figure 10:</u> Hepatic glycogen levels. Glycogen content of HepG2 cultures in the presence of 0.1 µM insulin was measured by the anthrone test for carbohydrates. Glycogen content is expressed as a percentage of the MCDB-201 control. Statistical analysis performed using one-way ANOVA (n = 3). ** = $p < 0.005$, *** = $p < 0.0005$ (compared to control), ## = $p < 0.005$, ### = $p < 0.0005$ (compared to either IF or PB). IF = Insulin and Fructose in MCDB-201 medium, IFM = IF supplemented with 1 µM metformin, IFSF = IF supplemented with 12 µg/mL *S. frutescens* aqueous extract, PB = Palmitate-BSA conjugate in MCDB-201 medium, PM = PB supplemented with metformin, PSF = PB supplemented with *S. frutescens* aqueous extract.

Decreased glycogen synthesis is induced by fructose due to fructose-induced decrease in GSK-3 phosphorylation through CREB activity. Furthermore, CREB affects expression of *G6Pase* and *PEPCK*. Therefore, apart from increasing SIRT1 activity, fructose also increases PEPCK and G6Pase activity (Wei *et al*., 2007). Of these, PEPCK is involved in converting oxaloacetate to PEP during the first glycolytic bypass reaction of gluconeogenesis, while G6Pase is involved in conversion of G6P to glucose in the hepatic ER; promoting glucose production (Matte *et al*., 1997).

To further induce the insulin-resistant state, high levels of chronic insulin exposure leads to a decrease in insulin receptor autophosphorylation and subsequent IRS1 and IRS2 phosphorylation. Chronic exposure to high levels of insulin has also been shown to decrease the protein levels of the IR and IRS1/2 in HepG2 cells (Yuan *et al*., 2013). The inhibition of IRS1/2 activities result in a decrease in PI3K and GS activities, while relieving the inhibitory effect of insulin on PEPCK. The combination of these effects of high insulin and fructose levels results in attenuation of insulin signalling, promoting gluconeogenesis and

glycogenolysis, thus making these key markers for the detection of insulin-resistance during the establishment of insulin-resistant cell culture models.

Palmitate-induced gluconeogenesis may act through a different mechanism to that of the IF model. There are several proposed mechanisms by which palmitate may induce insulin-resistance (Figure 11). Emerging studies show that insulin-resistance may be induced by fatty liver (Stefan and Häring, 2011). In hepatic steatosis, FFAs and triacylglycerol (TAG) metabolites, such as DAG and fatty acyl-CoA, accumulate. Palmitate has been implicated in increasing β-oxidation with concomitant increases in acetyl-CoA (Noguchi *et al*., 2009). Fatty acid oxidation involves the transport of acyl-CoAs into the mitochondrial matrix by the addition of carnitine to acyl-CoA. Once inside the mitochondrial matrix, acyl-carnitine is converted back into acyl-CoA by carnitine acyltransferase. This allows for successive rounds of β-oxidation of the fatty acids to yield acetyl-CoA. From here, acetyl-CoA enters the citric acid cycle for ATP production in the same fashion as acetyl-CoA derived from glycolysis. As the acetyl-CoA levels rise, it acts as a signal for the activation of acetyl-CoA carboxylases, resulting in production of malonyl-CoA. Malonyl-CoA functions as a negative feedback signal by inhibiting the transfer of carnitine to acyl-CoA for the transportation of fatty acids into the mitochondrial matrix. Furthermore, acetyl-CoA acts as an inducer of pyruvate carboxylase activity while inhibiting the activity of pyruvate kinase, promoting the gluconeogenic pathway (Noguchi *et al*., 2009). Fatty acids can induce inflammation by stimulating the nuclear factor-κB (NF-κB) pathway or via induction of ER and oxidative stress by the activation of JNK. In this particular case, the saturated fatty acid palmitate plays an important role (Stefan and Häring, 2011).

In the present study, the effects of an aqueous extract of *S. frutescens* on insulin-resistance were investigated. It was found that the plant extract has the ability to decrease hepatic glucose output and recover the activity of glycogen synthase, seen as increased levels of glycogen (Figures 9 and 10). This effect is similar to that of metformin. Metformin acts through AMPK activation by its mild and specific inhibition of the mitochondrial respiratory-chain complex I, resulting in increased AMP levels which activate AMPK (Viollet *et al*., 2012). In turn, AMPK regulates TORC2 phosphorylation, which in turn regulates HGP in response to fasting by directing transcriptional activation of gluconeogenesis. Phosphorylated TORC2 is not able to translocate to the nucleus, preventing PGC-1α activation. In the liver, PGC-1α drives expression of the gluconeogenic genes, *PEPCK* and

G6Pase, which are therefore inhibited (Viollet *et al*., 2012; Viollet and Foretz, 2013). Although *S. frutescens* has the same effect as metformin here, it cannot be concluded that they work through the same mechanism of action.

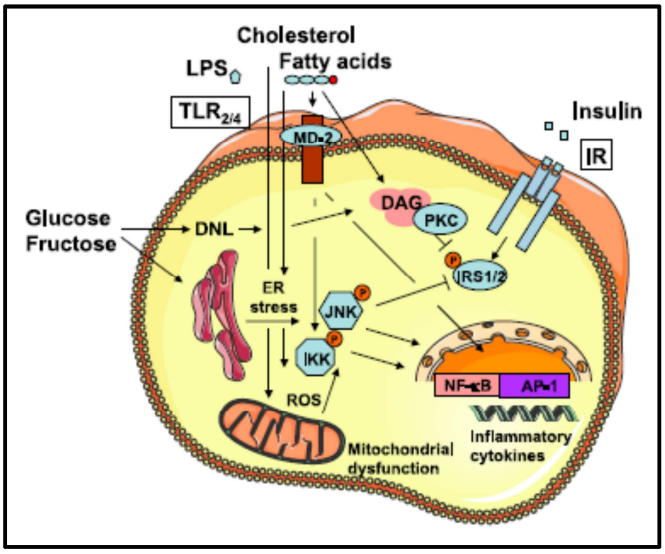

<u>Figure 11:</u> Pathways involved in inflammation and metabolism in human fatty liver disease. Abundant levels of glucose, fructose, and free fatty acids induce ER stress. Fatty acids and free cholesterol are also thought to induce mitochondrial dysfunction and increase ROS production. This leads to the activation of inflammatory pathways involving JNK and IKK, which then induce the transcription of inflammatory cytokines and consequently play a role in the inhibition of insulin signalling via IRS1 and 2. By increasing hepatic *de novo* lipogenesis, fatty acids, glucose, and fructose increase the DAG pool which, through activation of PKCs, also impairs insulin signalling. IR = insulin receptor, P = phosphorylation, MD-2 = myeloid differentiation protein-2 (Stefan and Häring, 2011).

This study shows that insulin-resistance may be induced using either a combination of high levels of insulin and fructose or oversupply of the saturated fatty acid, palmitate. The insulin-resistant state causes the liver to increase glucose output and glycogen breakdown, while inhibiting glycolysis and glycogen synthesis. Insulin-stimulated glycogen synthesis and suppression of glucose production is restored upon treatment of hepatic cells with metformin and *S. frutescens* (Figures 9 and 10). The treatments used here provided two working cell models of insulin-resistance which were used to elucidate some of the mechanisms underlying the development of insulin-resistance in each via investigation of lipid accumulation, ROS, nitric oxide (NO), acetyl-CoA, and genetic studies in later chapters. We also investigated the effects of *S. frutescens* on these parameters in comparison to metformin.

Chapter 3
Changes in Cellular Physiology

During insulin-resistance, the normal functioning of insulin-sensitive tissues becomes altered. These alterations lead to changes in cellular physiology such as changes in lipid accumulation, NO and ROS production, and changes in acetyl-CoA levels.

Using the two models of insulin-resistance, these changes in cellular physiology in each model were investigated. Lipid accumulation was studied using three methods, namely: Oil-Red-O staining, Nile Red staining, and thin-layer chromatography (TLC). These allow for the elucidation of the lipid profiles of the cells, while also quantifying these. Previous studies have shown that fructose and FFAs are capable of inducing liver steatosis in cell cultures (Samuel, 2011; Tappy *et al*., 2010; Gao *et al*., 2010). Nitric oxide has been implicated in palmitate-induced insulin-resistance, while ROS has been shown to be involved in both fructose- and palmitate-induced insulin-resistance (Yuzefovych *et al*., 2010; Tappy *et al*., 2010; Gao *et al*., 2010). Increased levels of FFAs lead to increased rates of β-oxidation and subsequent increased levels of acetyl-CoA. Acetyl-CoA acts as an intracellular signal of high energy levels, thus promoting pyruvate carboxylase activity during the first bypass reaction of gluconeogenesis (Hers and Hue, 1983). It also promotes activation of acetyl-CoA carboxylases which leads to the inhibition of β-oxidation through prevention of FFA transfer into the mitochondrial matrix, promoting lipotoxicity, mitochondrial dysfunction, ROS production, and ultimately insulin-resistance (Noguchi *et al*., 2009; Coll *et al*., 2008).

This chapter investigates the effects of *S. frutescens* on these changes in cellular physiology in comparison to metformin. This will allow for possible elucidation of the mechanism of *S. frutescens* anti-diabetic action.

Methods

1. Lipid Accumulation Assays

Two lipid stains, Oil-Red-O and Nile Red, were used quantify lipid accumulation in hepatocytes. The Oil-Red-O assay detects cellular neutral lipids, while Nile Red staining is used for the detection of neutral lipids (yielding a yellow-gold fluorescent colour) and phospholipids (yielding an orange-red fluorescence).

Previous studies have shown oleate to be a strong inducer of lipid accumulation in the form of TAG and phospholipids (Lee *et al*., 2010). Oleate was thus used as a positive control for lipid accumulation in HepG2 cells in the Oil-Red-O and Nile Red assays. The treatment was performed following the same procedure as the palmitate-BSA induction model, but instead used 0.25 mM oleate (OB). The OB medium was also supplemented with either 12µg/mL *S. frutescens* (OSF) or 1 µM metformin (OM) as treatment of the OB-treated cultures.

1.1. Oil-Red-O Assay

HepG2 cells were exposed to the various conditions as described in Chapter 2 for 24 hours, after which, the medium was removed and cells fixed in 10% (v/v) formaldehyde in 1× PBS (pH 7.4) for 10 min. Cells were rinsed with ddH_2O followed by 70% (v/v) ethanol, and stained with 3% (v/v) Oil-red-O solution (6 parts Oil-Red-O stock in isopropyl alcohol + 4 parts water) for 15 min. The stain was removed and cells washed with 70% (v/v) ethanol and finally water. The stain was then extracted by addition of isopropyl alcohol and the absorbance measured at 520 nm (Gao *et al*., 2010).

1.2. Nile Red Assay

After 24 hour exposure to the various conditions as in section 1.1, the cells were washed with 1× Hanks Balanced Salts Solution (HBSS; pH 7.4), and background fluorescence determined (535nm excitation, 580nm emission) on a Synergy MX (BioTek) plate reader. Freshly diluted Nile Red (1 µM Nile Red in 1% (w/v) Pluronic F127 in HBSS) was added to each well. After 4 hours incubation in the dark at room temperature, the Nile Red was removed

and cells washed once with HBSS. After a further incubation for 8-16 hours in HBSS in the dark at room temperature, fluorescence was determined as above and the background subtracted to determine the bound Nile Red fluorescence (Williams, 2010).

1.3. Thin Layer Chromatography

After 24 hour exposure to the conditions indicated in section 1.1, the medium was aspirated and cells gently scraped into 1 mL growth medium. Cells were then transferred to 2 mL microcentrifuge tubes and centrifuged for 5 min at 400 ×*g*. The supernatant was removed and the pellet re-suspended in 0.75 mL chloroform-methanol (1:2, v/v) and the phases separated by addition of 0.25 mL ddH_2O and 0.25 mL chloroform, followed by centrifugation at 1000 ×*g* for 5 min. The lower phase was dried and re-dissolved in 50 µL chloroform and spotted on silica gel TLC plates (Sigma). The total lipid extract was separated using diethylether-heptane-acetic acid (75:25:1, v/v/v). The solvent used to resolve the TLC plates causes the separation of the neutral lipid class. Thus, waxes and sterol esters migrate most quickly, followed by TAG, FFAs, DAG, and MAG, while polar lipids remain at the sample origin. Once the solvent has run to approximately ¾ of the length of the TLC plate, the TLC plates were stained using 0.003% (w/v) Coomassie blue in 100mM NaCl in 30% (v/v) methanol for 30 min. The plates were de-stained in dye-free solution for 5 min. (Baldanzi *et al*., 2010). Developed TLC plates were imaged using an AlphaImager™ 3400 (Alpha Innotech) and spot densities analysed using Alphaview software (version 3.2.2.0, 2010).

2. Nitric Oxide Quantification

After 24 hours exposure to the various conditions indicated in section 1.1, aliquots (50 µL) of medium were taken from each sample and analysed using the Griess system for nitrite detection. Briefly, the 50 µL samples were transferred to wells of a 96-well microtitre plate, followed by addition of 50 µL 1% sulfanilimide in 5% phosphoric acid (w/v) and incubated at room temperature for 10 minutes in the dark. Next, 50 µL 0.1% (w/v) *N*-1-naphthylethylenediamine dihydrochloride (NED) was added and incubated as before (a pink colour developed). The absorbance of the resultant mixture was measured at 520 nm. Nitrite concentrations were compared to the absorbance readings obtained from a nitrite standard curve using sodium nitrite (Sigma) (0-100 µM).

3. Measurement of Reactive Oxygen Species

For the quantification of ROS production, the dye 2',7'-dichlorodihydrofluorescin diacetate (DCFH-DA) was used. It is freely permeable and incorporates into the hydrophobic lipid regions of the cell. The acetate moieties are cleaved by cellular esterases, leaving non-fluorescent 2',7'-dichlorodihydrofluorescin (DCFH). This is oxidised by hydrogen peroxide and peroxidases into dichlorofluorescein (DCF), which is fluorescent (Robinson *et al*., 1994). After 24 hours exposure to the various conditions indicated in section 1.1, the medium was aspirated and cells washed twice with 1× PBS (pH 7.4). Thereafter, the cells were loaded with the DCFH-DA dye (20 µM in DMSO) for 30 minutes in the dark at 37 °C. Excess dye was removed by washing cells with PBS as before. Cells were then harvested, transferred into polypropylene tubes in phenol red-free EMEM, centrifuged at 400 ×*g* and incubated in phenol red-free EMEM for 10 minutes at 37 °C in the dark. Cells were centrifuged as before, washing with PBS. Once washed, the cells were re-suspended in 500 µL PBS and DCF fluorescence analysed by flow cytometry using the fluorescein isothiocyanate (FITC) channel (excitation/emission: 480 nm/530 nm).

4. Quantification of Acetyl-CoA

After 24 hours exposure to the various conditions indicated in section 1.1, the medium was aspirated from the cells and acetyl-CoA levels determined using the method of Hovik *et al*. (1991). The cells were harvested, by accutase (HyClone) treatment, into 200 µL hypotonic buffer (10 mM KPO_4 containing 1% (v/v) Triton X-100) and sonicated for five seconds. Thereafter, 1 M $ZnSO_4$ was added to a final concentration of 0.1 M, the solutions mixed thoroughly, and centrifuged at 1900 ×*g* for 15 minutes. The supernatants were collected and 1 mM L-carnitine (0.1 mM final concentration in 50 mM HEPES) added, pH adjusted (pH 7.0-7.5) using 15% (w/v) KOH, L-carnitine acetyltransferase (1 U/mL) (CAT, Sigma) added, and incubated at 37 °C for 10 minutes. Aldrithiol-4 (2 mM stock in 50 mM HEPES) (Sigma) was added to a final concentration of 0.2 mM and incubated as before. The absorbance readings were obtained at 324 nm and compared to a standard curve (1-5 µg) of acetyl-CoA (Sigma).

5. Data Analysis

All data were normalised to cell number as determined by the MTT assay and expressed as a percentage of the control (MCDB-201). Statistical analysis was performed by ANOVA (one- or two-way depending on the data set) with post-test analyses performed (Newman-Keuls or Bonferroni post-tests). Confidence levels were set to 95%.

Results and Discussion

1. Lipid Accumulation

After the confirmation of successful insulin-resistance induction using the two methods of induction (insulin/fructose and palmitate) (Chapter 2), HepG2 cells were subjected to lipid accumulation analyses. Lipid accumulation is related to the development of insulin-resistance, therefore this change in cellular physiology within the two models was investigated. HepG2 cells were exposed to the various media conditions for 24 hours, and then subjected to Oil-Red-O or Nile Red staining, or TLC of the lipid fractions.

The Oil-Red-O staining of the insulin-resistant cells showed a significant increase ($p < 0.05$ for IF and $p < 0.0005$ for PB and OB) in cellular lipid content. Significant decreases in lipid content were seen compared to the insulin-resistant cells following the metformin or *S. frutescens* treatments of the IF ($p < 0.05$) and OB ($p < 0.0005$) insulin-resistant cells, but no significant effect on the lipid content of palmitate-treated insulin-resistant cells was observed (Figure 12A). Visual representation of the cells containing Oil-Red-O-lipid droplet complexes can be seen in figure 12B. Compared to the control, it can be seen that the amount of stained lipid droplets is increased or decreased in a corresponding fashion to what is seen in the absorbance data (Figure 12A).

The Oil-Red-O dye stains predominantly TAG and other neutral lipids. In the IF model, there is an oversupply of fructose. Fructose, although having the same chemical formula as glucose, is quite distinct from glucose. Thus, the metabolism of fructose is directed by different biochemical mechanisms. In the case of hepatocytes, fructose is predominantly transported by GLUT2 into the cytosol, where it is rapidly phosphorylated to yield fructose-1-phosphate, due to the high levels of fructokinase in hepatocytes (Samuel, 2011; Wei et al., 2007). Fructokinase activity is not regulated by ATP levels, and thus is less responsive to the energy levels of the cell. This results in fructose being metabolised more favourably than glucose due to the fructolysis being less tightly regulated (Samuel, 2011). Once fructose-1-phosphate is cleaved to yield glyceraldehyde 3-phosphate, it may enter the glycolysis pathway and proceed to acetyl-CoA production.

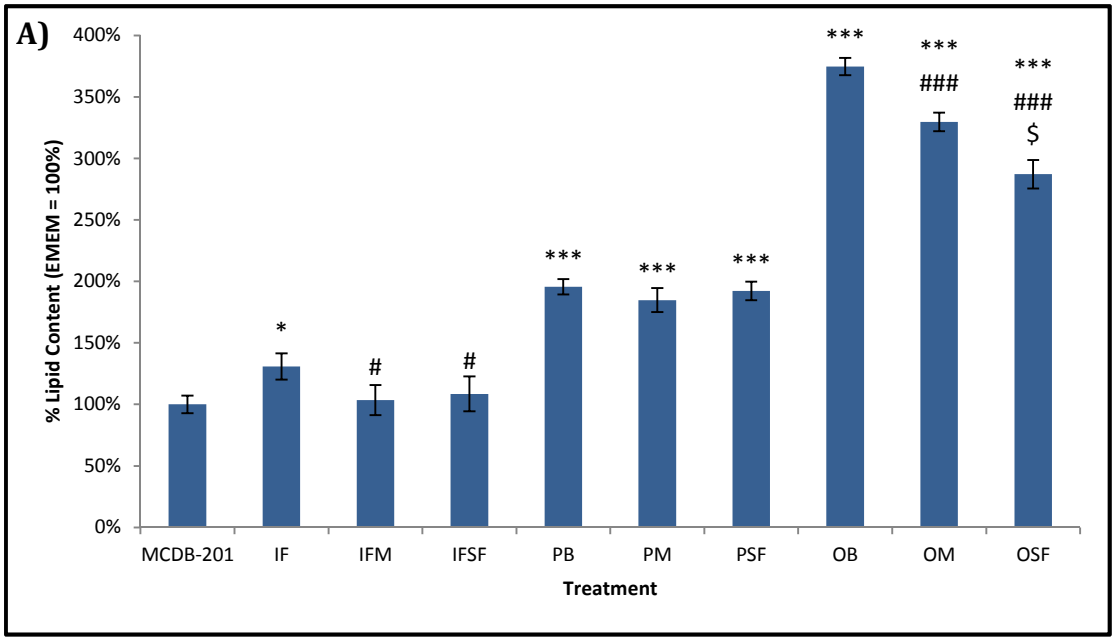

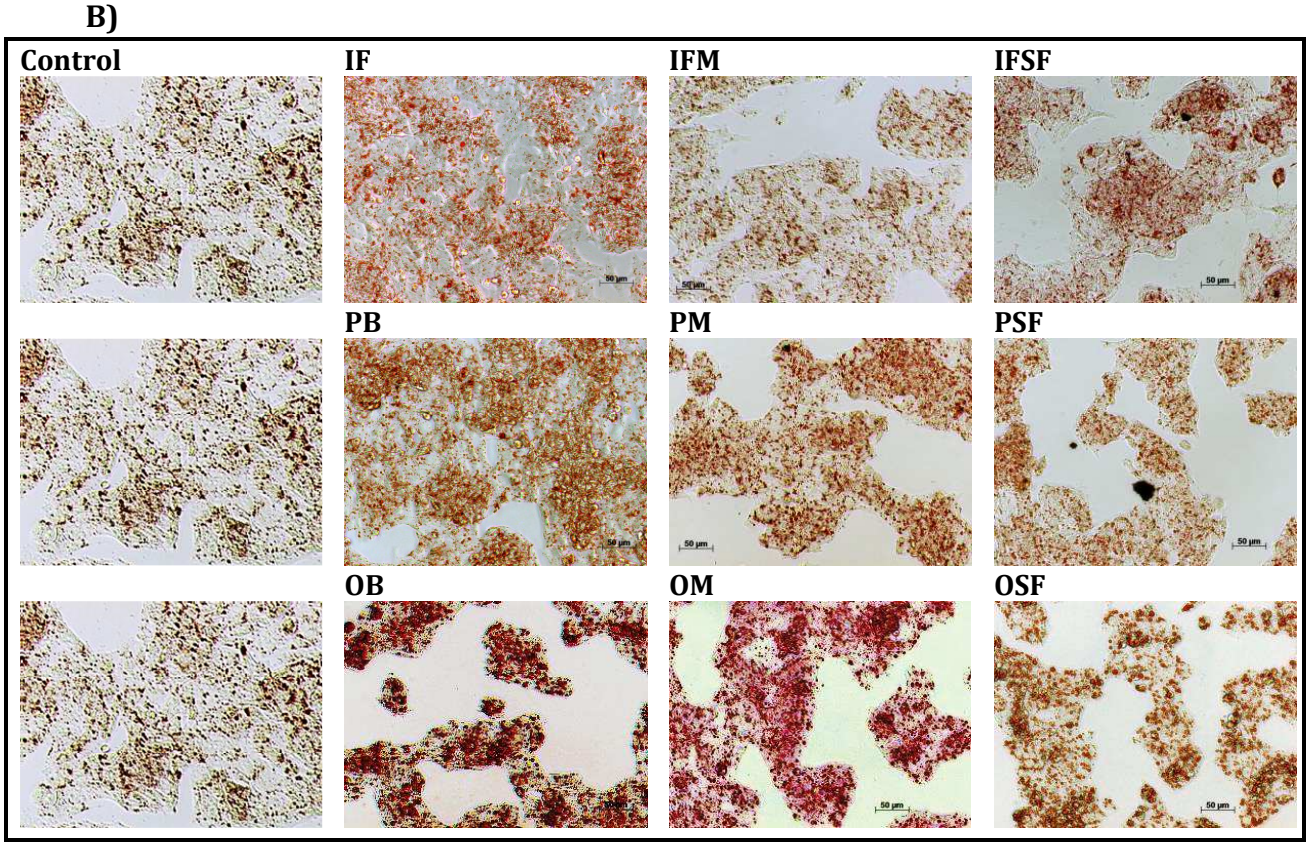

<u>Figure 12:</u> Neutral lipid and triacylglycerol accumulation in HepG2 cells. The cellular lipid content of HepG2 cells grown for 24 hours in various conditions was measured by Oil-Red-O staining. **A)** Data are represented as mean percentage of the control (MCDB-201) ± S.D., **B**) Oil-Red-O stained lipid droplets within cells as viewed under light microscopy using a 20× objective. Scale bar 50 µm. Statistical analysis was performed using one-way ANOVA (n = 3). * = $p < 0.05$, *** = $p < 0.0005$ (compared to control), # = $p < 0.05$, ### = $p < 0.0005$ (compared to either IF or OB), $ = $p < 0.05$ (Compared to metformin treatment of the positive control).

Acetyl-CoA in turn may enter the tricarboxylic acid (TCA) cycle or be directed to fatty acid synthesis. Further, trioses can be used for glycerol 3-phosphate synthesis, which forms the backbone of TAG. Thus, fructose contributes to TAG synthesis either by forming the glycerol backbone or a fatty acyl moiety. Several studies have shown the contribution of fructose to increased TAG levels (Samuel, 2011; Wei et al., 2007).

An alternative lipid specific dye was also used, namely Nile Red. The Nile Red dye predominantly stains cholesterol and phopsholipids and fluoresces when exposed to light at a wavelength of 535 nm. In the current study, no significant changes in both cholesterol and phospholipids were observed in any of the insulin-resistant models when compared to the control (MCDB-201). However, oleate was seen to induce a significant ($p < 0.0005$) increase in the fluorescent signal, indicating a significant increase in either cholesterol or phopspholipids, or both. Metformin and *S. frutescence* treatment of the OB-induced cells showed a mean decrease in lipid accumulation, however this was not significant (Figure 13). Associated with non-alcoholic fatty liver disease is the impaired secretion of very low density lipoprotein (VLDL) and high density lipoprotein (HDL) (Stefan and Häring, 2011). This impaired secretion will lead to elevated cholesterol within the liver, hence the increase in Nile Red fluorescence may be attributed to this accumulation of VLDL within the hepatocytes. Zhang *et al*., showed the involvement of FoxO1 in increasing lipid metabolism and decreasing plasma cholesterol levels using transgenic mice wherein FoxO1 was constitutively expressed. Furthermore, FoxO1 activation through hepatic stress signals (such as increased JNK activity) during the development on insulin-resistance may exacerbate this condition (Gao *et al*., 2010). However this is seen only under elevated FFA levels and concomitant β-oxidation of short-chain fatty acids, such as oleate.

The mechanism by which fructose induces lipogenesis is still not fully understood, but some pathways have been proposed (Figure 14). One such mechanism involves the fructose-induced alteration of specific lipogenic enzymes (Samuel, 2011). Fructose is able to alter the activity of pyruvate dehydrogenase (PDH) by inhibiting PDH kinase (PDK) (Figure 14). This is in line with previous studies which showed decreased PDK activity and increased PDH activation in rats fed a fructose-rich diet (Park et al., 1992). PDH activity causes a rise in acetyl-CoA levels, which is directed to lipid synthesis. This leads to increased DAG production which inhibits insulin signalling via PKCε activation. DAG levels do not remain

elevated, however, but are converted to TAG under the control of SREBP1c for subsequent exportation as VLDL.

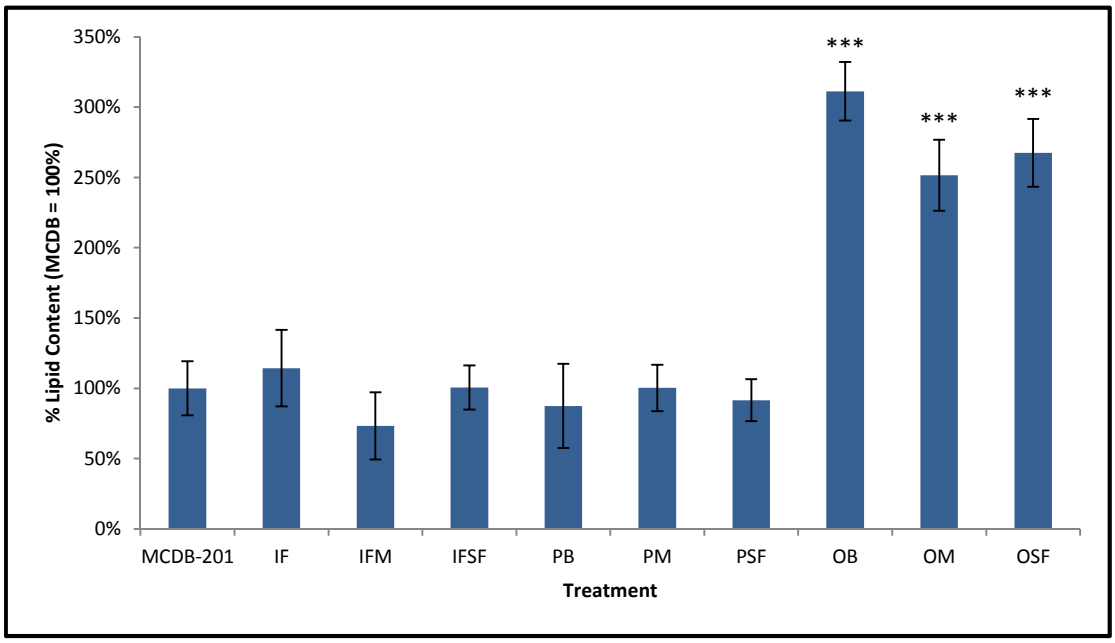

Figure 13: Cholesterol and phospholipid accumulation in HepG2 cells. The cellular lipid content of HepG2 cells grown for 24 hours in various conditions was measured by Nile Red staining. Data are represented as mean percentage of the control (MCDB-201) ± S.D. Statistical analysis was performed using one-way ANOVA (n = 3). *** = $p < 0.0005$ (compared to control).

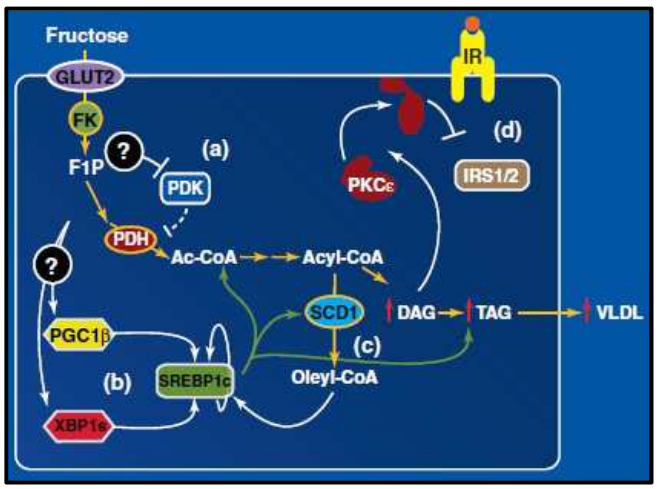

Figure 14: Proposed mechanism of fructose-induced lipogenesis. Fructose promotes lipogenesis by (a) increasing PDH activity by inhibiting PDK and (b) stimulating increases in SREBP-1c transcription, (c) SCD-1 catalysed desaturation of fatty acyl-CoA to produce monounsaturated fatty acids such as oleyl-CoA, which may also increase *SREBP-1c* expression, and (d) DAG activates PKCε, which attenuates insulin signalling, leading to hepatic insulin-resistance (Samuel, 2011).

Another proposed mechanism of fructose-induced lipogenesis is through PGC-1β activity (Samuel, 2011). PGC-1β acts as a nuclear receptor co-activator which can increase the expression of many transcription factors, such as the peroxisome proliferator-activated receptors α and γ (PPARα and PPARγ). Furthermore, PGC-1β can bind to and transactivate

SREBP1, linking PGC-1β-induced lipogenesis to the aforementioned PDH/PDK-induced mechanism of fructose-induced lipogenesis.

The signal by which fructose activates these pathways is still unknown; however some suggestions have been made. The carbohydrate response element binding protein (ChREBP) is key to connecting glucose metabolism to increased expression of glycolytic and lipogenic enzymes. In this case, X5P produced from glucose via the pentose-phosphate pathway, acts in protein phosphatase 2A (PP2A) activation, enhancing nuclear translocation of ChREBP. In the case of fructose, X5P is not increased *per se*, since fructose is rapidly metabolised into trioses. These trioses are destined for incorporation into TAG, thus feeding into the lipogenic action of fructose (Samuel, 2011). Studies have shown increased activity of ChREBP in the absence of increased X5P, suggesting another means of ChREBP activation (Koo *et al*., 2009). G6P is capable of activating ChREBP directly without X5P accumulation and PP2A activation, providing a link to fructose metabolism.

Gonzalez *et al*. (2011) showed the involvement of the hyperinsulinaemic state in lipid accumulation. Here, a state of selective insulin-resistance develops, causing an uncoupled insulin action wherein FoxO1's insulin responsiveness is maintained. This uncoupling is due to the high sensitivity of FoxO1 to insulin stimulation. During insulin-resistance, inhibition of hepatic gluconeogenesis by insulin is disrupted due to deregulation of FoxO1, while regulation of fatty acid and TAG biosynthesis through SREBP-1c remains functional, which in turn contributes to hyperglycaemia and hypertriglyceridaemia (Matsumoto *et al*., 2007). Furthermore, regulation of FoxO1 by insulin may be tissue-specific and thus respond differently under hyperinsulinaemic states. In the liver, FoxO1 modulates carbohydrate metabolism and is exposed to higher levels of insulin than other tissues (such as adipose), both in the fasted and postprandial state. FoxO1's transcriptional activity is negatively regulated by insulin-activated Akt and positively regulated by JNK, which promotes its translocation into the nucleus (Guo *et al*., 2012).

This involvement of FoxO1 in the development of insulin-resistance may be a key component in the models investigated in this study. In the IF-induced cells, it was observed that gluconeogenesis was elevated (Chapter 2). This may be due to the elevated activity of FoxO1 through either 1) its ability to be still responsive to insulin signalling under hyperinsulinaemic states and insulin-resistance or 2) the hyperglycaemic-induced (high

fructose content) stress activation of JNK and consequent FoxO1 activation, or 3) a combination of both. FoxO1 in turn regulates the expression of gluconeogenic genes, resulting in dysregulation of carbohydrate metabolism and homeostasis (Guo *et al*., 2012). This may be why the IF-induced cells exhibit a different lipid profile than the PB-induced cells. In the IF-induced cells, the oversupply of fructose will be directed to increased lipogenesis through the lipogenic mechanism described above. Therefore, it is expected to see increased TAG levels in the cells exposed to IF (Figure 15). Models of lipogenesis previously described provide the explanation for the increased TAG in IF-induced cells. Palmitate-induced DGAT2 inhibition result in no TAG being produced and lipogenesis arresting at the DAG stage, thus increasing DAG. The IF-induction does not inhibit DGAT2, allowing TAG synthesis to proceed. This same response may be at work in the palmitate model (PB) where it is known that palmitate activates JNK, which would then cause this activation of FoxO1, providing a link between the hyperinsulinaemic (and consequent hyperglycaemic) and hyperlipidaemic states associated with T2DM.

In contrast, palmitate-induced lipogenesis results in a different lipid profile to that of fructose-induced lipogenesis. Palmitate is thought to alter the expression of genes involved in TAG synthesis, such as *Dgat2*, which is involved in the conversion of DAG to TAG (Chavez and Summers, 2010). Palmitate is mainly directed to incorporation into DAG which, together with palmitate-induced diacylglycerol acetyltransferase 2 (DGAT2) inhibition, results in accumulation of DAG (Coll *et al*., 2008). In the present study, palmitate-induction (PB) significantly increased DAG levels ($p < 0.0005$) while having no significant effect on either monoacylglycerol (MAG) or TAG levels. Further, DAG was significantly reduced by metformin and *S. frutescens* ($p < 0.05$), although these remained significantly higher than that of the control ($p < 0.0005$) (Figure 15). In the liver, DAG activates the novel PKC isoform, nPKCε via palmitoylation (Sampson and Cooper, 2006). Novel PKCε is involved in serine phosphorylation of IRS1, inhibiting insulin signalling, and impairment of HMGA1 activity, which results in decreased insulin receptor expression, contributing to insulin-resistance (Dasgupta *et al*., 2011).

It is suggested that the anti-lipogenic activity of metformin is directed through AMPK and the concomitant decrease in ChREBP and SREBP-1 activity, leading to decreased hepatic steatosis, thus alleviating the lipotoxic and insulin-resistant states (Viollet *et al*., 2012). In the current study, metformin and *S. frutescens* treatment showed a significant decrease in lipid

accumulation (Figures 12 and 15) ($p < 0.05$) in comparison to the IF-treated cells, while having no significant effect on the palmitate-induced lipid accumulation. This decrease in lipid accumulation in the IFM and IFSF treatments is accompanied by increased insulin responsiveness, as measured by insulin-induced suppression of gluconeogenesis (Chapter 2).

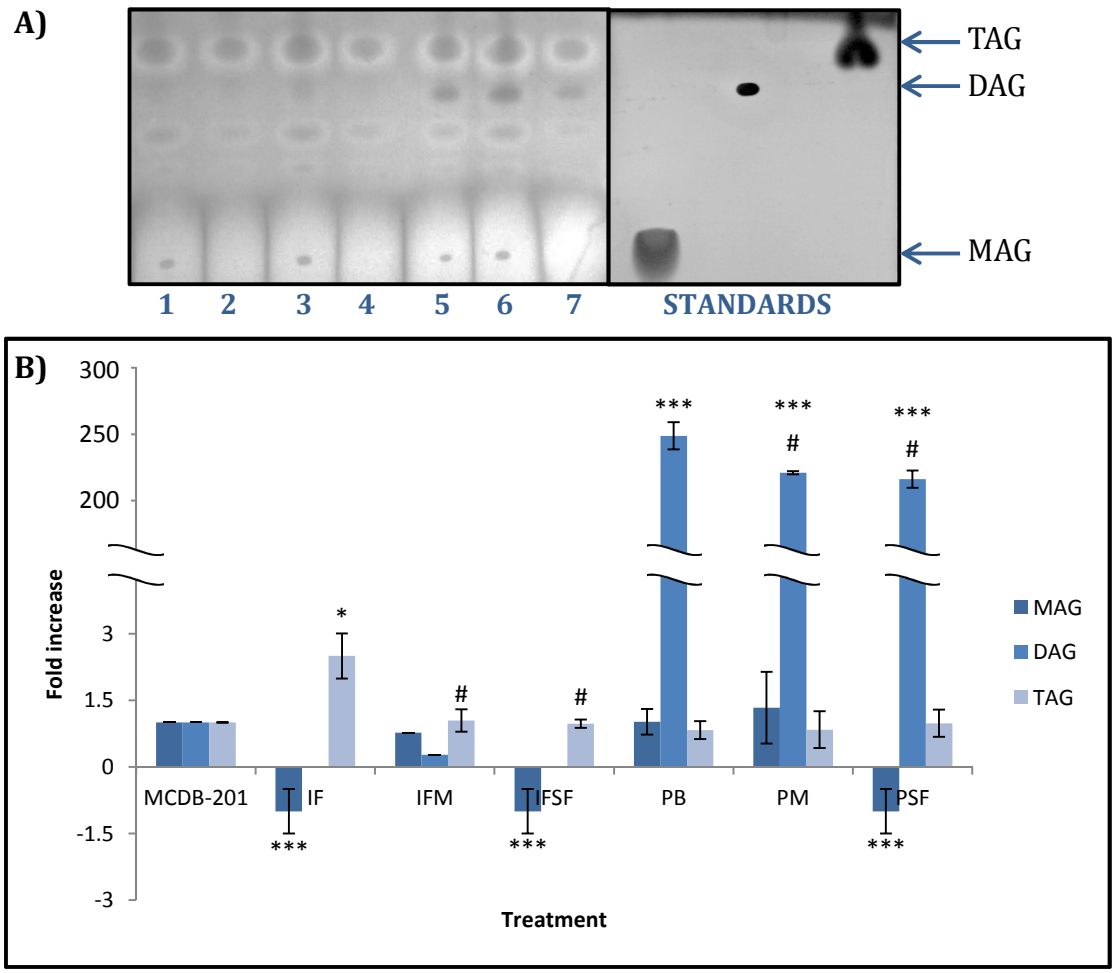

Figure 15: Thin layer chromatography of lipid fractions. The cellular lipid profile of HepG2 cells grown for 24 hours in various conditions was analysed by **A)** representative thin layer chromatograph and **B)** subsequent densitometry. In the chromatograph, lanes represent the samples as **1)** MCDB-201, **2)** IF, **3)** IFM, **4)** IFSF, **5)** PB, **6)** PM, and **7)** PSF. Data are represented as fold increase compared to the control (MCDB-201) ± S.D. Statistical analysis was performed using two-way ANOVA (n = 3). * or # = $p < 0.05$ (compared to control or insulin-resistant model, respectively), *** = $p < 0.0005$ (compared to control). MAG = monoacylglycerol, DAG = diacylglycerol, TAG = triacylglycerol.

A possible reason for the lipid accumulation not being decreased in the palmitate-treated cells by either metformin or *S. frutescens* is due to the type of lipid accumulated in these cells. Here, DAG is accumulated in contrast to the TAG accumulation as seen in the IF model. Metformin increases β-oxidation, thus increasing palmitate metabolism, alleviating the

inhibitory effect of palmitate on DGAT2. This allows the excess of DAG to continue into TAG synthesis. Hence, metformin appears to not reduce lipid accumulation as seen in the Oil-Red-O experiments, but does reduce DAG levels as seen in the TLC analyses (Figure 15).

This study shows that the changes in cellular lipid metabolism involved in the two models of insulin-resistance are directed through different mechanisms and toward different fates. In the hyperinsulinaemic/hyperglycaemic state (IF model), lipid accumulation in the form of TAG is directed by fructose-induced increased PDH and PGC-1α activities, resulting in increased lipogenesis. This increased activity of PGC-1α is also involved in the induction of insulin-resistance (Chapter 2). In the palmitate model, DAG accumulation is observed due the inhibitory effect of palmitate on lipolysis and the predominant incorporation of palmitate into DAG (Coll *et al*., 2008). Furthermore, palmitate, but not IF, inhibits the activity of DGAT2, resulting in DAG accumulation, which in turn induces insulin-resistance through inhibition of IRS1/2. Treatment of these models with either metformin or *S. frutescens* yielded different effects on the observed lipid accumulation (Figures 12 and 15). Thus, palmitate causes an initial increase in β-oxidation, resulting in increased levels of acetyl-CoA. This in turn stimulates the gluconeogenic pathway and TAG synthesis. However, palmitate-induced down-regulation of DGAT2 activity prevents the conversion of DAG to TAG during TAG biosynthesis. DAG levels rise as a result (while TAG levels remain low), causing increased activation of JNK and subsequent serine phosphorylation of IRS1/2 either directly by JNK or via activation of PKC isoforms, inhibiting insulin signal transduction and ultimately increasing HGP and decreasing activity of glycogen synthase (Sampson, 2006; Lee *et al*., 2010).

2. Oxidative Stress

In the liver, NO has several functions. Exogenous NO down regulates gluconeogenesis, although this effect is only mild, during states of inflammation such as sepsis and endotoxaemia. A more important effector function of NO is on mitochondrial respiration. Here, NO decreases respiratory activity by interacting with the cytochromes of the electron transport chain and also affects mitochondrial permeability. This results in a net decrease in the metabolic rate of hepatocytes. It must be noted that many of the effector functions of NO are not regulated directly by NO itself, but rather by its more stable form, peroxynitrite. Furthermore, the nitric oxide synthase (NOS) enzymes are also capable of forming

superoxide instead of NO when the substrate (arginine) or cofactor (tetrahydrobiopterin) is limited. This results in co-generation of both NO and superoxide (O_2^-) by the same enzyme, which may be implicated in inflammatory states where inducible nitric oxide synthase (iNOS) up-regulation results in depletion of arginine and tetrahydrobiopterin (BH_4). The most significant direct effect of NO is that of its effect of apoptosis. At high levels, NO induces apoptosis, which is primarily mediated by peroxynitrite's ability to increase mitochondrial permeability, either directly or through DNA damage with subsequent activation of the polyadenylate ribose synthase pathway. This leads to release of cytochrome *c* from the mitochondria, initiating the apoptotic signal, while uncoupling of NOS activity from NO production leads to mitochondrial DNA damage (Clemens, 2001).

Given the involvement of oxidative stress in the development of insulin-resistance, the levels of NO (as nitrite) and reactive oxygen species (ROS) were analysed. As before, the HepG2 cells were exposed to the different induction media or treatments for 24 hours (nitrite assayed at 1, 3, and 6 hours post-treatment or post-induction, as well as 24 hours) after which the cells were subjected to oxidative stress analyses. The time points for the nitrite assays were chosen based on previous work done by Yuzefovych *et al*. (2010). Nitrite levels were found to be significantly elevated within the first six hours post-induction with palmitate ($p < 0.0005$) while the levels had reverted to the control level after 24 hours (Figure 16). The IF model showed no significant change in nitrite levels and neither metformin nor *S. frutescens* showed any effect on the nitrite levels. At 24 hours post-induction, the levels of cellular ROS were found to be significantly elevated in the IF ($p < 0.005$) and PB ($p < 0.0005$) models, and significantly reduced in the IFM ($p < 0.05$), IFSF ($p < 0.05$), PM ($p < 0.0005$) and PSF ($p < 0.0005$) treatments. However, the PM treatment still yielded significant ROS levels ($p < 0.005$) (Figure 17).

Fructose metabolism leads to an increase in pyruvate levels which may be converted to acyl-CoA by PDH; however, pyruvate is also the precursor molecule to the TCA cycle. Pyruvate enters the mitochondrial matrix where it commits to the TCA cycle, which in turn produces the electron carriers, nicotinamide adenine dinucleotide (NADH) and flavin adenine dinucleotide (FADH2). The NADH and FADH2 are then used in the mitochondrial electron transport chain during ATP synthesis. The elevated mitochondrial activity leads to increased ROS production (superoxide and hydrogen peroxide). Through this increase in ROS

production, fructose may induce increased activity of JNK, leading to attenuation of insulin signalling (Stefan and Häring, 2011).

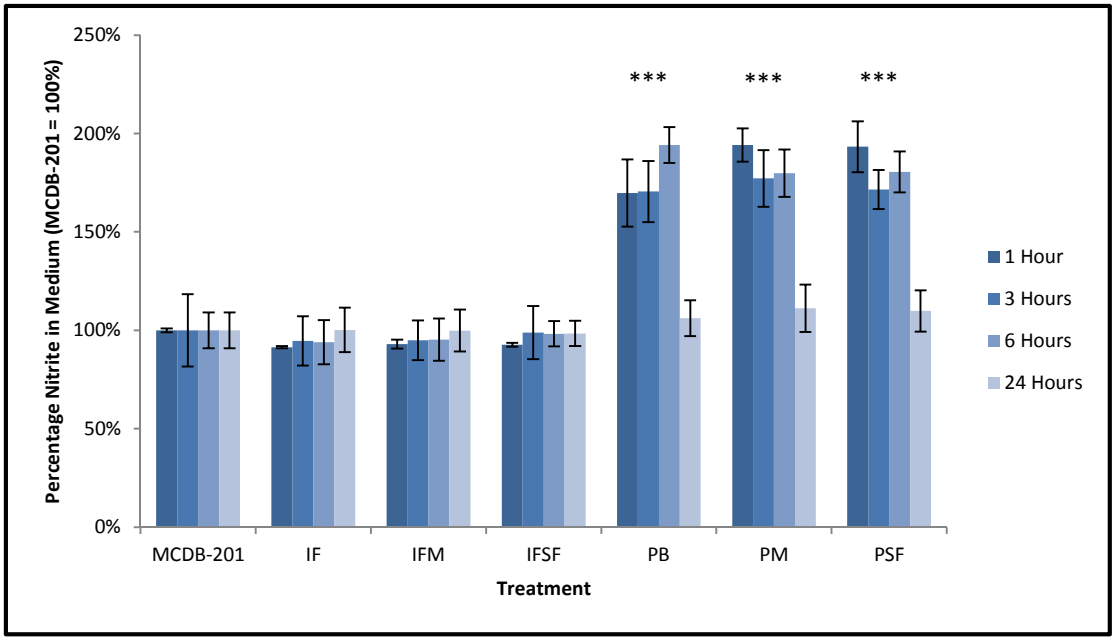

Figure 16: Nitrite levels within the culture medium. After exposure to the various induction media or treatments, aliquots of the medium were analysed for nitrite levels at 1, 3, 6, and 24 hours post-induction or post-treatment. The data are represented as mean percentage of the control (MCDB-201) ± S.D. Statistical analysis was performed using two-way ANOVA (n = 3). *** = $p < 0.0005$ (compared to control).

The palmitate-induced insulin-resistant cells showed an increase in NO production (Figure 16) prior to ROS production. It is suggested that this initial production of NO is responsible for significant mitochondrial DNA damage, which in turn causes increased mitochondrial ROS production, detected at the later time point. Palmitate has been found to inhibit insulin signalling through the activation of JNK (Gao *et al*., 2010). One way in which palmitate-induced JNK activation occurs is through the consequential increase in ROS production, related to increased electron flux in the mitochondrial respiratory chain due to increased β-oxidation of palmitate. The high mitochondrial oxidative phosphorylation fuelled by palmitate metabolism, therefore, may induce increased ROS production and result in the development of insulin-resistance (Stefan and Häring, 2011).

Treatment with either metformin or S. frutescens yielded decreased ROS, but not NO, production (Figures 16 and 17). Metformin's ability to decrease ROS production is likely due to its effect on the mitochondrial electron transport chain, where it results in mild

inhibition of mitochondrial chain complex I (Viollet and Foretz, 2013). Through this inhibition, ATP production is decreased and thus consequent superoxide production is decreased. The same effect is seen in the PM treatment, although ROS levels were still significantly higher than the control. This may be due to the increased metabolism of palmitate, induced by metformin, which leads to ROS being produced. Thus, in the case of the PM culture, metformin may be involved in both directly decreasing ROS production through inhibition of the mitochondrial electron transport chain and increasing palmitate β-oxidation and concomitant ROS production.

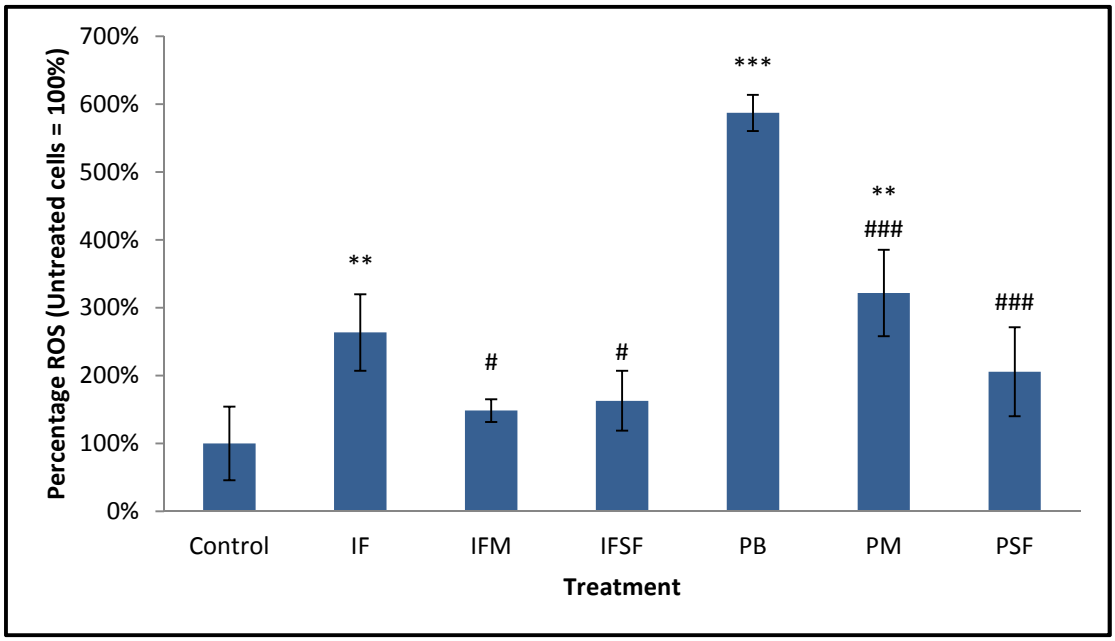

Figure 17: Reactive oxygen species levels in HepG2 cells. After 24 hours exposure to the various induction media or treatments the cells were loaded with DCFH-DA and relative fluorescence measured by flow cytometry. The data are represented as mean percentage of the dye-loaded, untreated cells (control) ± S.D. Statistical analysis was performed using one-way ANOVA (n = 3). # = $p < 0.05$ (compared to IF), ** = $p < 0.005$ (compared to control), *** or ### = $p < 0.0005$ (compared to control or PB, respectively).

Sutherlandia frutescens yielded significantly lower ROS levels than in both the PB and PM cultures, suggesting that it has a better anti-oxidant capacity than metformin (in the case of the palmitate-induced insulin-resistant cultures) and may also act through similar mechanisms. Fernandes *et al*. (2003) investigated the anti-oxidant activity of *S. frutescens* using a hot water, whole plant extract in two systems: *in vivo* cell culture and a cell-free system. *Sutherlandia. frutescens* was found to exert a significant anti-oxidant activity in both systems, decreasing ROS production in the *in vivo* cell model at concentrations as low as 10 µg/mL and 0.62 µg/mL in the cell-free system. This anti-oxidant activity is suggested to be related

to the phenolic compounds, such as tannins and flavonoids present in *S. frutescens*. Furthermore, Tai *et al*. (2004) demonstrated this ROS scavenging capability, while also indicating a lack of suppression and stimulation of NO production. Although L-canavanine is a selective inhibitor of iNOS, the lack of NO suppression may be concentration related. This is supported by the use of 0.5 mM L-canavanine and 10 mM pinitol (far higher than present in the hot aqueous extracts), which exhibited an inhibitory effect on NO production. Therefore, *S. frutescens* possesses a significant ROS scavenging ability as demonstrated by this study and others (Fernandes *et al*., 2003; van Wyk and Albrecht, 2008).

3. β-oxidation

After the 24 hour exposure to the various treatments, cellular acetyl-CoA levels were determined as acetyl-CoA reflects the level of β-oxidation (primarily) occurring within the cells. This study shows that in the IF-induced insulin-resistant cells a significant increase ($p < 0.05$) in acetyl-CoA is present as compared to the control cells (MCDB-201), while the palmitate model yielded a greater increase ($p < 0.0005$). Metformin and *S. frutescens* treatment of the IF-induced insulin-resistant cells yielded no significant change in the acetyl-CoA levels, although the levels were decreased (9% and 1%, respectively). Interestingly, metformin and *S. frutescens* caused an increase in acetyl-CoA levels in the palmitate model. Cellular acetyl-CoA in the metformin-treated cells was significantly higher than in the control ($p < 0.0005$), while *S. frutescens* significantly further increased the acetyl-CoA levels beyond those of the PB and PM cultures ($p < 0.0005$) (Figure 18).

As seen in the previous experiments, high doses of fructose cause a metabolic burden upon the cells. Here, fructolysis results in production of fructose-1-phosphate, which is cleaved to yield glyceraldehyde 3-phosphate. This in turn may enter the glycolysis pathway and proceed to acetyl-CoA production (Samuel, 2011). The significant increase in acetyl-CoA levels in the IF model reflects this metabolism of fructose, which in turn may feed the lipogenic and/or gluconeogenic pathways, leading to the increase in lipid accumulation and HGP seen with this model. Furthermore, an increase in acetyl-CoA due to increased fructolysis allows for increased activity of the TCA cycle and subsequently results in electron transport chain dysfunction and increased ATP production. This in turn increases ROS production (Figure 17). In the case of palmitate, acetyl-CoA levels are elevated due to increased β-oxidation of palmitate. The acetyl-CoA produced may be used again for

increased lipid accumulation or HGP. Furthermore, acetyl-CoA is also implicated in the induction of pyruvate carboxylase activity and inhibition of pyruvate kinase activity, promoting the gluconeogenic pathway (Noguchi *et al*., 2009). Thus, both IF and PB induction leads to increased acetyl-CoA production, which is a major factor in the increases in lipid accumulation and HGP seen in these insulin-resistant models. Interestingly, metformin and *S. frutescens* treatment resulted in increased acetyl-CoA production in the palmitate-induced model, although these improved the insulin-resistant state (through decreasing HGP). This may be through the increased β-oxidation of the palmitate present in the induction media, resulting in increased acetyl-CoA production. Although the acetyl-CoA levels are increased, insulin responsiveness is improved in the PM and PSF treatments. This may be due to the usage of the acetyl-CoA in the production of glycogen, as seen in Chapter 2, instead of HGP and lipogenesis as metformin (and possibly *S. frutescens* inhibits the latter two pathways). Furthermore, through the anti-oxidant activities of both metformin and *S. frutescens*, a protective effect is inferred upon the cells, preventing mitochondrial dysfunction and subsequent insulin-resistance.

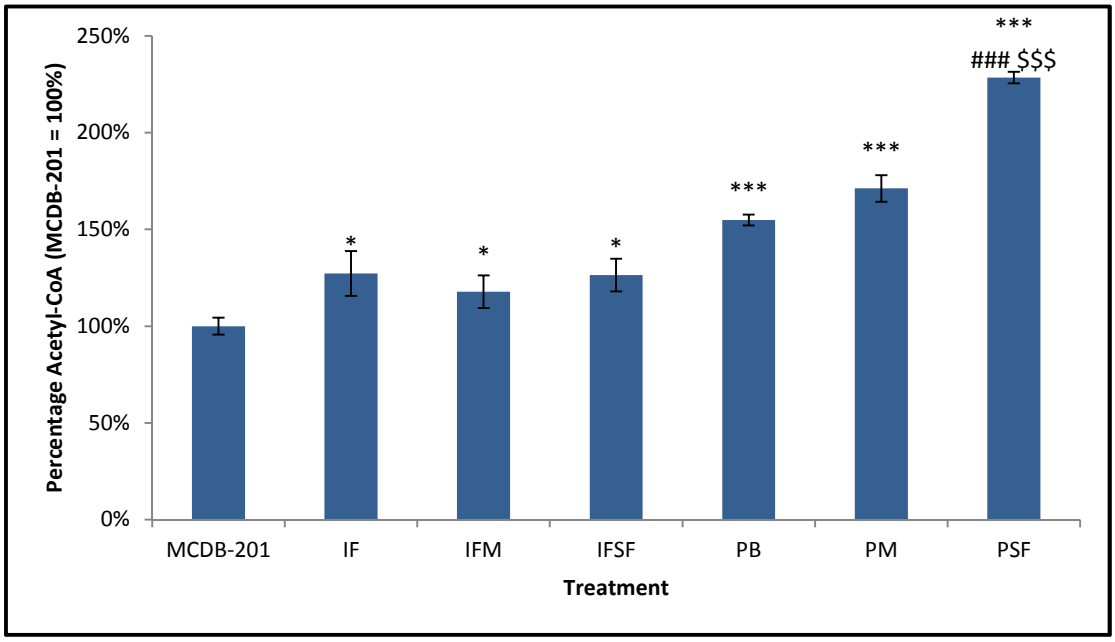

Figure 18: Acetyl-CoA levels in HepG2 cells. After 24 hours exposure to the various media conditions, the cells were lysed and assayed for acetyl-CoA levels. The data are represented as mean percentage of control (MCDB-201) ± S.D. Statistical analysis was performed using one-way ANOVA (n = 3). * = $p < 0.05$ (compared to control), *** or ### or $$$ = $p < 0.0005$ (compared to control, PB, or PM, respectively).

4. Summary

In the liver, the development of insulin-resistance is governed by several factors which are induced by the oversupply of insulin, fructose, and FFAs acting through several mechanisms, such as changing enzyme activity and gene expression (Figure 19).

Hyperinsulinaemia causes deregulation of FoxO1, leading to decreased glycogenesis and increased translocation of FoxO1 to the nucleus. FoxO1 stimulates the expression of the gluconeogenic genes *PEPCK* and *G6Pase*, increasing gluconeogenesis. Fructose is taken up by the liver in an unregulated fashion, and is rapidly metabolised to fructose 1-phosphate (F1P) due to the high levels of fructokinase in the liver. Together with fructose-induced inhibition of PDK, F1P induces the activity of PDH, increasing the conversion of pyruvate to acetyl-CoA. Furthermore, glyceraldehyde 3-phosphate derived from F1P may be metabolised to yield acetyl-CoA via the glycolytic pathway. From this fructose-derived acetyl-CoA, lipogenesis is stimulated through the high-energy signal provided by acetyl-CoA and increased SREBP-1c activity (induced by acetyl-CoA derived oleyl-CoA) during which glycerol 3-phosphate (derived from F1P) is used as the glycerol backbone. Fructose may also be converted to fructose 6-phosphate (F6P) by phosphohexose isomerase. This then enters the pentose phosphate pathway (PPP), where it is converted to X5P, which in turn induces PP2A activity and subsequent increased nuclear translocation of ChREBP; inducing lipogenesis. The fructose-induced lipogenesis results in increased levels of DAG, which inhibits insulin action through activation of JNK. Diacylglycerol is converted to TAG and stored in lipid droplets, resulting in liver steatosis. The increased production of acetyl-CoA from fructose metabolism is also further metabolised via the TCA cycle. The increased activity within the mitochondria place a metabolic burden upon the cell, resulting in electron transport chain dysfunction which causes increased ROS production. These ROS are implicated in the activation of stress signalling via JNK. The increased acetyl-CoA metabolism also increased the ATP output, which increases the ATP/AMP ratio and subsequently inhibits AMPK's anti-gluconeogenic activity. Acetyl-CoA is further capable of promoting the gluconeogenic pathway via induction of pyruvate carboxylase, PEPCK, and G6Pase and inhibition of pyruvate kinase (Noguchi *et al*., 2009).

On the other hand, palmitate induces lipogenesis via increased acetyl-CoA derived from increased β-oxidation. The elevated acetyl-CoA levels have the same fate as the fructose-derived acetyl-CoA: increasing gluconeogenesis, ROS, ATP, and TAG levels. However, the lipogenic pathway, in the presence of high levels of palmitate, becomes impeded through palmitate-induced inhibition of DGAT2. This results in the prevention of TAG synthesis from DAG, causing DAG accumulation. The increased levels of DAG, in turn, activates JNK via palmitoylation, leading to increased FoxO1 and PKCε activity and consequent increased serine phosphorylation of IRS1/2, *PEPCK* and *G6Pase* expression. Furthermore, PKCε is implicated in the inhibition of HMGA1, leading to decreased expression of the insulin receptor (Dasgupta *et al*., 2011). Palmitate metabolism is not limited to mitochondria alone, but β-oxidation also occurs within peroxisomes. Here, palmitate metabolism results in the direct production of hydrogen peroxide (H_2O_2) as opposed to TCA cycle derived H_2O_2. Thus, palmitate induces the insulin-resistant state via increased ROS production, and concomitant JNK activation, and increased acetyl-CoA production which leads to increased gluconeogenesis and lipogenesis (Stefan and Häring, 2011; Gao *et al*., 2010; Noguchi *et al*., 2009).

Metformin and the hot aqueous extract of *S. frutescens* show the ability to improve the insulin-resistant state by inhibiting gluconeogenesis, lipogenesis, and oxidative stress and related stress signalling. Furthermore, metformin and *S. frutescens* induce glycogenesis, glycolysis, and lipolysis. In the case of metformin, these effects are achieved through activation of AMPK by metformin's ability to inhibit the mitochondrial transport chain (Stephenne *et al*., 2011), resulting in decreased ATP production and thus decreasing the ATP/AMP ratio and ROS production. *S. frutescens*, on the other hand, decreases ROS production through its inherent ROS scavenging characteristics. Furthermore, *S. frutescens* may act in increasing β-oxidation as seen in its ability to increase cellular acetyl-CoA levels. Thus, lipid accumulation, oxidative stress, and the related stress signalling are decreased. However, investigation of the metabolic enzymes involved in glycolysis/gluconeogenesis, lipolysis/lipogenesis, and stress signalling (such as JNK and IkkB) may elucidate the cellular mechanisms involved in the anti-diabetic activity of *S. frutescens*.

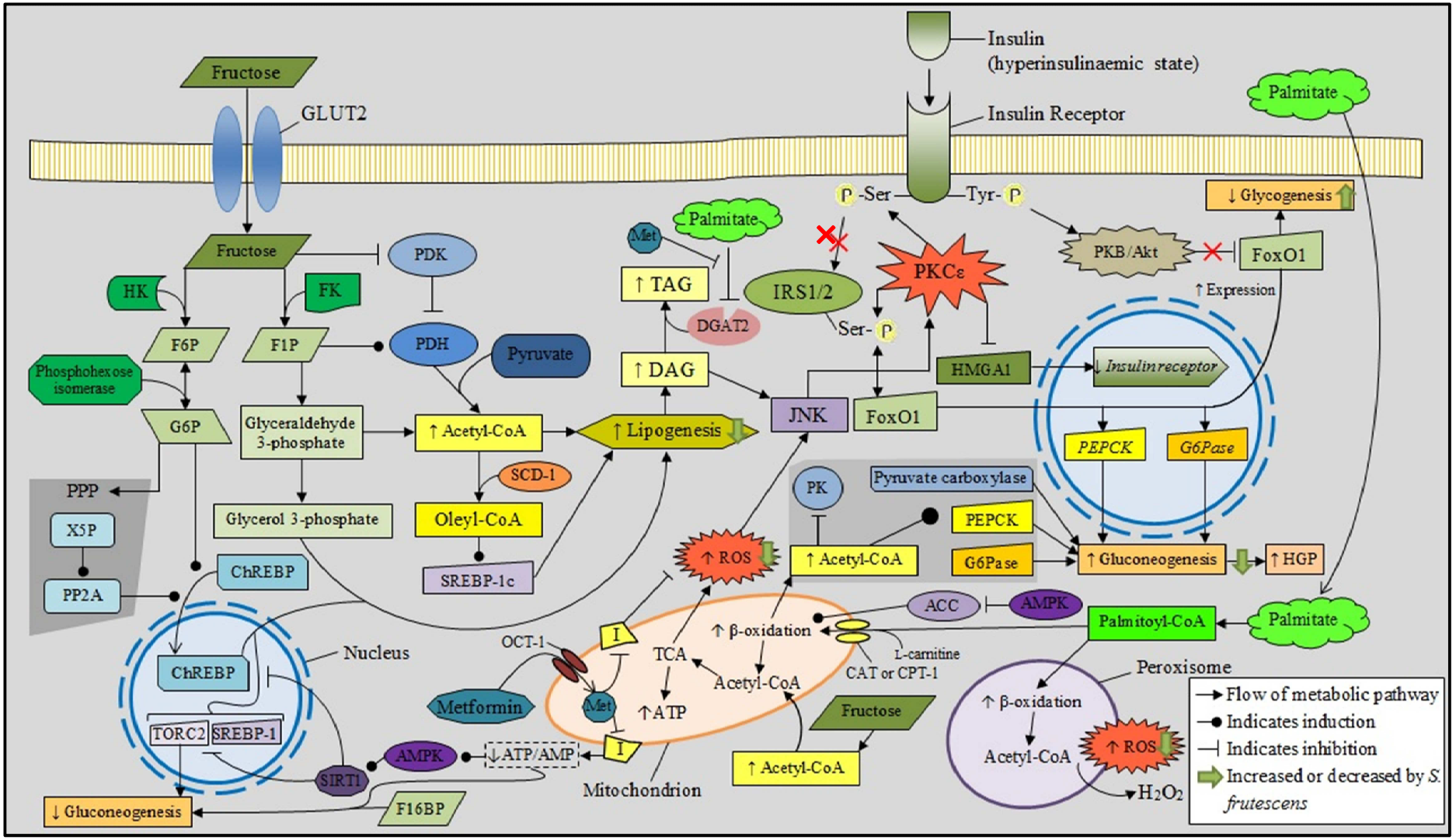

Figure 19: Summary of the cellular mechanisms involved in the development of insulin-resistance. In the liver, high levels of the combination of insulin and fructose and high levels of palmitate induce the insulin-resistant state via several mechanisms, resulting in the development of specific cellular physiologies, including steatosis, increased ROS levels, and increased levels of acetyl-CoA. ACC = Acetyl-CoA carboxylase, AMPK = AMP-activated kinase, AMP = adenosine monophosphate, ATP = adenosine triphosphate, CAT = carnitine acetyltransferase, ChREBP = carbohydrate response element binding protein, CPT-1 = carnitine palmitoyltransferase-1, DAG = diacylglycerol, DGAT2 = diacylglycerol acetyltransferase 2, F16BP = fructose 1,6-bisphosphate, F1P = fructose 1-phosphate, F6P = fructose 6-phosphate, FK = fructokinase, FoxO1 = forkhead box protein O1, G6P = glucose 6-phosphate, G6Pase = glucose 6-phosphatase, HGP = hepatic glucose production, HK = hexokinase, HMGA1 = high-mobility group protein 1, I = mitochondrial respiratory chain complex I, IRS1/2 = insulin receptor substrate 1/2, JNK = c-Jun N-terminal kinase, Met = Metformin, OCT-1 = Organic Cation Transporter 1, PDH = pyruvate dehydrogenase, PDK = pyruvate dehydrogenase kinase, PEPCK = phosphoenolpyruvate carboxykinase, PK = pyruvate kinase, PKB/Akt = protein kinase B, PKCε = protein kinase Cε, PP2A = protein phosphatase 2A, PPP = pentose phosphate pathway, ROS = reactive oxygen species, SCD-1 = Stearoyl-CoA Destaturase-1, SIRT1 = Sirtuin 1, SREBP-1c = sterol regulatory element binding protein 1c, TAG = triacylglycerol, TCA = tricarboxylicacid cycle, TORC2 = transducer of regulated CREBP 2, X5P = xylulose 5-phosphate (Adapted from: Sanuel 2011; Park *et al.*, 1992; Koo *et al.*, 2009; Gonzalez *et al.*, 2011; Matsumoto *et al.*, 2007; Guo *et al.*, 2012; Coll *et al.*, 2008; Sampson and Cooper, 2006; Dasgupta *et al.*, 2011; Viollet *et al.*, 2012; Lee *et al.*, 2010; Gao *et al.*, 2010; Noguchi *et al.*, 2009; Fernandez *et al.*, 2003).

Chapter 4
Changes in Gene Expression

During the development of insulin-resistance, several physiological changes occur within the hepatocytes. These changes may have an underlying genetic mechanism, which translates into changes in mRNA and possibly protein levels. These changes may include increased or decreased expression of metabolic enzymes, allowing for a shift in cellular metabolism from a glycolytic to a gluconeogenic state. For analysis of changes in the mRNA expression, the reverse transcriptase quantitative polymerase chain reaction (qRT-PCR) technique is used.

In order to investigate at this level of gene expression, RNA must first be isolated from the samples and linearly converted to cDNA, which is used in qPCR. The reverse transcription and PCR may be performed in a one-step reaction where both occur in the same tube or in a two-step process, where these occur in two separate tubes. This study employed the two-step procedure. The qRT-PCR method has developed into an important and powerful tool for the investigation of gene expression, accurately and reproducibly (Bustin and Nolan, 2004). This method, however, has several pitfalls, which will be discussed in this chapter alongside the experimental data. The method itself involves the collection of data throughout the PCR process, hence the "real-time" aspect of the method (Wong and Medrano, 2005). This data collection is achieved at the end of each PCR cycle through the use of a variety of fluorescent dyes and probes used with fluorescence detection equipment, which allow for the correlation of fluorescence to PCR-product concentration. For this study, SYBR Green was used to detect PCR progression, as it provides two main advantages over the probe-based procedures. Firstly, being a non-specific, interchelating dye, it can be incorporated into optimised and long-established PCR protocols, simply by adding the dye as a reagent to the PCR cocktail of standard reactions. Secondly, the cost is significantly lower than that of probe-based detection systems (Bustin and Nolan, 2004), since the dye can be incorporated into PCR reactions using any primer pairs, avoiding the need to use different probes for each gene to be examined and optimised. However, the non-specific nature of the dye results in its binding to any double-stranded DNA (dsDNA), which can result in fluorescence readings in so-called "no template controls" (NTCs) due to the dye binding to primer dimers. Primer dimers are short sequences of non-specific dsDNA formed as a consequence of the primer pairs annealing to non-target sequences. These non-target sequences may be of several origins, of

which the first two give rise to primer dimers: (1) primer pairs may recognise complementary sequences within one another. If this inter-primer association is stable enough, it may be amplified by the DNA polymerase in the PCR reaction mixture, (2) primers may self-anneal, forming what is called a hairpin loop. This occurs when a sequence in the 3' or 5' end is capable of stably annealing to a sequence within the primer itself, causing the primer to fold back onto itself and thus forming a hairpin loop, and (3) the primers may recognise other sequences in the target cDNAs which are either upstream, downstream, within the target gene, or in other gene sequences, resulting in amplification of incorrect amplicon lengths. The latter describes the formation of non-specific products and not primer dimers. This non-specific amplification is usually addressed by the use of melt curve analysis (Bustin, 2000). In this method, the fluorescence generated by SYBR green binding to dsDNA is plotted as a function of temperature, generating the melt curve. This is achieved by increasing the temperature from a starting temperature of 1 °C below the annealing temperature (T_a) of the primers by 1 °C every 30 seconds and measuring the fluorescence at each time point and plotting the differential of fluorescence against time. This generates a characteristic melting peak at the T_a of the amplicon (the dsDNA product formed during the PCR process) which distinguishes it from any other products, such as primer dimers, which form broad peaks at lower temperatures. Any amplification of other sequences not within the gene of interest will appear as separate distinct melt peaks (Bustin, 2000).

During the PCR process, there will be a PCR cycle at which the SYBR green-labelled target amplification is first detected to be significantly above background. This cycle is referred to as the quantification cycle (C_q). The greater the quantity of target cDNA in the sample, the earlier in the PCR process the C_q will be reached (Bustin, 2000). At the end of the qPCR procedure, amplification curves are generated which indicate the C_q-value, which is inversely proportional to the amount of cDNA in the original sample.

This amount of PCR template may be determined in two ways: relative or absolute quantification (Wong and Medrano, 2005). Relative quantification involves the measurement of the steady-state levels of a gene of interest relative to an invariant control gene. In contrast, absolute quantification requires the use of a sample of known quantity (also referred to as the copy number) of the gene of interest which may be diluted to generate a standard curve. The unknown samples are compared to this standard curve for absolute quantification (Valasek and Repa, 2005). This study used the relative quantification procedure. This procedure relies

on the use of control genes or sequences (referred to as reference or housekeeping genes) and a normalisation procedure. During the analysis of gene expression, several variables need to be controlled, such as the amount of starting material, enzymatic activity, and differences between the overall transcription activity of the experimental cells (Vandesompele *et al*., 2002). One strategy to normalise for these variations is the use of reference or housekeeping genes which should not vary in any of the experimental and control cells.

In this study, the mRNA levels of genes involved in the insulin signalling pathway were investigated after exposure to the various induction media or treatments. These included, IRS1, Akt1/PKB, JNK, and PKCε, of which the latter two are involved in the attenuation of insulin signalling (Gao *et al*., 2010; Dasgupta *et al*., 2011).

Methods

1. Quantitative Reverse Transcriptase Polymerase Chain Reaction (qRT-PCR)

1.1 RNA Extraction

After exposure to the various induction media or treatments as described in Chapter 2, the cells were exposed to either an equal volume of 1× PBS (pH 7.4) or 0.1 µM insulin for 30 minutes. Thereafter, the medium was removed from the cells. Cellular RNA was extracted using TriZol™ (BioRad). Briefly, TriZol™ reagent was added directly to the culture wells at 1 mL per 1×10^7 cells. The lysate was suspended and transferred to a 2 mL safe-lock microcapped tube. The homogenate was allowed to stand for 5 minutes at room temperature, followed by the addition of 200 µL chloroform. The mixture was vigorously vortexed for 15 seconds and left at room temperature for 3 minutes. The samples were then centrifuged at 12 000 ×*g* for 15 minutes at 4 °C. The upper aqueous phase (containing cellular RNA) was transferred to 1.5 mL RNase-free tubes.

1.2 RNA Precipitation and Quantification

The RNA was precipitated using the ethanol-precipitation technique. Absolute ethanol was added at 1× the volume of the RNA-containing sample and mixed thoroughly, but gently to avoid shearing of RNA. The samples were incubated on ice for 1 hour before centrifugation at 12 000 ×*g* for 30 minutes at 4 °C. The RNA pellet was re-suspended in 0.5 mL 75% ethanol and mixed gently. The samples were centrifuged as before and incubated for 15 minutes at room temperature. Centrifugation was again performed as before and the pellet air-dried for 5-10 minutes at room temperature. The RNA pellet was finally dissolved in RNase-free water (Ambion) and incubated for 15 minutes at room temperature before being stored at -80 °C. The RNA samples were quantified using a NanoDrop 2000c (Thermo Scientific)

1.3 cDNA Preparation and qPCR

cDNA was prepared from the RNA samples using the iScript cDNA synthesis kit from BioRad, according to the manufacturer's instructions. Each reverse transcriptase reaction was set up as indicated in Table 1.

Table 1: RT Reaction Mix. Relative amounts of each component from the iScript cDNA synthesis kit added per reaction.

Components	Volume per Reaction
5× iScript reaction mix	4 µL
iScript reverse transcriptase	1 µL
Nuclease free water	x µL
RNA template (1 µg total RNA)	x µL
Total volume	**20 µL**

The reactions were run using a thermocycler with the following reaction protocol as: 5 minutes at 25 °C, 30 minutes at 42 °C, 5 minutes at 85 °C, and a final hold at 4 °C. The generated cDNA was stored at -20 °C.

Table 2: qPCR reaction mix components and relative volumes used of each. The master mix described is suitable for use with multiple cDNA samples wherein a single target gene is to be analysed. cDNA is added into separate tubes to which this master mix is added.

Components	Volume per Reaction	Volume for 10 reactions
1× SoFast Evergreen Supermix	6 µL	60 µL
Sense Primer	1 µL	10 µL
Anti-sense Primer	1 µL	10 µL
cDNA	2µL	20µL
RNase-free PCR Grade Water	10 µL	100 µL
Total volume	**20 µL**	**200 µL**

Quantitative polymerase chain reaction was performed using the SoFast™ Evergreen Supermix (BioRad) in a 20 µL reaction. Each reaction contained a final concentration of 1× SoFastTM Evergreen Supermix, 500 mM final concentration forward and reverse primers, and 2 µL cDNA (50 ng/µL) in PCR-grade water (Ambion), in duplicate. Prior to performing qPCR, the total number of reactions in each experiment was calculated (plus one extra

reaction to accommodate pipetting error) in order to accurately prepare a qPCR master mix (Table 2).

The qPCR master mix was set up under sterile conditions as set out in Table 2, with the omission of the cDNA component, in a sterile microcapped Eppendorf tube. The master mix was then gently vortexed and briefly spun down. Thirty six µL of the master mix was transferred to pre-labelled, sterile microcapped Eppendorf tubes, each intended for one cDNA sample. Technical replicates were set up in the same tube. Thus, for the analysis of a single target gene or sequence, a total of 14 samples and 2 NTCs required the preparation of 35 reactions (each sample in duplicate plus 10% compensation for pipetting losses). Once each tube contained the aliquot of master mix, 4 µL cDNA (pre-diluted to 50 ng/µL in PCR-grade water (v/v)) was added to each tube corresponding to the cDNA sample. Thereafter, the completed qPCR reaction mix was gently vortexed, briefly centrifuged, and 20 µL transferred from each reaction mix to two adjacent wells of a 96-well PCR reaction plate (Bio-rad). The 96-well PCR reaction plate was kept on a chilled IsoFreeze plate holder to ensure all reactions remained cold while transferring the reactions to the plate. Thereafter, the plate was covered with optical tape (Bio-rad) and centrifuged at 1200 ×*g* for 2 minutes at 4 °C. The PCR reaction was performed in a Bio-rad iCycler as described below (Table 3). After each experiment, a melt curve analysis was performed to confirm production of a single product. The genes investigated are listed in Table 4, indicating the primer sequences and annealing temperatures used for each.

The T_a for each primer pair was determined by performing a temperature gradient experiment. This involves the preparation of a qPCR reaction as described above, but using a cocktail of the cDNA samples. This cocktail was set up by mixing equal volumes of each cDNA sample in a single tube from which 2 µL was used per qPCR reaction. For each primer pair, a theoretical T_a was reported by the supplier (Inqaba Biotech) which was used as a guideline for the temperature gradient experiment. The iCycler was programmed to run a temperature gradient ranging from ~2 °C below the theoretical T_a to ~65 °C, providing 8 temperatures for testing. Once the PCR reaction was completed, the highest T_a at which the amplification efficiency was still as high as the most-efficient lower T_a was chosen as the experimental T_a to be used. The qPCR data was recorded on the iCycler software, and the Cq values were exported for analysis by the qBasePLUS (version 2) software programme (BioGazelle). Relative changes in gene expression were compared.

Table 3: qPCR conditions used for each of the reference and target genes. The annealing temperature for each primer pair varied between genes (designated T_m) as listed in Table 3.

Step	Number of Cycles	Temperature (°C)	Time
Denaturation	1	95	3 minutes
Denaturation	40	95	30 seconds
Annealing		T_a	30 seconds
Extension		72	30 seconds
Denaturation	1	95	30 seconds
Melt Curve	1	Variable	30 seconds
Hold	1	18	∞

Table 4: Primers used for the reference genes or sequences and genes of interest. Primer sequences and respective annealing temperatures of each primer pair were determined using a temperature gradient of which the highest, most efficient temperature was chosen to be used.

Target	Accession Number	Primer Sequences		T_a (°C)
		Sense	Anti-sense	
TATABP	P20226	5'-AGTCCAATGATGGCTTACGG-3'	5'-TTGCTACTGCCTGCTGGTTG-3'	59
ATP5B	P06576	Obtained from GeNorm kit (Primer Design)	Obtained from GeNorm kit (Primer Design)	57
ALUsx	N/A	5'-TGGTGAAACCCCGTCTCTACTAA-3'	5'CCTCAGCCTCCCGAGTAGCT-3'	60
ALUsq	N/A	5'-CATGGTGAAACCCCGTCTCTA-3'	5'-GCCTCAAGCCTCCCGAGTAG-3'	60
IRS1	P35568	5'-TCTGTAAGTCTGTCTCCTA-3'	5'-CCTAATGTGATGCTCTGT-3'	59
PKCε	Q02156	5'-ATGAGTTCCAGTCTGAATACA-3'	5'-ATTGACAGCATCCACCTT-3'	60
PKB/Akt	P31749	5'-AAATGAATGAACCAGATT-3'	5'-CTAGGAAAGCAAAGAAAT-3'	56.5
JNK	P45983	5'-ATGTCCTACCTTCTCTATCA-3'	5'-TTACTACTATATTACTGGGCTTTA-3'	59

Results and Discussion

To investigate whether the various induction media or treatments used in the experimental conditions described in Chapter 2 have an effect on mRNA levels within the cells, qRT-PCR was performed on RNA samples isolated from cultures of the experimental HepG2 cells. Here, the method of relative quantification was used, which requires the use of reference housekeeping genes for relative quantification of the genes of interest in the samples.

1. Quantification of RNA

Before analysis of gene expression can be performed, RNA needs to be extracted from sample cells and quantified in order to use equal amounts of cDNA per sample in the qPCR procedure. For this, RNA was extracted from HepG2 cells treated with either 1× PBS (pH 7.4) or 0.1 µM insulin for 30 minutes after being treated with the various experimental conditions described in Chapter 2. The isolated RNA was subsequently quantified using a NanoDrop 2000c (shown in Table 5).

Table 5: RNA concentrations per experimental sample. Each sample represents the respective media conditions the cell cultures were exposed to followed by incubation in either PBS (designated "-") or 0.1 µM insulin (designated "+").

Sample	RNA concentration (ng/µL)	A 260/280	Sample	RNA concentration (ng/µL)	A 260/280
MCDB-201-	386.5	2.06	**IFSF+**	180.5	1.99
MCDB-201+	223.2	2.01	**PB-**	78.5	2.06
IF-	141.5	1.85	**PB+**	91.8	1.62
IF+	566.3	1.93	**PM-**	56.5	1.78
IFM-	446.3	2.1	**PM+**	145.9	1.76
IFM+	312.3	2.04	**PSF-**	50.9	1.64
IFSF-	680.8	2.06	**PSF+**	155.6	1.83

The use of the NanoDrop quantification of RNA provides the advantage of using very little sample per quantification (1 µL) and the quantification procedure is very fast. However, this quantification has the disadvantage of being unable to provide accurate insight into the quality of the RNA samples and does not discriminate between varying lengths of RNA. The only indication of the purity of RNA is through the A 260/280 ratio and absorption spectra reported by the software. In general, "pure" RNA has an A 260/280 ratio of approximately

2.0. In the experimental samples, it can be seen that in the various cultures there was some degree of variation in the A 260/280 ratios and thus indicates variations in RNA purity (Table 5). The less "pure" RNA was found in the IF- and all palmitate-treated samples (PB, PM, and PSF), except for the PB- sample which had a shift in the 260-280 nm peak. Inspection of the curve shape and absorption peaks may provide some insight into the quality of the sample. The curves generated for the experimental samples generated high absorption spectra between 220-240 nm (Figure 20). This indicates the presence of common contaminants such as guanine, phenol, or TriZol™, which in this case the peak between 220-240 nm is likely to be due to residual TriZol™ in the samples. More importantly, the presence of residual TriZol™ in the samples may result in a shift in the 260-280 nm peak, resulting in an overestimation of the RNA concentrations.

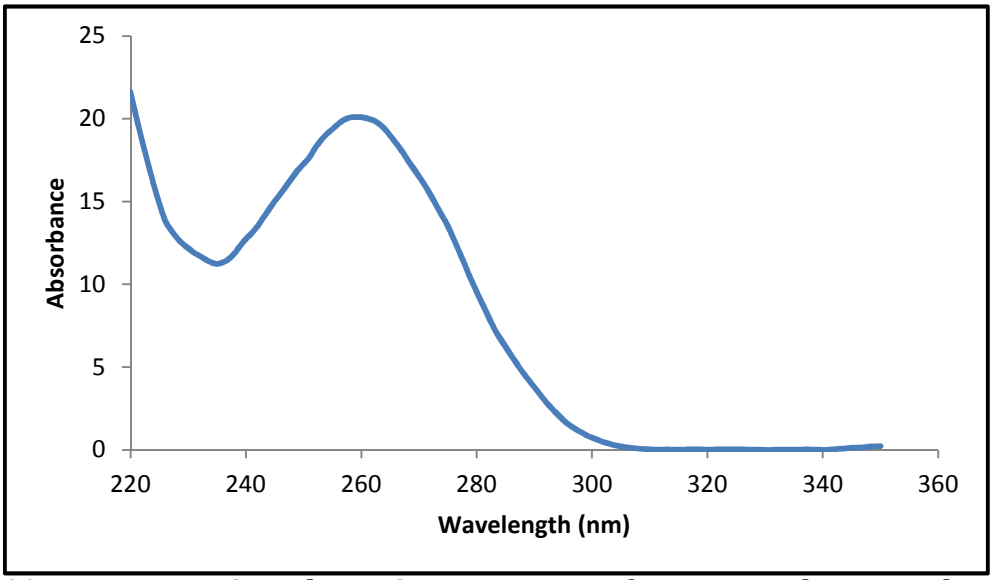

Figure 20: Representative absorption spectrum of RNA sample as analysed by a NanoDrop 2000c. The absorption spectrum ranges from 220-350 nm which indicates the characteristic peak at 260 nm for the RNA sample. Also seen is a peak at 220 nm, indicative of the presence of contaminants such as TriZol™.

Therefore, degraded and/or contaminated RNA may still provide high yields of RNA, which will result in complications at the qPCR stage. This may account for the differences seen in the expression levels of the reference genes analysed. The differences in RNA concentrations between the samples may be attributed to the effect each treatment has on gene expression or effects on apoptosis, as well as the presence of TriZol™ in some of the samples. Particularly, in the palmitate-treated cells, the lowest RNA yield was achieved and these cells showed the highest degree of cell death (Chapter 2). This high degree of cell death may be responsible

for the low yield through the small amount of cells present in the sample and the higher degree of apoptosis-induced DNA and RNA degradation. Therefore, quantification of the RNA using a different technique would be more beneficial to ascertaining the integrity of the RNA prior to cDNA synthesis.

1.1 Reference Genes

For the calculation of relative expression of the genes of interest, three reference genes should ideally be used. For this, four candidate genes or sequences were analysed by qPCR - these included the *Arthrobacter luteus* (ALU) repeat sequences, ALUsx and ALUsq, and the TATA binding protein (TATABP), and the ATP synthase β subunit (ATP5B) genes (Figure 21). The TATABP was excluded as the primers resulted in no amplification in the samples and could thus not be used as a reference gene. The ALU repeat sequences and ATP5B reference gene were selected to be used in this study as their GeNorm analysis yielded reference target stabilities in the acceptable range for a reference target to be used.

The ALU repeat sequences are short stretches of DNA originally characterised by the action of the Alu (*Arthrobacter luteus*) restriction endonuclease. These ALU elements are retrotransposons originating from human evolutionary ancestry and are thus present in all individuals with a common ancestor. They are comprised of repetitive DNA sequences of approximately 300 base pairs long and occur at high copy number in introns, 3' untranslated regions of genes and intergenic genomic regions. The ALU repeats are predominantly located in gene-rich regions of the human genome and account for more than 10% of the genome mass. Thus, these are the most abundant mobile element and are divided into several well-conserved subfamilies, namely the ALUsx, ALUsq, ALUy, ALUj, etc. Due to their genome-wide distribution, any changes in individual gene expression in the cells of interest will not influence the total ALU element expression. This makes the ALU repeat sequences valuable in normalisation of qRT-PCR experiments (Vossaert *et al*., 2013).

ALUsx, ALUsq, and ATP5B were subsequently subjected to analysis using the qBasePLUS software (version 2, 2010) to determine the reference gene stabilities and normalisation factors to be used in the calculation of the relative expression of the genes of interest (Table 6). During analysis, two parameters are calculated by the qBasePLUS software in order to verify the selected reference genes. The M value represents the gene expression stability

parameter as calculated by GeNorm, and CV represents the variation of the normalised relative quantities of a reference gene across all samples. The significance of these two values is that the lower the M value is, the greater the stability of the reference gene expression and the lower the CV value the more significant this stability becomes. Thus, one would select reference genes with the lowest M and CV values. In this study, the cut-off values for the validation of the reference genes were set to 1 and 0.5, respectively. Although the genes did not meet these criteria, they were near to them and so were used.

Table 6: Reference gene stability values. GeNorm calculated housekeeping gene stabilities, indicating the M and CV values.

Reference Target	M	CV
ALUsq	0.848	0.292
ALUsx	0.897	0.340
ATP5B	1.014	0.423
Average	**0.920**	**0.351**

For each of the reference genes, the fold expression per experimental sample was calculated in relation to the experimental control (MCDB-201–) (Figure 22). For ALUsx, the fold-expression varied between 1 and 8.20, 1 and 5.99 for ALUsq, and 1 and 4.65 for ATP5B. The variations seen in the fold-expression of the reference genes when compared individually illustrate the problems associated with using only a single reference gene for normalisation of qPCR data. Therefore, the use of the geometric mean of multiple reference genes is a more accurate method for normalisation (Vandesompele *et al*., 2002). The mean M value generated was thus 0.920 and the mean CV value 0.351.

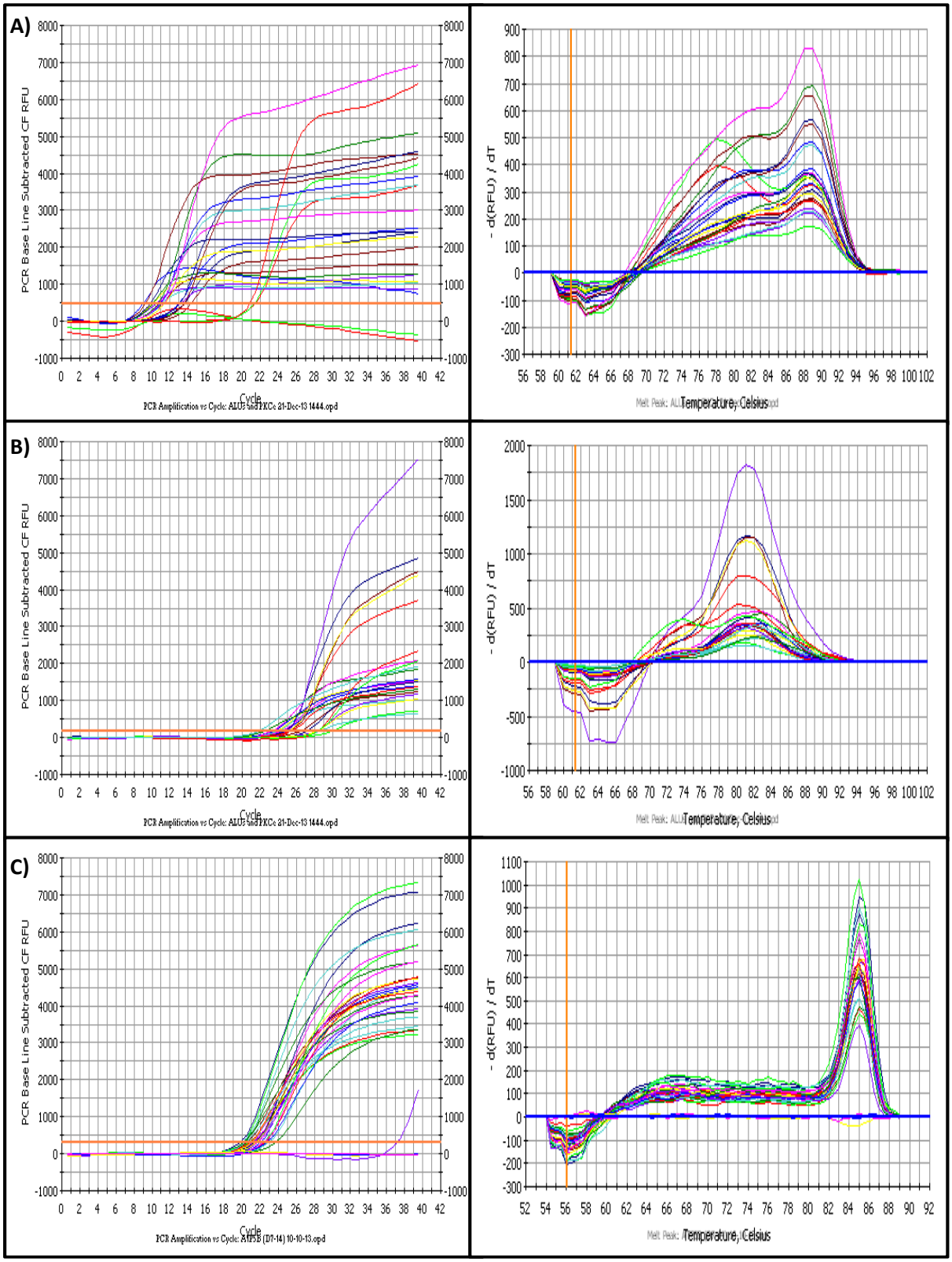

Figure 21: Amplification and melt curves of reference genes or sequences. A) ALUsx amplification and melt curve, respectively, **B)** ALUsq amplification and melt curve, respectively, and **C)** ATP5B amplification and melt curve, respectively.

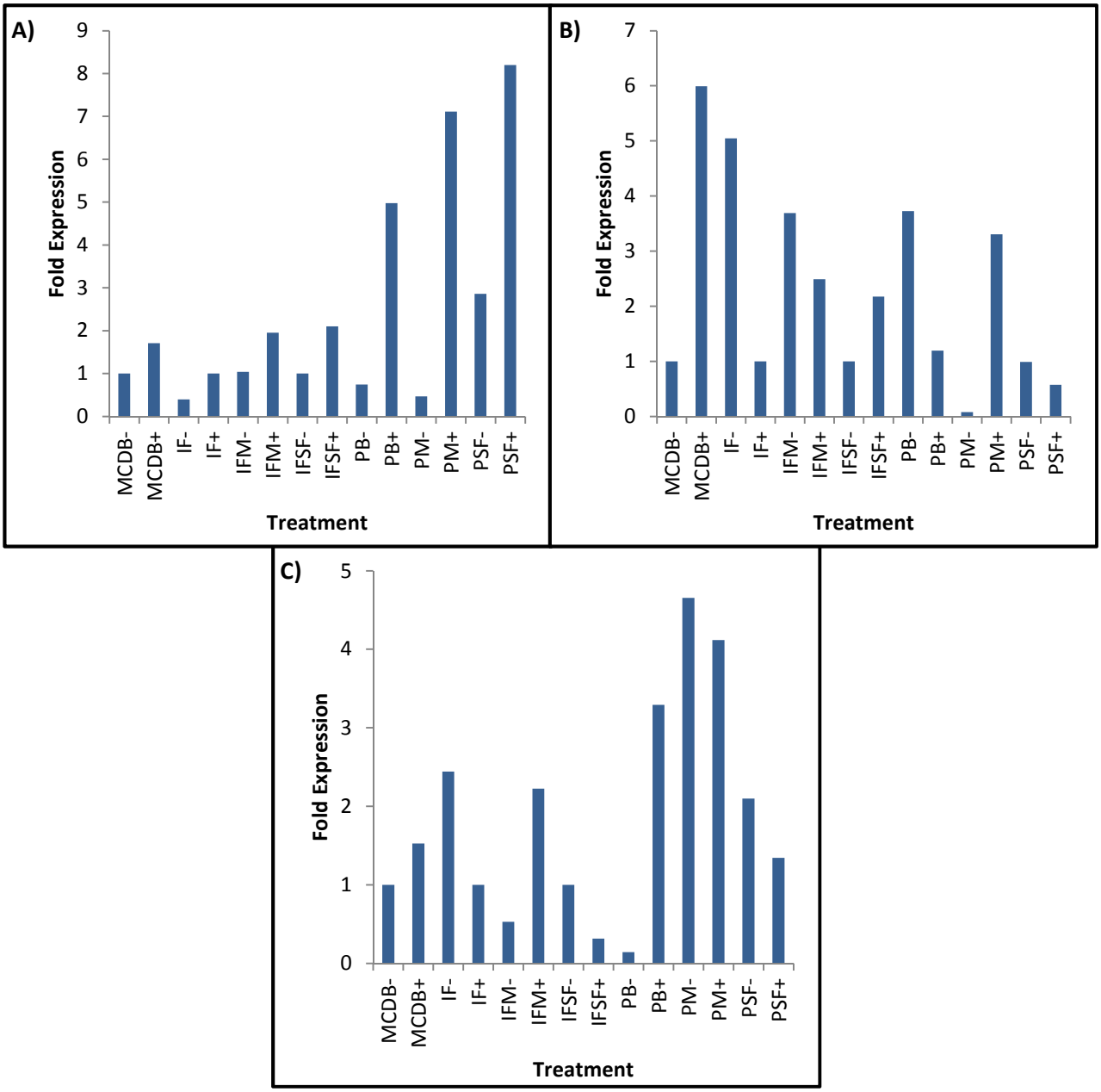

<u>Figure 22:</u> Fold-expression of the three reference genes. Data are represented as fold expression relative to the control sample (MCDB-201-). A) ALUsx, B) ALUsq, and C) ATP5B.

The variation in the fold-expression may be attributed to differences in the amount of input biological material in the qPCR procedure, which may be due to differences in the efficiency of cDNA synthesis, RNA integrity, and pipetting. However, the process of normalisation corrects for these differences as it would affect both the reference and target genes to the same degree. From the relative expression of the reference genes, normalisation factors were thus calculated based on the geometric mean of the fold expression of the three reference genes for all of the samples (Figure 23), which varied between 0.53 and 1.65.

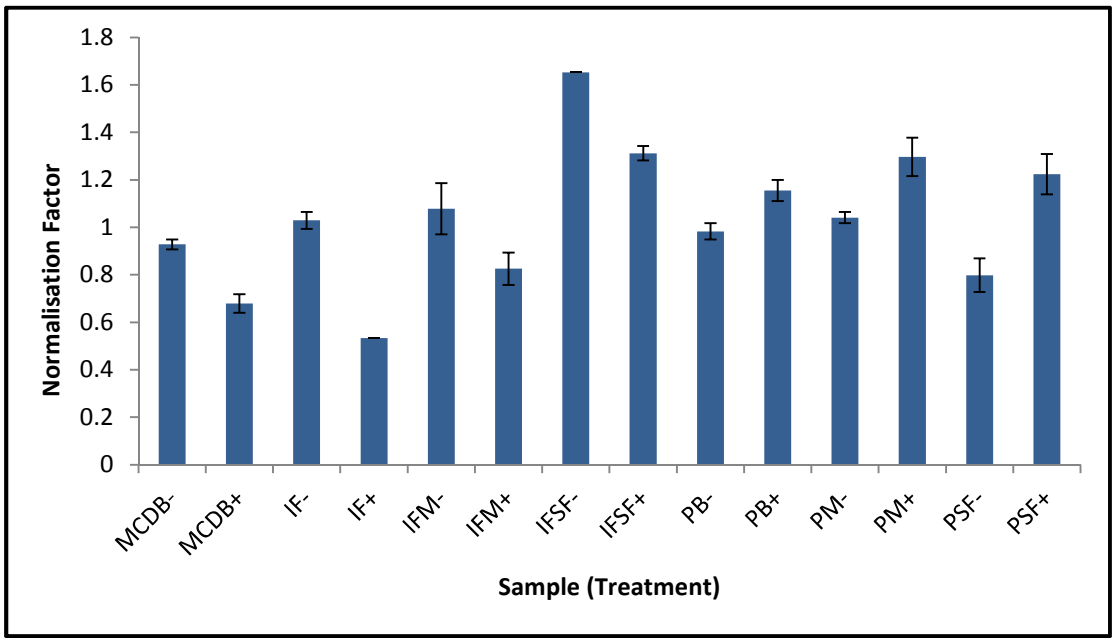

Figure 23: Normalisation factors used in the calculation of relative gene expression. The normalisation factor calculated for each experimental sample based on the average expression of the three reference genes (ALUsx, ALUsq, and ATP5B) as determined by the qBasePLUS qPCR data analysis software. Data represents the calculated normalisation factors ± S.E. Samples ending with a + or – indicate whether the experimental cells were incubated in the presence or absence of 0.1 µM insulin for 30 minutes prior to RNA extraction.

1.2 Genes of Interest

The amplification with the primer pairs for each of the genes of interest (*IRS1*, *PKB/Akt*, *JNK*, and *PKCε*) using the conditions indicated in Table 3 generated a single melt peak for *IRS1* and *PKB/Akt*, while non-specific melt peaks were generated for *JNK* and *PKCε* (Figures 24a and 24b). The NTCs generated non-specific amplicons after 32 cycles. The difference between the lowest NTC Cq values and the highest value in the experimental amplifications (true amplicons) was at least 6 cycles. This indicates that the non-specific amplicon formed was a late reaction, which would not affect the specific amplification of cDNA in the samples. In the case of *PKB/Akt*, the amplicons returned high C_q values of 31 and NTCs returned C_q values of 37. The same pattern was seen for the *JNK* expression and in the *PKCε* expression (Figure 24b); the NTCs did not yield any amplification. However, in the *JNK* and *PKCε* melt curves, additional peaks were present. This additional peak seen in each of these indicates the presence of non-specific amplification and must be considered in the interpretation of the data analysis, as it will result in inaccurate estimation of relative gene expression.

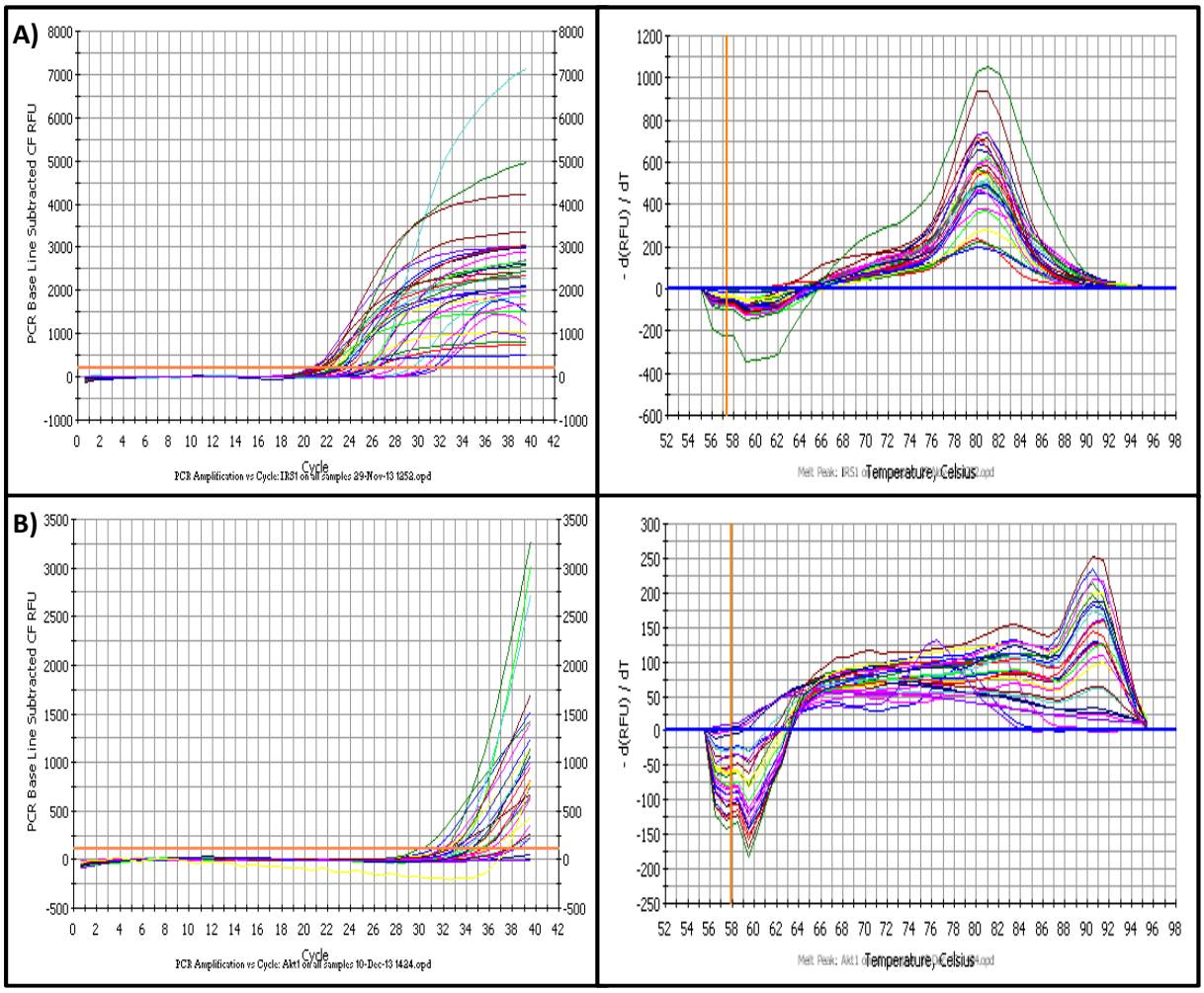

<u>Figure 24a:</u> Amplification and melt curves for genes of interest. A) Amplicon detection for the *IRS1* gene starts at the 21st cycle and the latest sample appears at cycle 26. The NTCs show amplification at cycle 32, **B)** *PKB/Akt* amplicon has a lowest C_q of 31 and the latest sample appears at cycle 32. The NTCs show amplification at cycle 37.

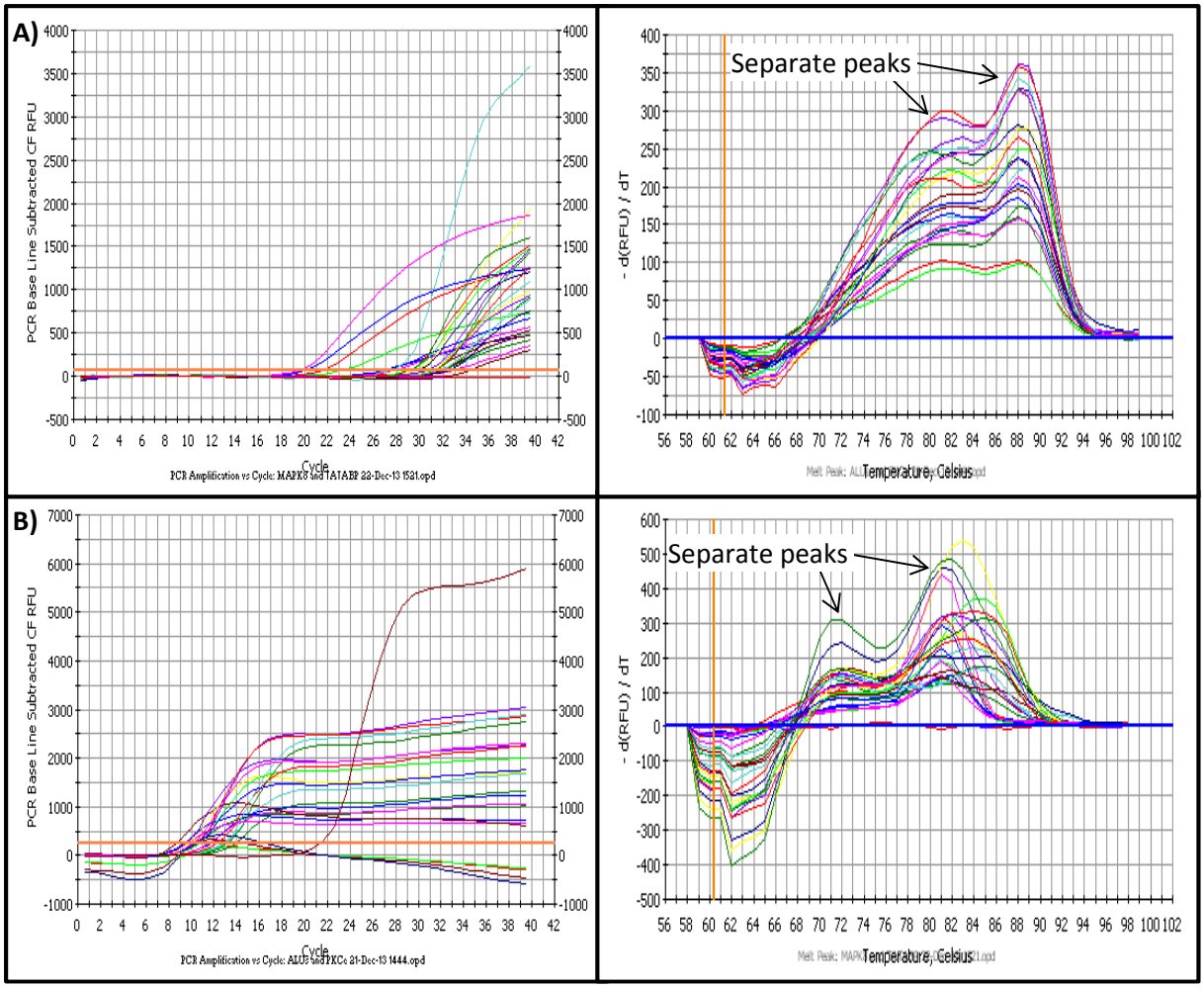

Figure 24b: Amplification and melt curves for genes of interest. A) The lowest C_q value for the *JNK* gene is 19 highest 26. The NTCs show amplification at cycle 32, and **B)** Amplicon detection for the *PKCε* gene starts at the 9th cycle and the latest sample appears at cycle 22. The NTCs show no amplification.

Using the normalisation factors, each target gene's expression was normalised to the expression of the reference genes and expressed as fold-change relative to the control sample (MCDB-201-) (Figure 25).

1.2.1 *IRS1* expression

In the control cultures (MCDB-201), insulin stimulation did not cause any clear changes in *IRS1* expression (Figure 25A). *IRS1* expression was found to be down-regulated in the cells made insulin-resistant by IF (0.11 fold change relative to the control non- insulin-resistant cells) while insulin stimulation of these cells resulted in an expression level similar to that of the control cultures (1 fold change relative to the control non-insulin-resistant cells). This one fold change indicates that the expression level of the sample was identical to that of the control sample, indicating some degree of insulin responsiveness and thus may imply

incomplete insulin-resistance in the IF-treated cultures. The PB-treated insulin-resistant cultures showed decreased *IRS1* expression (0.43 fold change relative to the control non-insulin-resistant cells) (Figure 25A).

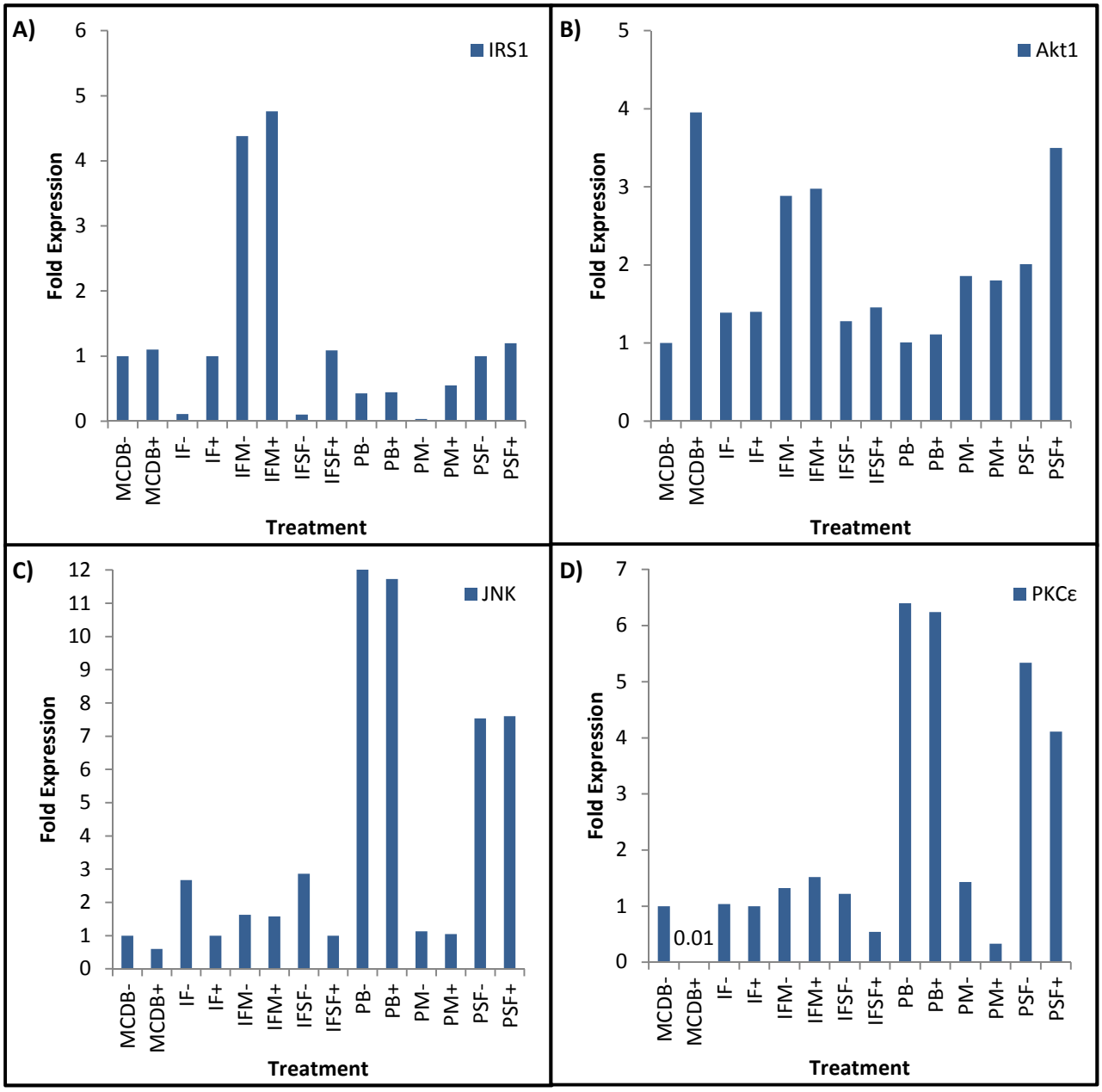

Figure 25: Fold expression of genes of interest. The relative fold expression (compared to MCDB-201-) for each sample normalised to the expression of the three reference genes or sequences. **A)** *IRS1*, **B)** *PKB/Akt1*, **C)** *JNK*, and **D)** *PKCε*.

1.2.2 *PKB/Akt* expression

The expression of *PKB/Akt* mRNA showed sensitivity to insulin stimulation in the control sample (Figure 25B). Pre-incubation with 0.1 µM insulin up-regulated the expression of *PKB/Akt* by 3.95 fold. This insulin-stimulated up-regulation was not observed in the IF- and PB-treated cells, although the expression levels were at the same level as the control non-insulin stimulated cells. Metformin treatment of the cells made insulin-resistant by IF-induction resulted in up-regulation of *PKB/Akt* expression in both insulin-stimulated and non-stimulated cultures. In contrast, *S. frutescens* treatment of the IF-induced insulin-resistant cultures did not change the expression of *PKB/Akt* relative to the insulin-resistant culture (IF). Furthermore, metformin had no distinct effect on the expression levels in the PM-treated cultures, while *S. frutescens* induced up-regulation of expression in the insulin-stimulated and non-stimulated cultures (2.01 and 3.5 fold change, respectively).

Both IRS1 and PKB/Akt are involved in eliciting the effector functions of insulin through transduction of the initial phosphorylation signal from the insulin receptor to IRS1. IRS1 in turn activates PKB/Akt through PI3K activity. PKB/Akt is involved in the promotion of glycogen synthesis and suppression of gluconeogenesis through phosphorylation of FoxO1 (Sesti, 2006). Therefore, the insulin-resistant state seen in the IF and PB cultures may be a consequence of, or exacerbated by, the down-regulation of the *IRS1* gene, leading to decreased signalling capacity upon insulin binding to the insulin receptor. Expression of *PKB/Akt* appears to be enhanced in the presence of insulin. The insulin-resistant samples (IF and PB) showed no increased expression in the presence of insulin. These changes in gene expression indicate the involvement of regulation or disruption of IRS1 and PKB/Akt gene expression in the development of insulin-resistance. Through down-regulation of *IRS1* and prevention of insulin-induced *PKB/Akt* up-regulation in the IF and PB cultures, insulin signalling becomes impeded, exacerbating the insulin-resistant state. This effect of the IF and PB induction media is reversed by metformin and *S. frutescens*, respectively. This is in line with previous studies where *S. frutescens* treatment up-regulated IRS1 expression above that of IF-induced cells (Williams *et al*., 2013).

1.2.3 *JNK* expression

It is thought that JNK is involved in the development of insulin-resistance through attenuation of insulin signalling and promoting HGP and liver steatosis (Gao *et al*., 2010; Dasgupta *et al*., 2011). Analysis of *JNK* expression showed decreased expression in the

insulin-stimulated control cells (0.6 fold change relative to the MCDB- culture) (Figure 25C). The IF culture resulted in increased *JNK* expression and cultures stimulated by insulin showed down-regulation of *JNK* expression, reflecting once again incomplete insulin-resistance in the IF-treated cultures. Metformin or *S. frutescens* treatment of the insulin-resistant IF-treated cultures resulted in no distinct change in *JNK* expression compared to the insulin-resistant cultures (IF). Palmitate-treated cultures, however, increased *JNK* expression in both insulin-stimulated and non-stimulated cultures (12.07 and 11.73 fold change, respectively). Metformin treatment of the insulin-resistant PB-cultures resulted in down-regulation of expression relative to the PB-culture, yielding an expression level similar to that of the control culture. The *S. frutescens*-treated PB insulin-resistant cultures still showed up-regulated levels of expression (7.54 and 7.6 in the insulin stimulated and non-stimulated cultures, respectively).

1.2.4 *PKCε* expression

It is known that PKCε is involved in the JNK-induced insulin-resistance (Dasgupta *et al*., 2011). The expression levels of *PKCε* showed a similar pattern to that of *JNK* expression (Figure 25D). In the control cultures, insulin stimulation down-regulated *PKCε* expression by 0.01 fold relative to the non-insulin stimulated culture. In the insulin-resistant cultures treated with IF, this insulin-related down-regulation of *PKCε* expression was abolished – having the same expression levels as the control culture. Metformin treatment of these insulin-resistant cultures did not show any distinct effect on *PKCε* expression, while *S. frutescens* treatment (PSF) resulted in recovery of the insulin-related down-regulation of *PKCε* expression (having a 0.54 fold change in the insulin stimulated culture). In contrast, PB-treated cultures yielded a distinct increase in *PKCε* expression, but insulin stimulation of these cultures did not have any effect on the expression levels (6.4 and 6.24 fold change, respectively, relative to the control). Metformin treatment of the insulin-resistant PB cultures caused the expression of *PKCε* to revert back to the level of the control and to be insulin-responsive once more (1.43 and 0.33 fold change in the non-insulin and insulin-stimulated cultures, respectively). Similarly, *S. frutescens*-treatment recovered the insulin-related effect on *PKCε* expression; however the levels were still higher than that of the control culture (5.34 and 4.11 fold change in the non-insulin and insulin-stimulated cultures, respectively).

The up-regulation of the *JNK* and *PKCε* genes may lead to attenuation of insulin signalling through increased activity of both JNK and PKCε. Interestingly, the expression of these

genes is up-regulated in the PB-culture, wherein palmitate-induced insulin-resistance acts mainly through the activities of both JNK and PKCε. However, this change in gene expression may not be a direct consequence of palmitate induction, but rather an indirect consequence due to the oxidative stress induced by palmitate, which activates the cellular stress signalling response in which JNK and PKCε are functional (Gao *et al*., 2010).

S. frutescens shows potential as an anti-diabetic treatment through its ability to recover insulin-responsive expression of genes involved in insulin signalling (*IRS1* and *PKB/Akt*) and recover the insulin-responsive expression of genes involved in attenuating insulin-resistance (*JNK* and *PKCε*). The expression of these genes may, however, not be causative factors in the development of insulin-resistance, but may be consequences of the insulin-resistant state. This cause and effect relationship between gene expression and insulin-resistance is difficult to elucidate and it may also be a complex combination of both causative and consequent responses. Furthermore, it must be noted that the expression of *JNK* and *PKCε* may be misrepresented due to the presence of non-specific peaks in the melt curve analyses. In addition, the qPCR experiment was performed using only a single run per gene which contained duplicate samples. This affects the statistical analysis of data such that no reasonable statistics can be performed due to a lack of replicate experiments (n = 1 in this study).

Chapter 5

Summary

Recent studies into the molecular mechanisms underlying T2DM have shown that high levels of insulin and fructose and high fat diets are capable of inducing the insulin-resistant state (Williams *et al*., 2013; Ruddock *et al*., 2008). Furthermore, the potential of the South African medicinal plant (*S. frutescens*) as an anti-diabetic agent was investigated in this study.

The primary objective of the current study was to investigate the changes in cellular physiology during the development of insulin-resistance and the effect a hot aqueous extract of *S. frutescens* has on the insulin-resistant state and related physiologic changes. In order to do this, two models of insulin-resistance were established, using the hepatocyte cell line HepG2, which reflected two causative factors in the development of insulin-resistance, namely hyperglycaemia and the compensatory hyperinsulinaemia, and hyperlipidaemia. HepG2 human hepatocyte cultures were chronically exposed to high levels of a combination of insulin and fructose (IF) (0.1 µM and 1 mM, respectively) or high levels of palmitate (PB) (0.25 mM). After 24 hours, the insulin-resistant state was confirmed by measuring hepatic glucose metabolism and homeostasis in the presence of 0.1 µM insulin by, monitoring gluconeogenesis and glycogenolysis (Chapter 2).

Upon chronic exposure to the IF and PB induction media, gluconeogenesis and glycogenolysis were significantly increased, characteristic of the insulin-resistant state, as insulin normally supresses these metabolic pathways. It is suggested that the unregulated metabolism of fructose in the liver results in increased TCA cycle activity, causing increased activity in the mitochondrial electron transport chain and consequently increases ROS production. This in turn leads to ROS-induced JNK activation, which is implicated in attenuation of insulin signalling through increased serine phosphorylation of IRS1/2, either by JNK directly or JNK-induced PKCε activity. Furthermore, JNK causes activation of FoxO1, activity which causes decreased glycogenesis and increased expression of the gluconeogenic genes *PEPCK* and *G6Pase*, HGP (Gao *et al*., 2010). In addition to this, increased fructolysis causes an increase in acetyl-CoA levels through metabolism of the fructolysis product, glyceraldehyde 3-phosphate and fructose-induced inhibition of PDK, and subsequently increased PDH activity. The activity of PDH is further induced by fructose 1-

phosphate and acts in conversion of pyruvate to acetyl-CoA, further increasing acetyl-CoA levels derived from fructose metabolism. Acetyl-CoA induces pyruvate carboxylase, PEPCK, and G6Pase activities and inhibits pyruvate kinase – promoting gluconeogenesis (Noguchi *et al*., 2009). Hyperinsulinaemia is implicated in uncoupling of insulin action wherein deregulation of FoxO1 results in increased gluconeogenesis, while SREBP-1c insulin responsiveness remains intact, resulting in insulin-induced lipogenesis still being active (Gonzalez *et al*., 2011).

Palmitate-induced gluconeogenesis and glycogenolysis occurs through a similar mechanism to that induced by fructose. The main difference is that palmitate metabolism occurs within the mitochondria and peroxisomes where successive rounds of β-oxidation lead to increased acetyl-CoA production. Acetyl-CoA may enter the TCA cycle leading to increased ATP production. Apart from the oxidative stress this induces, it also results in an increase in the cellular ATP/AMP ratio, leading to inactivation of AMPK, which in turn alleviates the AMPK-induced inhibition of TORC2 and SREBP-1c activity – increasing gluconeogenesis and lipogenesis (Viollet and Foretz, 2013). In addition to this, inactivation of AMPK alleviates its inhibitory effect on acetyl-CoA carboxylase (ACC). This allows ACC to convert acetyl-CoA to malonyl-CoA, which in turn inhibits the activity of CAT. This prevents the transfer of acyl-CoAs into the mitochondrial matrix for subsequent β-oxidation. Thus, cytoplasmic levels of palmitate increases, which in turn inhibits DGAT2, leading to increased DAG accumulation (Coll *et al*., 2008).

In chapter 2, the successful establishment of two insulin-resistant cell models using elevated levels of insulin and fructose and elevated levels of palmitate is described. Treatment of these cultures using a hot aqueous extract of *S. frutescens* improved the insulin-resistant state through decreasing the amount of hepatic gluconeogenesis and glycogenolysis.

After the establishment of the insulin-resistant models, the next step was to investigate the changes in cellular physiology under the insulin-resistant condition. Changes in lipogenesis, as measured by the amount of lipid accumulation, oxidative stress, and β-oxidation were analysed in Chapter 3.

Lipid accumulation was seen to be increased in both IF and PB models as measured by the Oil-Red-O assay, which predominantly measures the levels of TAG. In contrast, the Nile Red assay detected no significant increases in lipid accumulation, except in the positive control. This may indicate that the insulin-resistant models do not accumulate phospholipids. Due to the differences in lipid accumulation detected using the two staining methods for cellular lipids, it was decided to analyse the cellular lipid profiles within the different treatments. This was achieved by running TLC plates of total lipid extracts from cells exposed to the various induction media or treatments. The TLC analysis indicated differences in lipid profiles within the two models of insulin-resistance and treatments. The IF model showed mainly significant TAG accumulation, while the PB model showed mainly DAG accumulation. The differences in lipid accumulation reflect the different mechanisms through which the IF- and PB-treatments induce insulin-resistance. Treatment with IF predominantly involves fructose-induced insulin-resistance and liver steatosis. On the other hand, palmitate-induced DAG accumulation results in activation of JNK, which in turn elicits the insulin-resistant state. Thus, in the IF model, lipid accumulation may be more a symptomatic effect, while in the PB-model the lipid accumulation may be a causative factor in the development of insulin-resistance.

Oxidative stress is involved in the development of insulin-resistance. This study investigated the levels of NO and ROS after induction and treatment. The NO levels were to be elevated only in the PB model 1 hour post-induction, and remained elevated for up to 6 hours. After 24 hours, the NO levels returned to normal, while ROS levels were significantly increased in both the IF and PB models. It is suggested that NO is implicated in the palmitate-induced ROS production through initiating mitochondrial DNA damage, exacerbating mitochondrial dysfunction. Reactive oxygen species are generated by mitochondria during the metabolism of FFAs and acetyl-CoA derived from metabolic pathways, such as glycolysis and fructolysis. The increased metabolism of palmitate and fructose was reflected by the increase in acetyl-CoA and ROS levels. Increased acetyl-CoA allows for increased ROS production through the TCA cycle and subsequent ATP production via the electron transport chain. Elevated ROS levels in turn induce JNK activity, which leads to the insulin-resistant state (Gao *et al*., 2010).

The aim of this study was to investigate the anti-diabetic activity of *S. frutescens*. Treatment of the IF- and PB-treated cultures with the plant extract resulted in reversal of the insulin-resistant state as indicated by the glucose oxidase and anthrone assays described in chapter 2. This reversal is attributed to the ability of *S. frutescens* to decrease lipid accumulation of both TAG and DAG, as found in the lipid accumulation study described in chapter 3. Furthermore, *S. frutescens* is implicated in reducing the amount of ROS, but not NO, leading to decreased oxidative stress and subsequently decreased activation of JNK. This in turn prevents JNK-induced gluconeogenesis and impaired insulin signalling. In the IF model, ROS levels were returned to the control level, while in the PB model, although being significantly reduced, the levels were still above the control level. This may be explained by the increased acetyl-CoA levels measured in the PSF treatment. *S. frutescens* may be implicated in increasing β-oxidation of the free palmitate contained in the induction medium, increasing acetyl-CoA production. The ROS levels may also be decreased by the anti-oxidant activity of L-canavanine contained in the *S. frutescens* extract. Thus, *S. frutescens* shows potential as anti-diabetic treatment through its ability to induce suppression of gluconeogenesis, lipid accumulation, and oxidative stress.

The work described in chapter 4 focussed on determining whether the various models and treatments described in Chapter 2 had any effect on the mRNA expression of two genes involved in the insulin signalling pathway (*IRS1* and *PKB/Akt*) and two genes involved in attenuating insulin signalling (*JNK* and *PKCε*).

From the relative fold expression of the genes of interest, it was determined that the IF-induction resulted in incomplete insulin-resistance, as it causes down-regulation of the expression of *IRS1*, but insulin-stimulated up-regulation of the gene remains intact. In contrast, *PKB/Akt* expression does not maintain insulin-responsive up-regulation. However, in both the insulin-stimulated and non-stimulated cultures, the gene expression was still seen to be at control level. Thus, the IF model does not seem to induce changes in the expression of *PKB/Akt* but rather prevents the insulin-induced changes in expression. Similarly, IF-induced cultures showed up-regulation of *JNK*, while being down-regulated in the presence of insulin. *PKCε* expression did not respond to the insulin stimulus. Hence, some degree of insulin sensitivity must remain intact.

The palmitate model yielded different results. *IRS1* expression was down-regulated and did not maintain insulin responsiveness; while *PKB/Akt* exhibited the same expression as in the IF-induced cultures. Furthermore, both *JNK* and *PKCε* expression was up-regulated in the PB-induced cultures and insulin stimulation had no effect on their expression. This pattern of expression indicates that the mechanism by which insulin-resistance develops is complex and may be different depending on the causative factor, i.e. whether hyperinsulinaemia and hyperglycaemia or hyperlipidaemia is responsible.

Treatment of the insulin-resistant cultures with either metformin or *S. frutescens* had differing effects on gene expression, suggesting that these treatments for insulin-resistance may be acting through different mechanisms, as also indicated by data presented in chapter 3. Metformin treatment of the cells made insulin-resistant by the IF model produced up-regulation of *IRS1* and *PKB/Akt* in both insulin-stimulated and non-stimulated cultures. In the PB-induced cultures, *IRS1* and *PKB/Akt* expression remained down-regulated. *JNK* and *PKCε* expression were down-regulated in comparison to the PB-induced cultures, but recovered insulin responsiveness. In contrast, *S. frutescens* was able to recover the expression of *IRS1* and *PKB/Akt* to the same level of the control in non-insulin treated cultures, as well as the insulin responsiveness of these genes following insulin stimulation. *JNK* expression was down-regulated by *S. frutescens*, compared to the PB culture, however it was still above that of the control non-insulin-resistant MCDB culture, and insulin responsiveness was not recovered. *PKCε* expression remained up-regulated, although insulin responsiveness appeared to be recovered.

The changes in gene expression indicates two main points. First, the method of insulin-resistance induction influences the expression of these genes in specific ways and hence may act via different mechanisms. Second, metformin and *S. frutescens* exhibit anti-diabetic activity as indicated by their differing effects on the recovery of gene expression to the level on non-insulin-resistant cultures. This indicates that these treatments act through different mechanisms in order to reverse the insulin-resistant state.

It must be noted that the RNA extracts may have been compromised and thus the gene expression data may not fully represent the expression levels of the respective genes and reference genes. Furthermore, mRNA expression levels do not reflect the functional protein expression levels. This is due to different RNA processing mechanisms, RNA silencing

which can prevent translation of the mRNA, RNA degradation which may affect the levels of protein (if any) expressed, differing translation efficiencies, differing protein half-lives and post-translational modification or activation of the protein product (Bustin and Nolan, 2004; Bustin, 2010). For full elucidation of gene expression, it was intended to analyse the protein expression levels of the genes of interest and to determine the phosphorylation states of these under the various induction or treatment conditions by flow cytometry. However, due to time constraints this analysis could not be performed.

Conclusion

In conclusion, the two models of insulin-resistance indicate that the development of insulin-resistance may be through different mechanisms. Treatment of the insulin-resistant cells with either metformin or *S. frutescens* showed different effects in each model, suggesting different modes of action.

Future studies would include repetition of the qRT-PCR experiment and the addition of flow cytometric analysis of protein levels and phosphorylation. Firstly, the purification of RNA may be performed by using RNA spin columns which would decontaminate the samples. Furthermore, RNA quantification may be performed using the Agilent RNA 6000 Nano kit which will allow for more accurate quantification of RNA and provide a so-called RIN-value which indicates the quality of the RNA sample. This RIN-value would enable the selection of the most "intact" RNA samples for cDNA generation and further analysis by qPCR. This approach would ensure that the cDNA used in the qPCR analysis are of the highest quality and thus avoid the complications encountered in the current study. Additional genes may be investigated by qRT-PCR, such as genes involved in the metabolic pathways described in chapters 2 and 3. These would include gluconeogenic genes such as *PEPCK* and *G6Pase*, and lipogenic genes such as *TORC2* and *SREBP-1c*. The analysis of these genes may reveal other mechanisms at work in the two models and during treatment with either metfromin or *S. frutescens*. Flow cytometric analysis of proteins and nuclear factors involved in changing gene expression such as FoxO1, HMGA1, and ChREBP would also be informative. This would reveal more about how the two models induce the insulin-resistant state. Additionally, the investigation of the lipid fractions may be done by using alternative methods such as gas chromatography (GC) or GC-mass spectrometry (GC-MS) would allow for more accurate and specific quantification of different lipid subtypes not limited to a single class, as seen with the TLC plates in this study. Alternatively, liquid chromatography tandem mass

spectrometry (LC-MS/MS) can be used to analyse specific subtypes of lipids more in detail in order to identify the different proportions of each type of lipid. The analysis of acetyl-CoA may be performed using high performance liquid chromatography (HPLC), reverse phased-HPLC, or LC-MS/MS as this would be more sensitive and accurate in the determination of each type of acyl-CoA. This will allow investigation of important mediators of hepatic steatosis such as stearoyl-CoA, acetyl-CoA, and malonyl-CoA. Finally, analysis of ATP levels and mitochondrial membrane potential would help determine whether *S. frutescens* acts through a similar mechanism to metformin with regards to decreasing lipid accumulation and gluconeogenesis.

This study therefore indicates the promising ability of *S. frutescens* to reverse the insulin-resistant state, and associated cellular physiological changes through decreasing gluconeogenesis, glycogenolysis, liver steatosis, and oxidative stress, making it a strong candidate for the development of a novel alternative treatment for insulin-resistance and T2DM.

References

Akaogi J., Barker T., Kuroda Y., *et al*. (2006) **Role of non-protein amino acid L-canavanine in autoimmunity**, *Autoimmunity Reviews* **5**:429-435.

Amod A., Ascott-Evans B.H., Berg G.I., *et al*. (2012) **The 2012 SEMDSA Guideline for the Management of Type 2 Diabetes (Revised)**, *Journal of Endocrinology, Metabolism, and Diabetes of South Africa* **17**(2):S1-S95.

Baldanzi G., Alchera E., Imarisio C., *et al.* (2010) **Negative regulation of diacylglycerol kinase *θ* mediates adenosine-dependent hepatocyte preconditioning**, *Cell Death and Differentiation* **17**:1059-1068.

Boden G. and G.I. Shulman (2002) **Free fatty acids in obesity and type 2 diabetes: defining their role in the development of insulin resistance and beta-cell function**, *European Journal of Clinical Investigation* **32**(2):14-23.

Bustin S.A. (2000) **Absolute quantification of mRNA using real-time reverse transcription polymerase chain reaction assays**, *Journal of Molecular Endocrinology* **25**:169-193.

Bustin S.A. (2010) **Why the need for qPCR publication guidelines? – The case for MIQE**, *Methods* **50**:217-226.

Bustin S.A. and T. Nolan (2004) **Pitfalls of Quantitative Real-Time Reverse Transcription Polymerase Chain Reaction**, *Journal of Biomolecular Techniques* **15**(3):155-166.

Caton P.W., Nayuni N.K., Khan N.Q., *et al*. (2011) **Fructose induces gluconeogenesis and lipogenesis through a SIRT1-dependent mechanism**, *Journal of Endocrinology* **208**:273-283.

Chadwick W., Roux S., van de Venter M., Louw J. and W. Oelofsen (2007) **Anti-diabetic effects of *Sutherlandia frutescens* in Wistar rats fed a diabetogenic diet**, *Journal of Ethnopharmacology* **109**:121-127.

Chavez J.A. and S.A. Summers (2010) **Lipid oversupply, selective insulin resistance, and lipotoxicity: Molecular mechanisms**, *Biochimica et Biophysica Acta* **1801**:252-265.

Chen D., Bruno J., Easlon E., Lin S.J., Cheng H.L., Alt F.W. and L Guarente (2008) **Tissue-specific regulation of SIRT1 by calorie restriction**, *Genes and Development* **22**:1753–1757.

Chen S., Lam T.K.T., Park E., Burdett E., Wang P.Y.T., Wiesenthal S.R., Lam L., Tchipashvili V., Fantus I.G. and A. Giacca (2006) **Oleate-induced decrease in hepatocyte insulin binding is mediated by PKC-δ**, *Biochemical and Biophysical Research Communications* **346**:931-937.

Chen X., Iqbal N. and G. Boden (1999) **The effects of free fatty acids on gluconeogenesis and glycogenolysis in normal subjects**, *Journal of Clinical Investigation* **103**:365-372.

Chun Y. and Z.D. Yin (1988) **Glycogen Assay for Diagnosis of Female Genital *Chlamydia trachomatis* Infection**, *Journal of Clinical Microbiology* **36**:1081-1082.

Clemens M.G. (2001) **The liver: Biology and Pathobiology** (4th ed.) Lippincott Williams & Williams, Philadelphia.

Coll T., Eyre E., Rodriguez-Calvo R., *et al*. (2008) **Oleate Reverses Palmitate-induced Insulin Resistance and Inflammation in Skeletal Muscle Cells**, *Journal of Biological Chemistry* **283**(17):11107-11116.

Cornier M., Dabelea D., Hernandez T.L., Lindstrom R.C., Steig A.J., Stob N.R., Van Pelt R.E., Wang H. and R.H. Eckel (2008) **The Metabolic Syndrome**, *Endocrine Reviews* **29**(7):777-822.

Dasgupta S., Bhattacharya S., Maitra S., Pal D., Majumdar S.S., Datta A. and S. Bhattacharya (2011) **Mechanism of lipid induced insulin resistance: Activated PKCε is a key regulator**, *Biochimica et Biophysica Acta* **1812**:495-506.

Dey D., Bhattacharya A., Roy S. and S. Bhattacharya (2007) **Fatty acid represses insulin receptor gene expression by impairing HMGA1 through protein kinase Cε**, *Biochemical and Biophysical Research Communications* **357**:474-479.

Diaz-Guerra M.J., Junco M. and L. Bosca (1991) **Oleic acid promotes changes in the subcellular distribution of protein kinase C in isolated hepatocytes**, *Journal of Biological Chemistry* **266**:23568-23576.

Fernandes A.C., Cromarty A.D., Albrecht C. and C.E.J. van Rensburg (2003) **The antioxidant potential of *Sutherlandia frutescens***, *Journal of Ethnopharmacology* **95**:1-5.

Foufelle F. and P. Ferre (2002) **New perspectives in the regulation of hepatic glycolytic and lipogenic genes by insulin and glucose: a role for the transcription factor sterol regulatory element binding protein-1c**, *Biochemical Journal* **366**:377-391.

Fröjdö S., Vidal H. and L. Pirola (2009)**Alterations of insulin signaling in type 2 diabetes: A review of the current evidence from humans**, *Biochimica et Biophysica Acta* **1792**:83-92.

Gao D., Nong S., Huang X., *et al*. (2010) **The Effects of Palmitate on Hepatic Insulin Resistance Are Mediated by NADPH Oxidase 3-derived Reactive Oxygen Species through JNK p38^{MAPK} Pathways**, *Journal of Biological Chemistry* **285**(39):29965-29973.

Gonzalez E., Flier E., Molle D., *et al*. (2011) **Hyperinsulinemia leads to uncoupled insulin regulation of the GLUT4 glucose transporter and the FoxO1 transcription factor**, *Proceedings of the National Academy of Sciences* (early edition):1-6.

Gorovits N., Cui L., Busik J.V., Ranalletta M., De-Mouzon S.H. and M.J. Charron (2003) **Regulation of Hepatic GLUT8 Expression in Normal and Diabetic Models**, *Endocrinology* **114**(4):1703-1711.

Gum R.J., Gaede L.L., Koterski S.L., Heindel M., Clampit J.E., Zinker B.A., Trevillyan J.M., Ulrich R.G., Jirousek M.R. and C.M. Rondinone (2003) **Reduction of protein tyrosine phosphatase 1B increases insulin-dependent signaling in *ob/ob* mice**, *Diabetes* **52**:21-28.

Guo H., Xia M., Zou T., *et al*. (2012) **Cyanidin 3-glucoside attenuates obesity-associated insulin resistance and hepatic steatosis in high-fat diet-fed and *db/db* mice via the transcription factor FoxO1**, *Journal of Nutritional Biochemistry* **23**(4):349-360.

Hall R.K., Yamasaki T., Kucera T., Waltner-Law M., O'Brien R. and D.K. Granner (2000) **Regulation of phosphoenolpyruvate carboxykinase and insulin-like growth factor-binding protein-1 gene expression by insulin. The role of winged helix/forkhead proteins**, *Journal of Biological Chemistry* **275**:30169-30175.

Hirosumi J., Tuncman G., Chang L., Gorgun C.Z., Uysal K.T., Maeda K., Karin M. and S. Hotamisligil (2002) **A central role for JNK in obesity and insulin resistance**, *Nature* **420**:333-336.

Hers H.G. and L. Hue (1983) **Gluconeogenesis and related aspects of glycolysis**, *Annual Review of Biochemistry* **52**:617-653.

Hovik R., Brodal B., Bartlett K. and H. Osmundsen (1991) **Metabolism of acetyl-CoA by isolated peroxisomal fractions: formation of acetate and acetoacetyl-CoA**, *Journal of Lipid Research* **32**:993-999.

Itani S.I., Ruderman N.B., Schmeider F. and G. Boden (2002) **Lipid-induced insulin resistance in human muscle is associated with changes in diacylglycerol, protein kinase C, and IkappaB-alpha**, *Diabetes* **51**:2005-2011.

Karaskov E., Scott C., Zhang L., *et al*. (2006) **Chronic Palmitate But Not Oleate Exposure Induces Endoplasmic Reticulum Stress, Which May Contribute to INS-1 Pancreatic *β*-Cell Apoptosis**, *Endocrinology* **147**(7):3398-3407.

Kawada T., Takahashi N., Goto T., Egawa K., Kato S., Kuroyanagi K., Kusudo T., Kim C. And R Yu (2005) **Herbal terpenoids act as ligands for PPAR-alpha and gamma to manage gene expression involved in lipid metabolism and inflammation**, In *75th EAS Congress April*, Prague, Czech Republic.

Koo H.Y., Miyashita M., Cho B.H. and M.T. Nakamura (2009) **Replacing dietary glucose with fructose increases ChREBP activity and SREBP-1 protein in rat liver nucleus**, *Biochemical and Biophysical Research Communications* **390**(2):285-289.

Kresge N., Simoni R.D. and R.L. Hill (2005) **Otto Fritz Meyerhof and the elucidation of the glycolytic pathway**, *Journal of Biological Chemistry* **280**, e3.

Leclercq I.A., Da Silva Morais A., Schroyen B., Van Hul N. and A. Geerts (2007) **Insulin resistance in hepatocytes and sinusoidal liver cells: Mechanisms and consequences**, *Journal of Hepatology* **47**:142-156.

Lee J., Cho H. and Y.H. Kwon (2010) **Palmitate induces insulin resistance without significant intracellular triglyceride accumulation in HepG2 cells**, *Metabolism Clinical and Experimental* **59**:927-934.

Liu H., Collins Q.F., Moukdar F., *et al*. (2007) **Prolonged Treatment of Primary Hepatocytes with Oleate Induces Insulin Resistance through p38 Mitogen-activated Protein Kinase**, *Journal of Biological Chemistry* **282**(19):14205-14212.

Matsumoto M., Pocai A., Rossetti L., *et al*. (2007) **Impaired regulation of hepatic glucose production in mice lacking the forkhead transcription factor FoxO1 in liver**, *Cell Metabolism* **6**(3):208-216.

Matte A., Tari L.W., Goldie H. and L.T.J. Delbaere (1997) **Structure and mechanism of phosphoenolpyruvate carboxykinase**, *Journal of Biological Chemistry* **272**:8105-8108

Meshkani R. and K. Adeli (2009) **Hepatic insulin resistance, metabolic syndrome and cardiovascular disease**, *Clinical Biochemistry* **42**:1331-1346.

Montell E., Turini M., Marotta M., Roberts M., Noe V., Ciudad C.J., Macé K. and A.M. Gómez-Foix (2001) **DAG accumulation from saturated fatty acids desensitizes insulin stimulation of glucose uptake in muscle cells**, *American Journal of Physiology – Endocrinology & Metabolism* **280**:E229-E237.

Mosmann T. (1983) **Rapid calorimetric assay for cellular growth and survival: application to proliferation and cytotoxicity assays**, *Journal of Immunological Methods* **65**(1):55-63.

Mosthaf L., Grako D., Dull T.J., Coussens L., Ullrich A. and D.A. McClain (1990) **Functionally distinct insulin receptors generated by tissue-specific alternative splicing**, *The European Molecular Biology Organization Journal* **9**:2409-2413.

Noguchi Y., Young J.D., Aleman J.O., *et al*. (2009) **Effect of Anaplerotic Fluxes and Amino Acid Availability on Hepatic Lipoapoptosis**, *Journal of Biological Chemistry* **284**(48):33425-33436.

Norgren S., Zierath J., Wedell A., Wallberg-Henriksson H. and H. Luthman (1994) **Regulation of human insulin receptor RNA splicing *in vivo***, *Proceedings of the National Academy of Sciences of the USA* **91**:1465-1469.

Pappas A., Anthonavage M. and J.S. Gordon (2002) **Metabolic Fate and Selective Utilization of Major Fatty Acids in Human Sebaceous Gland**, *The Journal of Investigative Dermatology* **118**(1):164-171.

Park O.J., Cesar D., Faix D., *et al*., (1992) **Mechanisms of fructose-induced hypertriglyceridaemia in the rat: Activation of hepatic pyruvate dehydrogenase through inhibition of pyruvate dehydrogenase kinase**, *Biochemical Journal* **282**:753-757.

Pessin J.E. and A.R. Saltiel (2000) **Signaling pathways in insulin action: Molecular targets of insulin resistance**, *Journal of Clinical Investigation* **106**:165-169.

Qatanani M and M.A. Lazar (2007) **Mechanisms of obesity-associated insulin resistance: many choices on the menu**, *Genes & Development* **27**:1443-1455.

Reeves R. (2001) **Molecular biology of HMGA proteins: hubs of nuclear function**, *Gene* **277**:63-81.

Robinson J.P., Carter W.O., and P.K. Narayanan (1994) **Oxidative product formation analysis by flow cytometry**, *Methods in Cell Biology* **41**:437-447.

Rodgers J.T., Lerin C., Haas W., Gygi S.P., Spiegelman B.M. and P. Puigserver (2005) **Nutrient control of glucose homeostasis through a complex of PGC-1alpha and SIRT1**, *Nature* **434**:113-118.

Ruddock M.W., Stein A., Landaker E., Park J., Cooksey R.C., McClain D. and M. Patti (2008) **Saturated Fatty Acids Inhibit Hepatic Insulin Action by Modulating Insulin Receptor Expression and Post-receptor Signalling**, *Journal of Biochemistry* **144**:599-607.

Saini V. (2010) **Molecular mechanisms of insulin resistance in type 2 diabetes mellitus**, *World Journal of Diabetes* **1**(3):68-75.

Sampson S.R. and D.R. Cooper (2006) **Specific protein kinase C isoforms as transducers and modulators of insulin signaling**, *Molecular Genetics and Metabolism* **89**:32-47.

Samuel V.T. (2011) **Fructose induced lipogenesis: from sugar to fat to insulin resistance**, *Trends in Endocrinology and Metabolism* **22**(2):60-65.

Sano H., Kane S., Sano E., Miinea C.P., Asara J.M., Lane W.S., Garner C.W. and G.E. Lienhard (2003) **Insulin-stimulated phosphorylation of a Rab GTPase-activating protein regulates GLUT4 translocation**, *Journal of Biological Chemistry* **278**:14599-14602.

Sesti G. (2006) **Pathophysiology of insulin resistance**, *Best Practice & Research Clinical Endocrinology & Metabolism* **20**(4):665-679.

Shulman G.I. (2000) **Cellular mechanisms of insulin resistance**, *Journal of Clinical Investigation* **106**:171-176.

Sicree R., Shaw J., P. Zimmet (2011) **The Global Burden: Diabetes and Impaired Glucose Tolerance**, *IDF Diabetes Atlas* **4**:1-105.

Stefan N. and H. Häring (2011) **The Metabolically Benign and Malignant Fatty Liver**, *Diabetes* **60**:2011-2017.

Stephenne X., Foretz M., Taleux N., *et al*. (2011) **Metformin activates AMP-activated protein kinase in primary human hepatocytes by decreasing cellular energy status**, *Diabetalogia* **54**:3101-3110.

Stumvoll M. (2005) **Fatty acids and insulin resistance in muscle and liver**, *Best Practice & Research Clinical Endocrinology & Metabolism* **19**(4):625-635.

Tai J., Cheung S., Chan E. and D. Hasman (2004) **In vitro culture studies of *Sutherlandia frutescens* on human tumor cell lines**, *Journal of Ethnopharmacology* **93**:9-19.

Tappy L., Lê K.A., Tran C. and N. Paquot (2010) **Fructose and metabolic diseases: New findings, new questions**, *Nutrition* **26**:1044-1049.

Toker A. and A.C. Newton (2000) **Cellular signaling: pivoting around PDK-1**, *Cell* **103**:185-188.

Valasek M.A. and J.J. Repa (2005) **The power of real-time PCR**, *Advances in Physiology Education* **29**:151-159.

Vandesompele J., De Preter K., Pattyn F., *et al*. (2002) **Accurate normalization of real-time quantitative RT-PCR data by geometric averaging of multiple internal control genes**, *Genome Biology* **3**(7):research 0034.1-0034.11.

Van Epps-Fung M., Williford J., Wells A. and R.W. Hardy (1997) **Fatty Acid-Induced Insulin Resistance in Adipocytes**, *Endocrinology* **138**(10):4338-4345.

Van Wyk B.E. and C. Albrecht (2008) **A review of the taxonomy, ethnobotany, chemistry and pharmacology of *Sutherlandia frutescens* (Fabaceae)**, *Journal of Ethnopharmacology* **119**:620-629.

Van Wyk B.E., B. van Oudtshoom and N. Gericke (2012) **Medicinal Plants of South Africa**, Briza Publications, Pretoria, p 336.

Viollet B. and M. Foretz (2013) **Revisiting the mechanisms of metformin action in the liver**, *Annales d'endocrinologie* **74**(2):123-129.

Viollet B., Guigas B., Garcia N.S., *et al*. (2012) **Cellular and molecular mechanisms of metformin: an overview**, *Clinical Science* **122**(6):253-270.

Vossaert L., O'Leary T., Van Neste C., *et al*. (2013) **Reference loci for RT-qPCR analysis of differentiating human embryonic stem cells**, *BMC Molecular Biology* **14**(21):1471-2199.

Wei Y., Wang D., Topczewski F. and M.J. Pagliassotti (2007) **Fructose-mediated stress signaling in the liver: implications for hepatic insulin resistance**, *Journal of Nutritional Biochemistry* **18**:1-9.

Wei Y., Bizeau M.E. and M.J. Pagliassotti (2004) **An acute increase in fructose concentration increases hepatic glucose-6-phosphatase mRNA via mechanisms that are independent of glycogen synthase kinase-3 in rats**, *Journal of Nutritional Biochemistry* **134**:545-551.

White M. (2002) **IRS Proteins and the Common Path to Diabetes**, *American Journal of Physiology – Endocrinology and Metabolism* **283**:E413-E422.
Williams S. (2010) **Chang liver cell line as a model for Type II Diabetes in the liver and possible reversal of this condition by Indigenous Medicinal Plants**, *PhD Thesis, Department of Biochemistry and Microbiology, Nelson Mandela Metropolitan University*.

Williams S., Roux S., Koekemoer T., *et al*. (2013) ***Sutherlandia frutescens* prevents changes in diabetes-related gene expression in a fructose-induced insulin resistant cell model**, *Journal of Ethnopharmacology* **146**:482-489.

Wong D.W. and J.F. Medrano (2005) **Real-time PCR for mRNA quantitation**, *Biotechniques* **39**(1):1-11.

Yuan L., Ziegler R. and A. Hamann (2003) **Metformin modulates insulin post-receptor signaling transduction in chronically insulin-treated HepG2 cells**, *ActaPharmacologica Sinica* **24**(1):55-60.

Yuzefovych L., Wilson G. and L. Rachek (2010) **Different effects of oleate vs. palmitate on mitochondrial function, apoptosis, and insulin signaling in L6 skeletal muscle cells: role of oxidative stress**, *American Journal of Physiology, Endocrinology and Metabolism* **299**(9):1096-1105.

Zhang W., Patil S., Chauhan B., *et al*. (2006) **FoxO1 Regulates Multiple Metabolic Pathways in the Liver: Effects on gluconeogenic, glycolytic, and lipogenic gene expression**, *Journal of Biological Chemistry* **281**(15):10105-10117.

Zick Y. (2001) **Insulin resistance: a phosphorylation-based uncoupling of insulin signaling**, *TRENDS in Cell Biology* **11**(11):437-441.